360

INSULATION CO-ORDINATION RELATED TO INTERNAL INSULATION OF GAS INSULATED SYSTEMS WITH SF_6 AND N_2/SF_6 GAS MIXTURES UNDER AC CONDITION

Working Group
C4.302

October 2008

WG C4.302

Insulation co-ordination related to internal insulation of gas insulated systems with SF_6 and N_2/SF_6 gas mixtures under AC condition

Members :

Hiroyuki HAMA(JP), Shigemitsu OKABE (JP), Redactors

Michael MUHR (AT), Convener

Tony BRITTEN (ZA)
Hiroyuki HAMA (JP)
Karsten JUHRE (DE)
Claus NEUMANN (DE)
Shigemitsu OKABE (JP)
Udo PRUCKER (DE)
Alain SABOT (FR)

ISBN: 978- 2- 85873-048-3

INSULATION CO-ORDINATION RELATED TO INTERNAL INSULATION OF GAS INSULATED SYSTEMS WITH SF_6 AND N_2/SF_6 GAS MIXTURES UNDER AC CONDITION

Contents

1. EXECUTIVE SUMMARY……..……5

2. INTRODUCTION…….……..11

REFERENCES of Chapter 1 & 2……13

3. CONVERSION IN SHAPE OF FIELD OVERVOLTAGE TO STANDARD IMPULSE WAVEFORM IN DETERMINING REPRESENTATIVE OVERVOLTAGES FOR GIS
…..14

3.1 Introduction……14

3.2 Non-standard lightning impulse waveform……14

3.3 Insulation characteristics of GIS element for non-standard lightning impulses……..15
3.3.1 Experimental results……...15
3.3.2 Duration time evaluation……15

3.4 Evaluation method for GIS……...……..18

3.5 Application to a lightning surge at GIS in the UHV system……...19

3.6 Conclusion……..19

REFERENCES of Chapter 3……...20

4. IN-SERVICE AGEING IN SAFETY FACTOR ……21

4.1 Long-term performance of SF_6 insulation system in GIS……21

4.2 V-t characteristics of SF_6 under clean and metallic particle contamination ……21

4.3 V-N characteristics of interface between insulator surface and SF_6……23

4.4 V-t and V-N characteristics of internal bulk of solid insulators……..25
4.4.1 Long-term V-t characteristics ……25
4.4.2 Influence of temperature and mechanical stress on the V-t characteristics……28
4.4.3 V-N characteristics of internal bulk at LI and SI……29

4.4.4 Critical field for ageing……..30

4.5 Performance of combined and SF_6 impregnated dielectrics……....32

4.6 Influence of VFT on internal potential connections in GIS equipment……..33

4.7 Ageing of gas insulated equipment and switchgear after long-term service operation……33
4.7.1 Example of 245 kV CT……..34
4.7.2 Example of epoxy spacer……...35
4.7.3 Example of 123 kV GIS…….37

4.8 Insulation performance after 50 years GIS service life……37

4.9 Conclusion……..38

REFERENCES of Chapter 4……...40

5. INFLUENCE OF PRESTRESS VOLTAGE ON INSULATION WITHSTAND OF GIS …..41

5.1 Insulation characteristics under impulse voltages superimposed to AC voltages……41

5.2 Insulation characteristics under impulse voltages superimposed to DC voltages……..41

5.3 Influence of AC and DC prestress on GIS insulation performance……48

5.4 Conclusion……..55

REFERENCES of Chapter 5……...56

6. TEST CONVERSION FACTORS IN SF_6 AND N_2/SF_6 GAS MIXTURES …….57

6.1 Breakdown properties at LI, SI and AC voltages in SF_6……57
6.1.1 Properties under quasi-uniform field…….57
6.1.2 Properties under non-uniform field……63
6.1.3 Conversion factors in SF_6……...70

6.2 Breakdown properties at LI, SI and AC voltages in N_2/SF_6 gas mixtures……..73
6.2.1 Properties under quasi-uniform field…….73
6.2.2 Properties under non-uniform field……79
6.2.3 Conversion factors in N_2/SF_6 gas mixtures……80

6.3 Most critical stress in SF_6 and N_2/SF_6 gas mixtures……80
6.3.1 Most critical stress in SF_6……...80
6.3.2 Most critical stress in N_2/SF_6 gas mixtures…….85

6.4 Conclusion……...85

REFERENCES of Chapter 6……88

7. SITE TESTING……90

REFERENCES of Chapter 7……90

8. CONCLUSIONS ……..94

EXECUTIVE SUMMARY

Introduction

The CIGRE Task Force focuses on the following study items of gas insulated system regarding insulation co-ordination related to internal insulation to make up the lack of information concerning "dielectric withstand characteristics of electrical insulation":

a) Conversion of field overvoltage to standard impulse waveform,
b) Combined safety factors in IEC60071-1,
c) In-service ageing of insulation,
d) V-t characteristics from the point of view as to whether there is sufficient information available for insulation co-ordination,
e) Influence of a prestress voltage on the insulation withstand,
f) Conversion factors relating to voltages above and below which switching impulse or power frequency tests may be substituted for each other,
g) Site testing.

Gas insulated system, which enables compactness and high reliability of the equipment, has now worldwide issues such as in-service ageing of the equipment, further compactness with high reliability and environmental problem to reduce SF_6 emission into the atmosphere.

On the other hand, the insulation techniques for the gas insulated system have been progressed steadily in the field of equipment reliability and insulation co-ordination.

This brochure reviews and discusses insulation co-ordination related to internal insulation of gas insulated equipment in SF_6 and also some aspects of N_2/SF_6 gas mixtures under AC condition, considering the above issues and referring to the latest research on the insulation properties and techniques. As the equipment of the gas insulated system, gas insulated switchgear (GIS) is dealt with in this brochure.

Scope of Studies

Insulation co-ordination process is explained by the flow chart for the determination of rated or standard insulation level of IEC 60071-1 as shown in Fig. 1. The process consists of four steps of calculating (1) representative voltages and overvoltages U_{rp}, (2) co-ordination withstand voltages U_{cw}, (3) required withstand voltages U_{rw}, (4) rated or standard insulation level: set of U_w.

Some essential factors such as co-ordination factor K_c in the step (2), altitude correction factors K_a (or atmospheric correction factor K_t) and safety factor K_s in the step (3), and test conversion factor K_{tc} in the step (4) are applied in the above insulation co-ordination process.

This brochure introduces a method of conversion in shape of field overvoltage to standard impulse waveform to determine representative voltages and overvoltages U_{rp}, and also deals with the safety factor K_s and the test conversion factor K_{tc} from the following viewpoints.

Regarding the safety factor K_s, the study on ageing of insulation performance during the long operation is essential. The influence of prestress voltages such as AC or DC on insulation performance of GIS is also important to evaluate "other unknown factors" in the safety factor K_s, since the prestress effects have not been well discussed for the latest power equipment applying IEC 62271-203.

The test conversion factors should be also reviewed for the equipment applying SF_6, reflecting the recent data on the insulation properties to develop the latest compact equipment. Also, there is a demand for the test conversion factor in N_2/SF_6 gas mixtures, since gas insulated line (GIL) applying the gas mixtures is now in service operation. Considering the above, the following items

are discussed in the brochure.

Conversion in Shape of Field Overvoltage to Standard Impulse Waveform in Determining Representative Overvoltages for GIS

In the chapter 3, a conversion method of field overvoltage to standard impulse waveform is introduced, which is effective to determine the representative voltages and overvoltages U_{rp} for GIS, referring to the recent experimental and analytical studies.

From the results of lightning surge and disconnector switching surge analyses, and so on, and measurements of ultra high voltage (UHV: 1000kV) and 500kV substations, representative non-standard impulse waveforms were extracted. The rise time of the wave crest is, as a whole, 0.1 - 1.0μs.

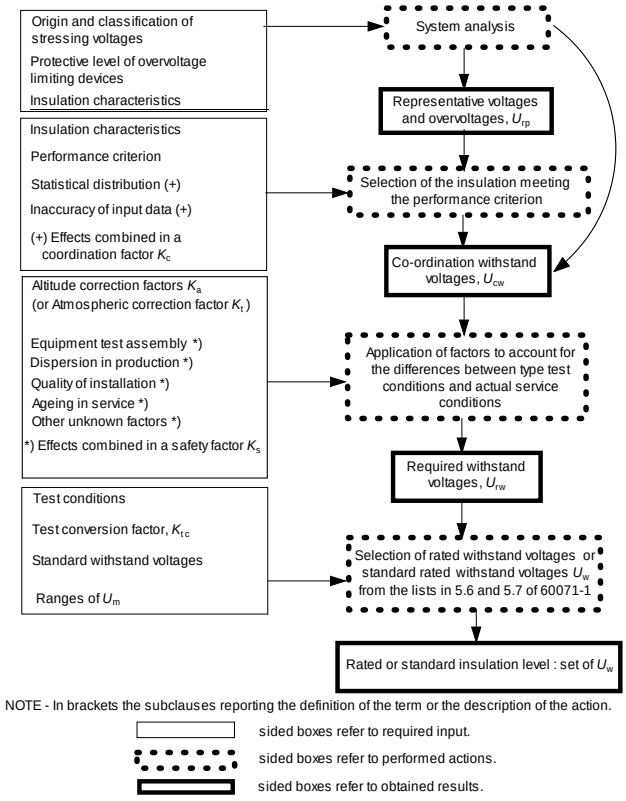

Fig. 1:Flow chart for the determination of rated or standard insulation level (IEC 60071-1)

(a) Waveform A: Pulse-shaped waveform
(b) Waveform B: The wave crest has a steep pulse-shaped part, and the wave tail is flat (Ratio between peak and flat part: 0.7 - 0.9)
(c) Waveform C: A damped oscillatory waveform whose first wave is a maximum (Frequency: 0.5 - 5.0MHz)
(d) Waveform D: A damped oscillatory waveform whose second wave is the crest value (Frequency: 0.5 - 5.0MHz)
(e) Waveform E: Double-frequency oscillatory waveform (Lower frequency: Approx. 1.0MHz, Upper frequency: Approx. 5.0MHz)

The waveform was resolved into elements including each oscillatory wave, the flat part, and so on. The crest value that was converted into an equivalent standard lightning impulse waveform as the overall waveform was calculated. Figure 2 shows the waveform evaluation flow for a GIS.

It is found that the insulation requirements could not be as severe as those of the standard lightning impulse waveform, since the decay of the field overvoltage is generally large. Consequently, it could be possible in some cases to use lower withstand test voltages for GIS using SF_6.

In-service Ageing in Safety Factor

In the chapter 4, the in-service ageing in safety factor is studied based on the recent data, discussing the insulation performance of GIS after 50 years service life.

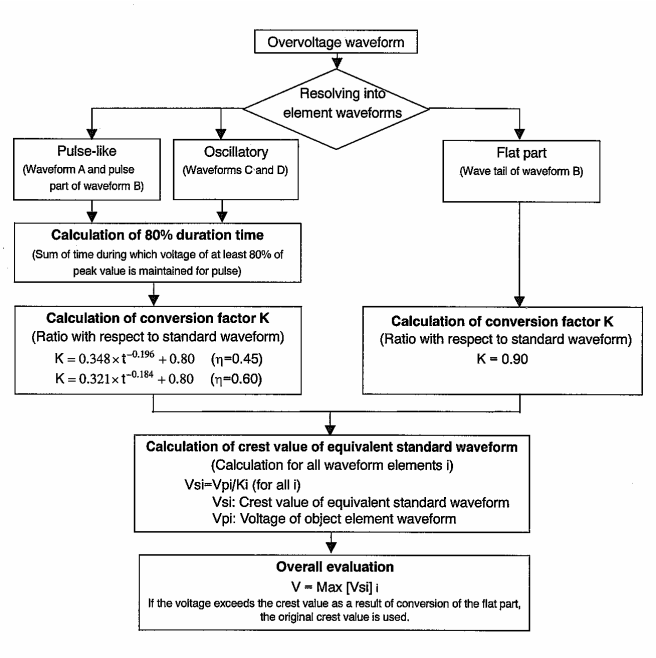

Fig. 2:Waveform evaluation flow for a GIS

The long-term performance of insulation system in GIS during the 50 years service life is summarized in Table 1, using the two parameter Weibull distribution together with the statistical coefficients representing the V-t and V-N characteristics. The insulation performance after 50 years operation is also estimated by each ageing factor.

The puncture field E_{50y} after 50 years operation of 5.9 – 7.0 kVrms/mm are larger than the maximum working stress 5 kVrms/mm reported in the literature, which shows that epoxy insulators would have enough performance even after 50 years operation. The enough insulation performance is also confirmed by the facts that the critical field for ageing is 12kVrms/mm during a long-term operation.

Table 1: Summary of statistical coefficients representing V-t and V-N characteristics of SF_6 insulated system in GIS at AC, LI and SI stress. Puncture field and reduction of insulation performance after 50 years service life are estimated.

Long-term insulation performance			Stress	*n*-value[*1]	*a*-value[*1]	Puncture field E_{50y} or Reduction rate after 50 years
Internal bulk of insulators	Room temperature	V-t	AC	13 [*5]	No data	8.1 kVrms/mm[*2]
				15 [*5]	0.4 -0.53, 0.9 [*4]	9.6 kVrms/mm[*2]
	90 - 105 degrees Centigrade			15.4 - 16	No data	10 % reduction from room temperature
	Room temperature	V-N	LI	35.7	0.37 - 0.53	10 %[*3]
			SI	45.5	0.21 - 0.38	10 %[*3]
Interface between insulator surface and SF_6 gas	Room temperature	V-N	-LI	124	0.2	3 %[*3]
			-SI	134	0.2 - 0.3	3 %[*3]
SF_6 gas	under clean condition	V-t	AC	78[*5]	0.25 - 0.50	20 %[*3]
	with metallic particles within quality control level			30 (< 10minutes)	0.88 - 0.98	-
				69 (> 10minutes)	0.4 - 0.46	22%[*3]

[*1] The values of *n* and *a* are the statistical coefficients representing V-t and V-N characteristics based on two parameter Weibull distribution given in the following equations:

$P(V,t) = 1-\exp[-(V/V_s)^m(t/t_s)^a]$ or $P(V,N) = 1-\exp[-(V/V_s)^m(N/N_s)^a]$, $m = n \times a$.

Here, $P(V,t)$ and $P(V,N)$ are the cumulative breakdown probability dependent on breakdown voltages V and time to breakdown t or number of voltage application N. The values of m and a are the shape parameters of V and t or N, respectively. The value of n gives the gradient $-1/n$ of V-t and V-N characteristics.

[*2] Puncture field E_{50y} after 50 years operation: $E_{50y} = E_{1m}t^{-1/n}$, here E_{1m} =30kVrms/mm (puncture field at 1 minute), t=50 years = 60x24x365x50 minutes. Considering other reduction of performance such as high temperature (10%), V-N characteristics (LI: 10%, SI: 10%), cumulative puncture field E_{c50y} after 50 years operation is estimated as E_{c50y}=8.1x0.9x0.9x0.9=5.9 kVrms/mm (for n=13) and E_{c50y}=9.6x0.9x0.9x0.9=7.0 kVrms/mm (for n=15). Therefore, E_{c50y}=5.9 - 7.0 > 5 kVrms/mm (maximum working stress).

[*3] V-N characteristics: Reduction rate = $[1-(N/N_0)^{-1/n}]$ x 100 (%), here N=50 at LI, N=100 at SI, N_0 = 1. V-t characteristics: Reduction rate = $[1-(t/t_0)^{-1/n}]$ x 100 (%), here t=50 years = 60x24x365x50 minutes, t_0 = 1 minute.

[*4] a=0.4 - 0.53 under service condition between 2.5 and 5.0 kVrms/mm, a=0.9 under high stress between 15 and 30 kVrms/mm.

[*5] Median of *n*-value. The variation of *n*-value is 10 to 16, 10 to 20 and 74 to 82, respectively.

Regarding the performance of interface between insulator surface and SF_6 gas, the reduction rate during 50 years is negligibly small, since the value is at most 6% for both lightning impulse (LI) and switching impulse (SI) voltage application.

As to the long-term performance of SF_6 gas under clean and particle contamination, the reduction rate of 20% and 22% is not critical again, since in the case of AC stress the reduction could be covered by the design margin *s* generally defined as the following Equation:

s = (minimum breakdown electric field of the system) / (design electric field) (A).

It is concluded that a GIS insulation system of a proper design has a service life of 50 years and in the recent reports no significant ageing is recognized in the actual GIS after long-term operations. However, some other aspects such as metallic particles generation from the contacts, mechanical/thermal performance and gas seal performance should also be considered in a practical GIS.

Influence of Prestress Voltage on Insulation Withstand of GIS

In the chapter 5, the influence of AC and DC prestress on insulation performance of GIS applying IEC 62271-203 is discussed, using the experimental results on insulation characteristics under impulse voltages superimposed to AC or DC.

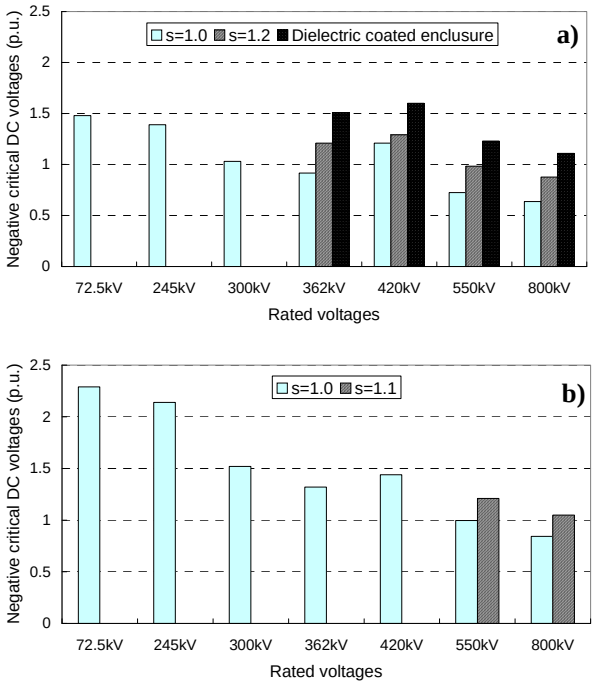

Fig. 3:Negative critical DC trapped charges that lower the dielectric strength of GIS

a) With small particles contamination under industrial clean conditions

b) With charge accumulation on spacer surface

Reduction of LI breakdown voltage is not observed when the superimposed AC component is within 70% of AC breakdown voltage (about 60% of LI breakdown voltage) for the three kinds of samples of sparkover, surface flashover and puncture. Therefore, there is no need to consider the influence of AC prestress on a GIS insulation performance under good quality control conditions up to the voltage class of 800kV and also UHV.

The influence of DC prestress on a GIS insulation performance is summarized in Figs. 3 (a) and (b), which shows the negative critical DC trapped charges U_{dc} that could lower the dielectric strength of a GIS. Here, the parameter *s* in the figures shows the design margin defined in the equation (A). The value of 1 p.u. corresponds to the crest value of the rated voltage. The figure suggests the following three points.

The effect of small particles contamination under industrial clean conditions is greater than that of charge accumulation on spacer surface in terms of the influence of DC prestress on a GIS

performance. The influence of DC prestress with charge accumulation on spacer surface could be neglected if an appropriate insulation design margin *s* is taken for a GIS. On the other hand the influence of DC prestress with small particles contamination under industrial clean conditions could be prevented by applying a thin dielectric coating such as epoxy resin and phthalic acid ester resin on the inner surface of GIS enclosure.

Test Conversion Factors in SF_6 and N_2/SF_6 Gas Mixtures

The test conversion factors in SF_6 and in N_2/SF_6 gas mixtures are studied in the chapter 6. Reviewing the most critical stress for the equipment when applying IEC 62271-203, the essential tests among lightning impulse, switching impulse and AC voltage tests are discussed.

Figures 4 (a) and (b) show the comparison between the rated withstand voltages and the voltages calculated by the test conversion factors under quasi-uniform field in SF_6 and in N_2/SF_6 gas mixtures, respectively. The values of lightning impulse withstand voltage (LIWV), switching impulse withstand voltage (SIWV) and AC withstand voltage (ACWV) are referred to those at the rated voltage of 550kV of IEC 62271-203.

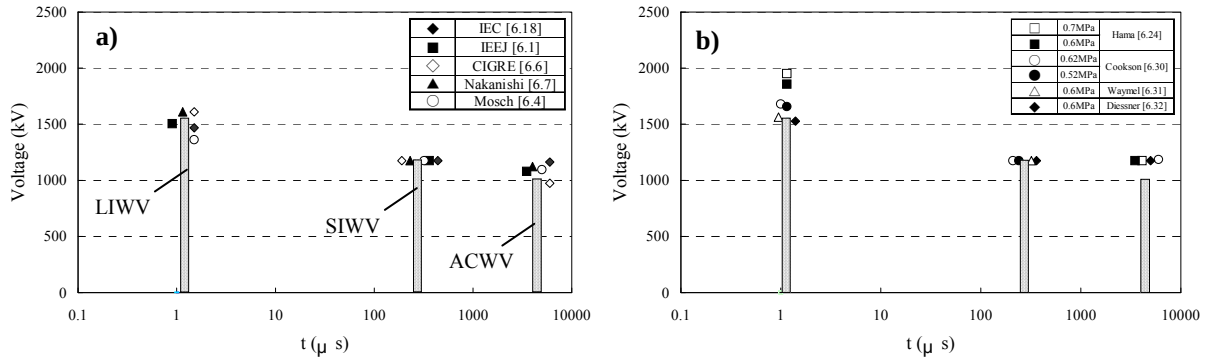

Fig .4:Comparison between the rated withstand voltage (LIWV, SIWV and ACWV at 550kV of IEC 62271-203) and the voltages calculated by the conversion factors under quasi-uniform field in SF_6 and in N_2/SF_6 gas mixtures. The number in the square brackets shows the reference in the brochure.

a) in SF_6 b) in SF6/N2 gas mixtures

Without the defects such as particle contamination and local field concentration at triple junction, LIWV is basically the most critical to the equipment applying SF_6. On the other hand, with the defects in SF_6, LI- and AC-voltage tests are essential to find out the defects in the equipment, while SI-voltage test could be eliminated due to corona stabilization effects.

However, for the equipment applying N_2/SF_6 gas mixtures and without the defects, SIWV is the most critical stress in the Range II (300kV or higher) of the IEC, while LIWV is basically the most critical in the Range I (245kV or lower).

Site Testing

In the chapter 7, the difference of a GIS site testing between IEC 62271-203 and other standards such as IEEE Std C37.122-1993 and JEC-2350-2005 (Standard of the Japanese electrotechnical committee: Gas insulated switchgear) is described in terms of purpose, test procedure and testing philosophy.

Regarding the purpose of the site testing, there is not an essential difference between them.

However, the test procedure and test voltage are different between IEC 62271-203/IEEE Std C37.122-1993 and JEC-2350-2005.

Conclusions and Further Work

Finally, in the chapter 8, the essential remarks of each chapter are briefly summarized. The studies on a GIS regarding insulation co-ordination related to internal insulation are useful to make up the lack of information concerning "dielectric withstand characteristics of electrical insulation". The results would contribute to the further compactness of a GIS with high reliability and to the reduction of SF_6 emission into the atmosphere.

As the next step, this work will be extended to internal insulation of oil-paper insulated systems.

KEYWORDS: Insulation co-ordination, Internal insulation, Dielectric withstand characteristics, Gas insulated switchgear, SF_6, N_2/SF_6 gas mixtures, Safety factor, Field overvoltage, In-service ageing, Prestress voltage, Test conversion factors, Site testing, V-t characteristics.

2. INTRODUCTION

SF_6 has been widely used as insulating and arc-quenching media for the high-voltage power equipment such as GIS, gas circuit breaker (GCB), gas insulated bus (GIB) and GIL, which contributes to achieve compactness and high reliability of the equipment.

However, in-service ageing of the equipment is now in great concern, since some of the equipment has been operated since the late 1960's and the equipment over 40 years old is increasing from now on as shown in Fig. 2.1 [2.1].

Several technical approaches [2.2] have been carried out to reduce the SF_6 emission into the atmosphere, since SF_6 is identified as one of the potent greenhouse gases. Development of compact gas insulated equipment [2.3] is conducted to enable the reduction of the SF_6 use, reviewing SF_6 insulation properties. SF_6 substitutes such as N_2/SF_6 gas mixtures have been studied to reduce the consumption and emission of SF_6 [2.4] - [2.6]. The GIL applying N_2/SF_6 gas mixtures, of which view is shown in Fig. 2.2, has been in a commercial operation in Geneva since 2001[2.6].

On the other hand, the insulation techniques have been progressed steadily in the field of equipment reliability and insulation co-ordination, for example, in the influence of unknown factors such as AC or DC prestress to insulation withstand of power equipment [2.7]- [2.9] and also in the insulation characteristics of the equipment for non-standard lightning impulse voltages [2.10].

Considering the above worldwide issues and referring to the latest research on the insulation properties and techniques, insulation co-ordination related to internal insulation of gas insulated equipment in SF_6 and also some aspects of N_2/SF_6 gas mixtures under AC condition has been reviewed and discussed. As the equipment of the gas insulated system, GIS is dealt with in this brochure.

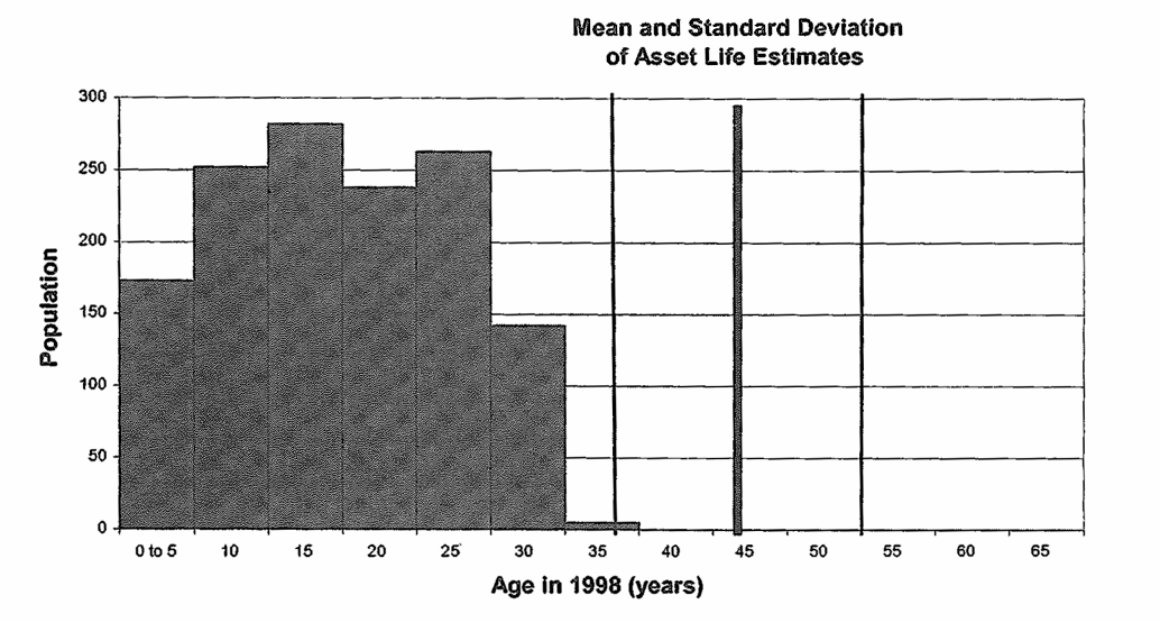

Fig.2.1: Age distribution of GIS as the example in Germany. The thick and the thin vertical lines show the medium value and the standard deviation for the estimated lifetime of GIS, respectively.

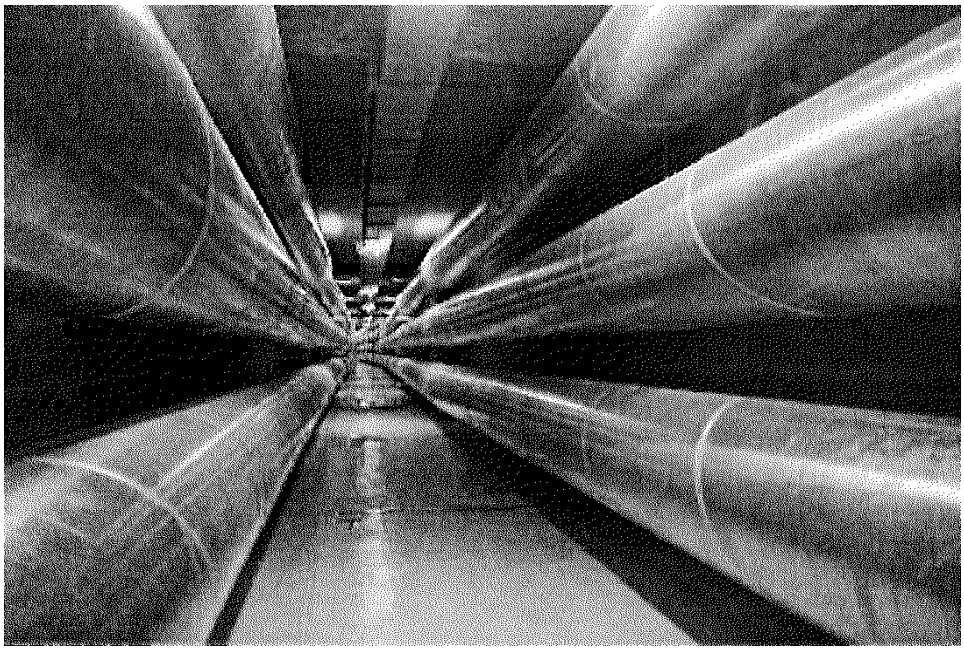

Fig.2.2: View of 245kV PALEXPO GIL installed in tunnel in Geneva. The insulating gas is 20%SF_6/80%N_2 at the pressure 0.7MPa.

REFERENCES of Chapter 1 - 2

[1.1] IEC 62271-203, "High- voltage switchgear and controlgear – Part 203: Gas-insulated metal-enclosed switchgear for rated voltages above 52kV".
[1.2] IEEE Std C37.122-1993, "IEEE standard for gas-insulated substations".
[1.3] JEC-2350-2005, "Standard of the Japanese electrotechnical committee: Gas insulated switchgear" (in Japanese).

[2.1] W.Degen, "Installation, Maintenance, and End of Life of a Gas-insulated Substation", *Gaseous Dielectrics X*, pp.363-373 (2004).
[2.2] L.G.Christophorou et al., "Gases for Electrical Insulation and Arc Interruption Possible Present and Future Alternatives to Pure SF_6", *NIST Technical Note* 1425 (1997).
[2.3] T.Kawamura, T.Yamagiwa, H.Hama and M.Meguro, "SF_6 Gas Handling in Japan Focused on Emission Reduction from Gas Insulated Electrical Equipment", *Gaseous Dielectrics IX*, pp.575-584 (2001).
[2.4] CIGRE WG 23.01 TF 02, "Guide for SF_6 Gas Mixtures", *Technical Brochure* No.163 (2000).
[2.5] CIGRE TF D1.03.10, "N_2/SF_6 Gas Mixtures for Gas Insulated Systems", *2004 CIGRE general session report*, D1-201.
[2.6] CIGRE WG 23/21/33-15 TF 2, "Gas Insulated Transmission Lines (GIL), Appendix B: GIL Insulation Coordination, On-site Test, Long Duration Test, Monitoring and Grounding", *Technical Brochure* No.218 (2002).
[2.7] G.Luxa, E.Kynast, W.Boeck, H.Hiesinger, A.Pigini, A.Bargigia, S.Schlicht, N.Wiegart, L.Ullrich, "Recent research activity on the dielectric performance of SF_6 with special reference to very fast transients", *1988 CIGRE general session report*, 15-06.
[2.8] Investigation R&D Committee Chaired by Prof. T. Kawamura, "Properties on Electrical Insulation Related to Testing Voltages and Power Equipment", *Technical Reports by IEE Japan*, No.518 (1994) (in Japanese).
[2.9] S.Okabe, T.Okada, S.Yuasa, T.Utsumi, F.Endo and K.Saitoh, "Effect of pre-stress on dielectric characteristics of an insulator in SF_6 gas", *12th ISH*, 4-30, pp.351-354 (2001).
[2.10] S.Okabe, S.Yuasa, M.Koto and E.Zaima, "Evaluation of lightning surge waveform for LIWV reduction of substation equipment", *13th ISH*, P.05.66 (2003).

3. CONVERSION IN SHAPE OF FIELD OVERVOLTAGE TO STANDARD IMPULSE WAVEFORM IN DETERMINING REPRESENTATIVE OVERVOLTAGES FOR GIS

3.1 Introduction

IEC 60071-1 "Insulation co-ordination Part1" [3.1][3.2] defines *representative overvoltages* U_{rp} *as standard shape overvoltage assumed to produce the same dielectric effect on the insulation* (3.19), and there is a note that *overvoltage shapes may have to be considered* (4.2)[3.1], (5.2)[3.2]. In the step of determining representative voltages based on system analysis results in the "flow chart for the determination of rated or standard insulation level" in IEC 60071-1, it is probable that real surge waveforms have different effects on equipment dielectrics from the standard impulse waveform (1.2/50μs).

As for this subject, it is described in IEC 60071-2 [3.3] "Insulation co-ordination Part2"(2.3.4.5) that *"As a general recommendation, the dependence on the overvoltage shape should also be considered in the determination of the representative amplitudes, in particular, for external insulation and oil-paper insulation"*. Further, Annex H illustrates with an example and states that *"if the assumed actual overvoltage has a shape different from test shape, the representative overvoltage may have to be modified accordingly so that tests truly verify the insulation strength"*.

Recent researches analyzed field surges [3.4], clarified insulating characteristics [3.5]-[3.7] for field real surges in comparison with for the standard impulse waveform in the lightning surge time region, and proposed the waveform evaluation method for a GIS as well as a transformer [3.8]. According to them, the decay of the field overvoltage is generally large, making the insulation requirements not as severe as those of the standard lightning impulse waveform. Consequently, it could be possible in some cases to use lower withstand test voltages [3.9].

3.2 Non-standard lightning impulse waveform [3.4]

From the results of lightning surge and disconnector switching surge analyses, and so on, and measurements of ultra high voltage (UHV: 1000kV) and 500kV substations, representative non-standard impulse waveforms were extracted. The rise time of the wave crest is, as a whole, 0.1 - 1.0μs.

(a) Waveform A: Pulse-shaped waveform
(b) Waveform B: The wave crest has a steep pulse-shaped part, and the wave tail is flat (Ratio between peak and flat part: 0.7 - 0.9)
(c) Waveform C: A damped oscillatory waveform whose first wave is a maximum
(Frequency: 0.5 - 5.0MHz)
(d) Waveform D: A damped oscillatory waveform whose second wave is the crest value
(Frequency: 0.5 - 5.0MHz)
(e) Waveform E: Double-frequency oscillatory waveform
(Lower frequency: Approx. 1.0MHz, Upper frequency: Approx. 5.0MHz)

Waveform B appears depending upon the positional relationship with protected points when the lightning arrester operates, and waveforms C and D occur as a result of a negative and/or positive reflection inside and/or outside the substation. Waveform A corresponds to the one when the decay of the DC component and/or oscillatory component of waveforms B, C and D is large. Also, waveform E occurs during a re-arcing surge inside the substation, such as a disconnector

surge, when there are two oscillation routes. Thus, in general, it can be said that these waveforms are representative waveforms in view of the mechanism under which they occur.

Figure 3.1 shows examples of waveforms A, B, C, D and E.

3.3 Insulation characteristics of GIS element for non-standard lightning impulses

3.3.1 Experimental results [3.5]-[3.7]

The SF_6 gas gap was used as the insulation element of a GIS. The electrodes used in the test generated quasi-equal electric fields whose utilization factors (η) were 0.60 and 0.45, and the gas pressure was an absolute pressure of 0.50MPa.

With changing waveform parameters such as the frequency, the decay time and so on, more than 100 cases were examined. Moreover, effects of other factors were investigated like the scale, the gas pressure, the voltage polarity, superposition with DC, electrode material, roughness and so on.

As an example of the results, Fig. 3.2 shows the characteristics with respect to waveforms A and E. In the case of waveform A, the minimum value of the insulation breakdown V-t characteristics is 264kV, which is 1.20 times that of the case of a standard lightning impulse. In other words, this means that it is possible to convert waveform A into a standard lightning impulse waveform with dividing the crest value by 1.20. This interpretation applies to the other experimental results as well.

3.3.2 Duration time evaluation

The insulation characteristics are arranged according to the waveform duration time of the 80% level of the peak value. Figure 3.3 explains how to calculate the duration time t_d: the sum of t_{d1}+t_{d2}. All of the characteristics for waveform A, the pulse parts of waveform B, and waveforms C and D, and the double-frequency oscillatory waveform E, lie roughly along one characteristic line as shown in Figure 3.4 [3.8].

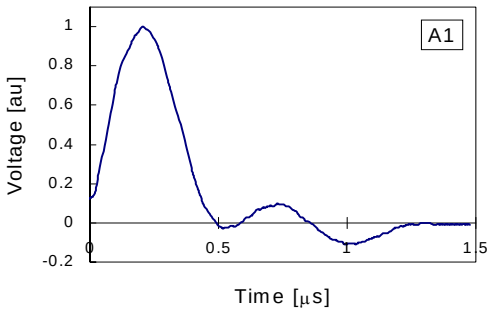

(a) Waveform A

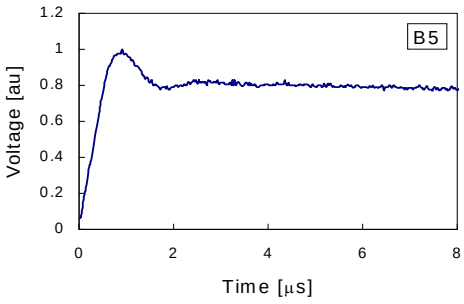

(b) Waveform B

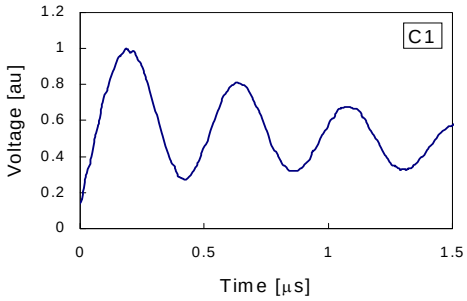

(c) Waveform C

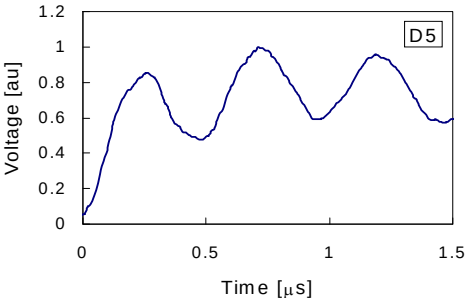

(d) Waveform D

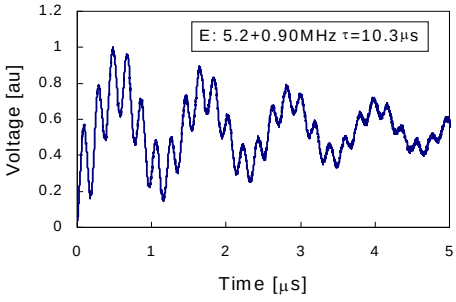

(e) Waveform E

Fig. 3.1: Examples of non-standard impulse waveforms.

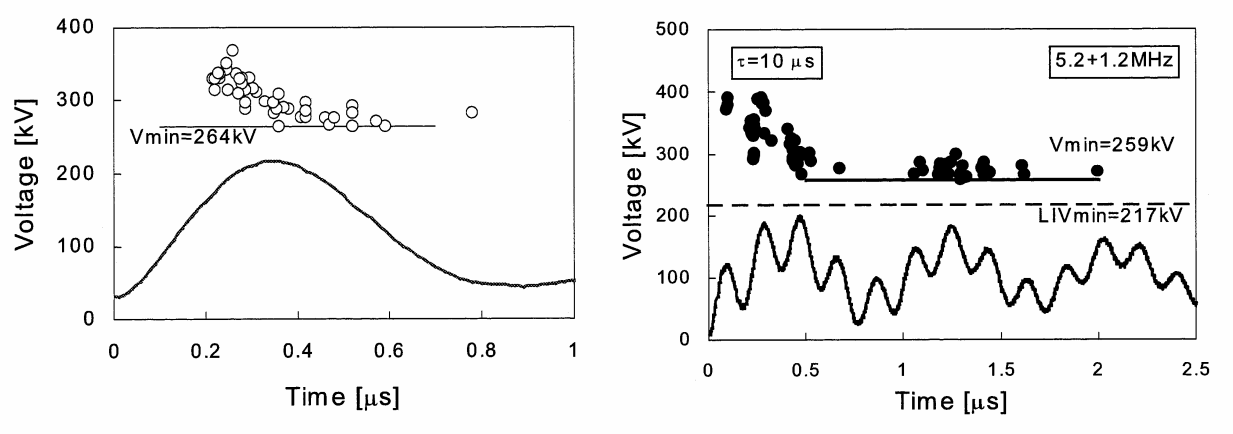

(a) Waveform A (b) Waveform E

Fig. 3.2: Examples of insulation characteristics with respect to the non-standard waveform of the gap.

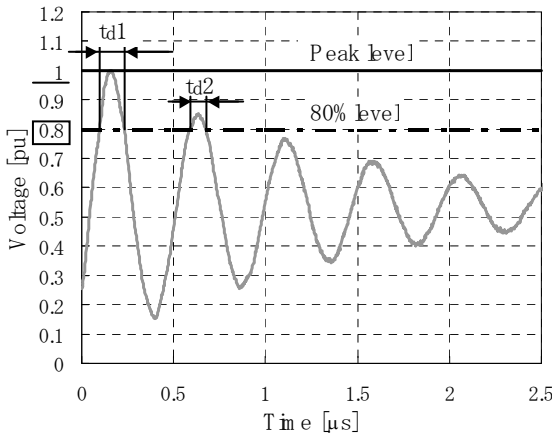

Fig. 3.3: Calculation of duration time t_d

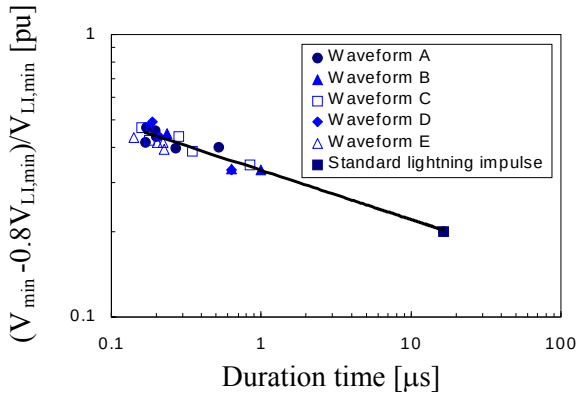

Fig. 3.4: $(V_{min} - 0.8V_{LI,min})/V_{LI,min}$ characteristics as a function of duration time over 80% voltage level. (V_{min}: minimum breakdown voltage at waveform A, B, C and D, $V_{LI,min}$: minimum breakdown voltage at standard lightning impulse waveform)

3.4 Evaluation method for GIS

The waveform was resolved into elements including each oscillatory wave, the flat part, and so on. It was then evaluated based on the characteristics of section 3.3, and finally the crest value that was converted into an equivalent standard lightning impulse waveform as the overall waveform was calculated.

Figure 3.5 shows the waveform evaluation flow for a GIS [3.8].

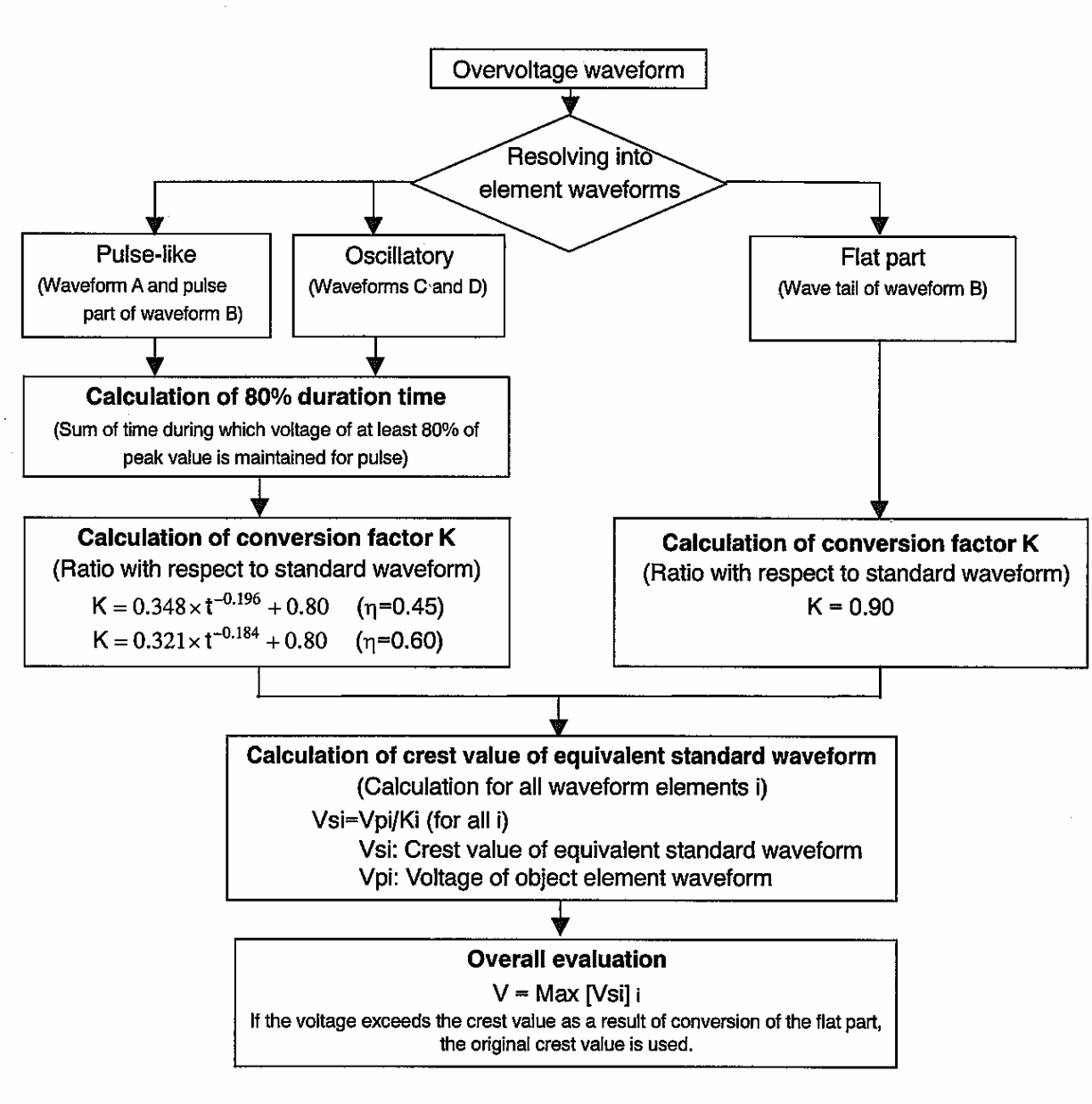

Fig. 3.5: Waveform evaluation flow for a GIS.

3.5 Application to a lightning surge at GIS in the UHV system

Figure 3.6 shows an example of the lightning surge analysis waveform applied to a GIS in a 1000kV UHV substation [3.10]. This waveform has the shape of waveform B whose wave tail maintains a level of about 60% with respect to the peak after the steep oscillatory surge has decayed.

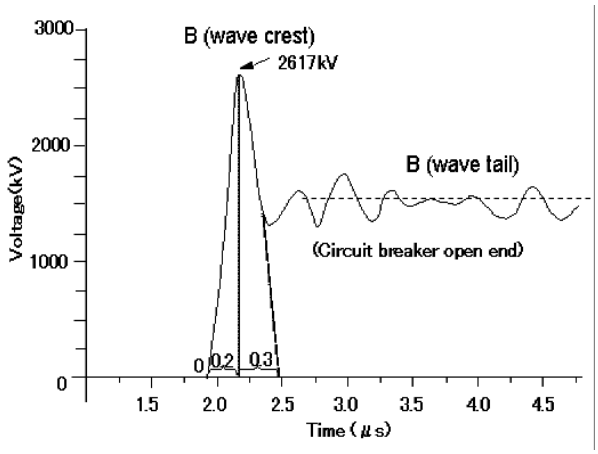

Fig. 3.6: Application to a GIS.

Table 3.1 shows the results of analyzing and evaluating this waveform using the flow of Fig. 3.5. In the case of this waveform and $\eta = 0.60$, the wave crest is severer than the wave tail, and the overall waveform is equivalent to a 2094kV standard lightning impulse waveform. In other words, the crest value was converted into a value that was about 25% lower [3.8].

Table 3.1: Evaluation of the lightning surge waveform in the GIS of a UHV system.

Waveform element	80% duration time	Peak voltage	Conversion ratio	Equivalent standard LI Vol.
B (wave crest)	0.16μs	2617kV	1.25 (1.30)	**2094kV** [η=0.60] **(2016kV** [η=0.45])
B (wave tail)	-	1517kV	0.90	1686kV

To think of the principle of construction, this method can be generally applicable to lower voltage classes as well as 500kV and UHV ones. In fact, it has been put into practical use in 66kV to UHV voltage classes at some electric power company.

3.6 Conclusion

Field real surges of non-standard lightning impulse waveform are analyzed and the SF_6 insulation characteristics for these actual surges in SF_6 are clarified to convert the surge waveform into the standard lightning impulse waveform. It was found that the insulation requirements could not be as severe as those of the standard lightning impulse waveform, since the decay of the field overvoltage is generally large. Consequently, it could be possible in some cases to use lower withstand test voltages for GIS using SF_6. The proposed conversion method for non-standard lightning impulse waveform is applicable up to 1000kV UHV system.

REFERENCES of Chapter 3

[3.1] IEC 60071-1, "Insulation co-ordination Part 1: Definitions, principles and rules" (1993-12).

[3.2] IEC 60071-1, "Insulation co-ordination Part 1: Definitions, principles and rules" (CDV: 2004-6).

[3.3] IEC 60071-2, "Insulation co-ordination Part 2: Application guide" (1996-12).

[3.4] S.Okabe, M.Koto, S.Yuasa, T.Suzuki, T.Rokunohe, T.Yamagiwa, "Analysis of Non-Standard Lightning Impulse Voltage for Actual Substation and Generation Circuit", *T. IEE Japan*, Vol. 123-B, No.2 (2003) (in Japanese).

[3.5] S.Okabe, M.Koto, K.Kato, S.Yuasa and E.Zaima, "Insulation Characteristics under Single- and Double-frequency Oscillatory Waveforms and Evaluation of Disconnector Switching Surges", *11-ISH*, Vol.3, 3.269.P3 (1999).

[3.6] S.Okabe, M.Koto, K.Kawashima, K.Kato and S.Yuasa, "Insulation Characteristics of GIS under Non-Standard Lightning Impulse Oscillations - Insulation Characteristics under high frequency Oscillations", *T. IEE Japan*, Vol. 121-B, No.11 (2001) (in Japanese).

[3.7] S.Yuasa and S.Okabe, "Breakdown Characteristics of SF_6 Gas under Non-Standard Lightning Impulse Voltage - Insulation Characteristics for Gas Gap and Spacer Surface under Single Pulse Waveforms", *T. IEE Japan*, Vol. 123-B, No.10 (2003) (in Japanese).

[3.8] S.Okabe, S.Yuasa, M.Koto and E.Zaima, "Evaluation of lightning surge waveform for LIWV reduction of substation equipment", *13-ISH*, P.05.66 (2003).

[3.9] W.Schmidt, R.Malewski, Special Report for Group33 (Power System Insulation Coordination), CIGRE Session-2000, No.33-00 (2000).

[3.10] T.Watanabe, Y.Yamagata and E.Zaima, "Insulation Co-ordination for UHV System", CIGRE, 33-101 (1998).

4. IN-SERVICE AGEING IN SAFETY FACTOR

4.1 Long-term performance of SF_6 insulation system in GIS

The following long-term performance should be considered to study in-service ageing of SF_6 insulation system in GIS.

(1) Voltage-time (V-t) characteristics of SF_6 under clean and metallic particle contamination,
(2) Voltage-number of times of voltage application (V-N) characteristics of the interface between insulator surface and SF_6,
(3) V-t and V-N characteristics of the internal bulk of solid insulators, e.g. the interface between embedded electrode and insulating material,
(4) Performance of combined and SF_6 impregnated dielectrics,
(5) Influence of VFT on internal potential connections in GIS equipment, e.g. bushings.

The above items are studied in the following sections from 4.2 to 4.6. The long-term field experience of a GIS and the key components is introduced in the section 4.7. The insulation performance during the 50 years service life of a GIS is evaluated in the section 4.8.

4.2 V-t characteristics of SF_6 under clean and metallic particle contamination

Figure 4.1 shows the V-t characteristics under clean condition and under metallic particle contamination within the quality control level in a factory and on-site [4.1]. The 72kV model bus is used and SF_6 gas pressure is 0.4MPa. In the experiment under metallic particle contamination, five aluminum wires of 0.25mm in diameter and 3mm in length are set in the enclosure and AC voltages are increased until the breakdown occurs.

The V-t characteristics are basically given by the following equation.

$$V = V_0 \, t^{-1/n} \tag{4.1}$$

Here V, t and V_0 are breakdown voltage, time to breakdown and a constant, respectively. The value of n is 82 under clean condition, while the value is 30 during short-term less than 10 minutes and is 69 during long-term more than 10 minutes under particle contamination.

Another experiment that determines the long term V-t characteristic of a coaxial electrode system in SF_6 is reported as shown in Fig. 4.2 [4.2]. Two cast epoxy spacers are within the test arrangement to position the center conductor. The breakdown voltage shows a slight time dependence under DC and 1 Hz AC voltage in the time range up to a few hundred hours. The best fit to the experimental data with Equation (4.1) is obtained for n=74. The observed time dependence is mainly attributed to the statistical nature of the gaseous breakdown, since the breakdown in compressed gas is always under the influence of micro-protrusions or particles.

The experimental data are also analyzed based on the two-parameter Weibull distribution given in the following equations which define the cumulative breakdown probability $P(V,t)$ dependent on the breakdown voltages V and the time to breakdown t.

$$P(V,t) = 1 - \exp[\, -(V/V_s)^m \, (t/t_s)^a \,] \tag{4.2}$$

$$m = n \times a \tag{4.3}$$

Here, V_s and t_s are the scale parameters. The values of m and a are the shape parameters. The value of n gives the gradient $-1/n$ of V-t characteristics in Equation (4.1).

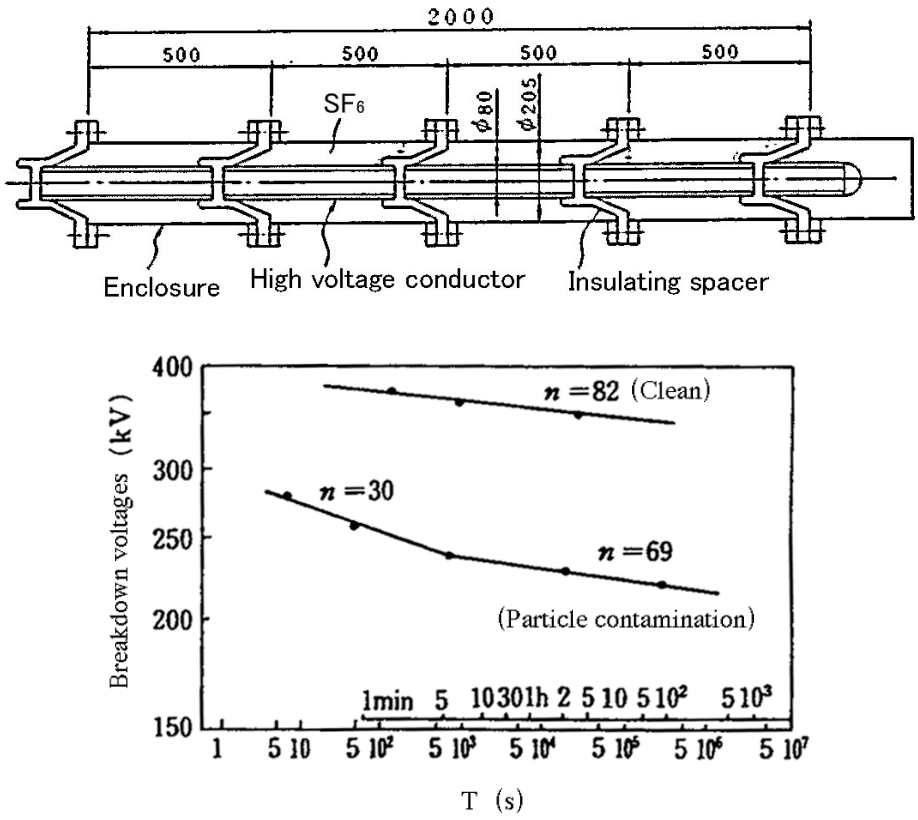

Fig. 4.1: Long-term V-t characteristics of SF_6 gas under clean condition and metallic particle contamination within the quality control level in a factory and on-site.

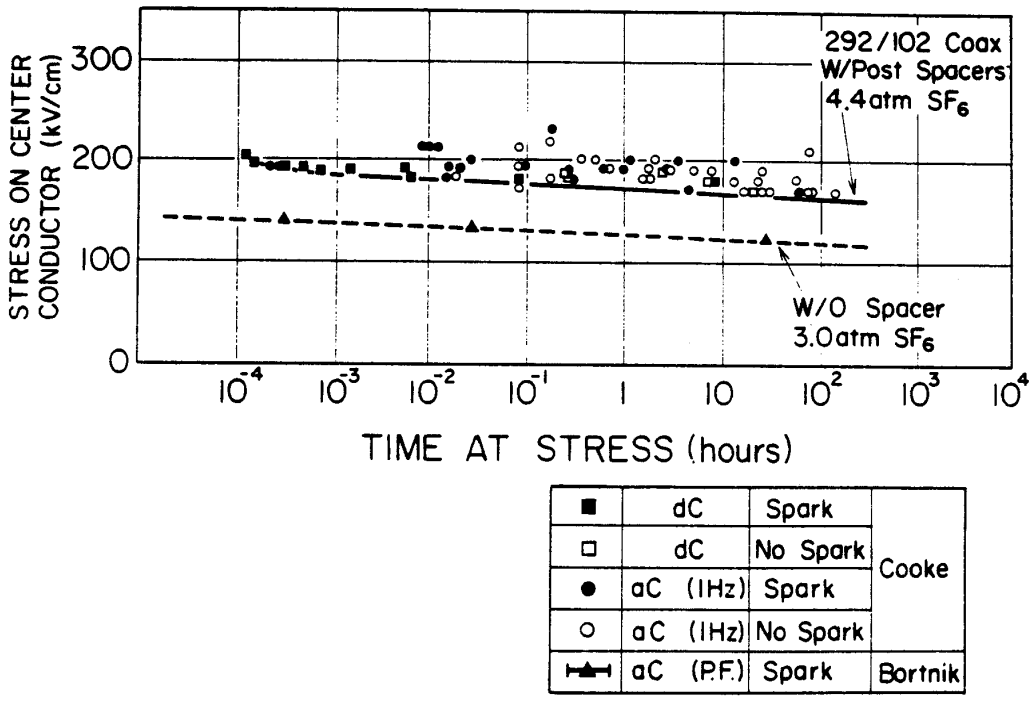

Fig. 4.2: Example of time dependence of breakdown in compressed SF_6 for coaxial cylinder electrodes.

Table 4.1 summarizes the statistical parameters *a*, *n* and *m* of the V-t characteristics calculated from the data in Fig. 4.1 based on Equations (4.2) and (4.3). On the other hand, the shape parameters *m* and *a* obtained from Fig. 4.2 are *m*=20-25 and *a*=0.25-0.5, respectively.

All the values *a* in the Table 4.1 and obtained from Fig. 4.2 are smaller than unity, which shows the breakdown under clean and metallic particle contamination is a teething fault.

Table 4.1: Statistical parameters *a*, *n* and *m* of V-t characteristics shown in Fig.4.1. In the case of "With particle", the upper and the lower values are for shorter and longer than 10 minutes, respectively.

	a					*n*	*m*
	V_1	V_2	V_3	V_4	V_5		
Clean	0.34 (370kV)	0.48 (360kV)	0.32 (350kV)	-	-	82	26 - 39
With particle	0.98 (280kV)	0.9 (260kV)	0.88 (240kV)	-	-	30	26 - 29
	-	-	-	0.46 (230kV)	0.4 (220kV)	69	28 - 32

4.3 V-N characteristics of interface between insulator surface and SF_6

Relation between surface flashover voltages and number of times of voltage application, that is V-N characteristics, is investigated at 0.4MPa under repetitive lightning impulse (LI) and switching impulse (SI) voltages using a model GIS spacer [4.3].

First, initial surface flashover probability $P(V)$ in terms of applied voltages V is investigated from the following equation.

$$P(V) = 1 - \exp[\, -(V/V_s)^m \,] \tag{4.4}$$

Here, V_s and m are the scale parameter and the shape parameter, respectively. The negative surface flashover voltages are lower than the positive ones for both LI and SI voltage application. It is reported that the values of m are 22 and 34 for negative LI and negative SI voltages, respectively.

Secondly, the V-N characteristics of surface flashover at negative LI and negative SI voltages are obtained as shown in Fig. 4.3. The V-N characteristics are given by the following equation.

$$V = V_{50\%} N^{-1/n} \tag{4.5}$$

Here, $V_{50\%}$ and N are 50% surface flashover voltage at N=1, number of times, respectively. The values of n are 124 and 134 for negative LI and negative SI voltages, respectively.

Thirdly, the surface flashover probability $P(N)$ in terms of number of times N at a constant applied voltage is studied by the following equation.

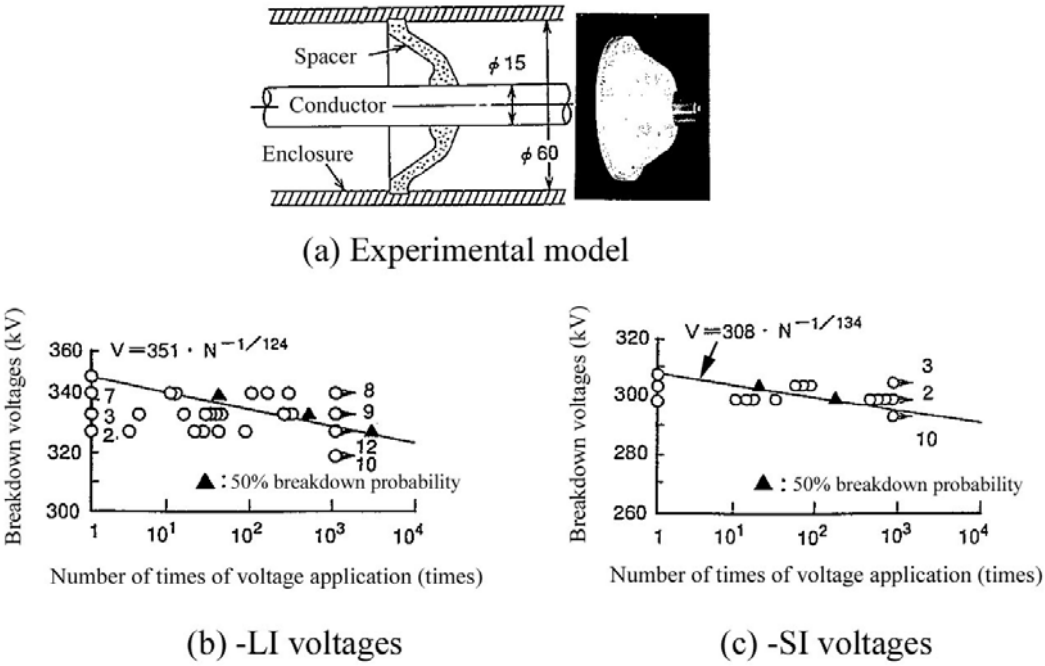

Fig. 4.3: V-N characteristics of surface flashover at -LI and -SI stress.

$$P(N) = 1 - \exp[\, -(N/N_s)^a \,] \tag{4.6}$$

Here, N_s and a are the scale parameter and the shape parameter, respectively. For two or three kinds of applied voltages, the values of a are obtained as 0.2 for negative LI and as between 0.2 and 0.3 for negative SI voltages.

Finally, the experimental data are checked if they are expressed by the similar two-parameter Weibull distribution as Equations (4.2) and (4.3). The cumulative breakdown probability $P(V,N)$ dependent on the surface flashover voltages V and number of times N are given in the following equations.

$$P(V,N) = 1 - \exp[\, -(V/V_s)^m (N/N_s)^a \,] \tag{4.7}$$

$$m = n \times a \tag{4.8}$$

The values of m given in Equation (4.4) are m=22 and m=34 for negative LI and negative SI voltages, respectively, while the values n x a in Equation (4.8) are 24.8 and between 27 and 40 for negative LI and negative SI voltages, respectively. Therefore, m is nearly equal to n x a, which suggests that the V-N characteristics can be analyzed by the two-parameter Weibull distribution given in Equations (4.7) and (4.8).

The statistical coefficients representing V-N characteristics are summarized in Table 4.2. Since the values a in Table 4.2 are a<1, the surface flashover is a teething fault. Considering the value N of LI and SI application during the service life would be at most 50 and 100, respectively [4.4], the reduction of insulation performance is within 3%, since n is large.

Table 4.2: Statistical coefficients representing V-N characteristics of surface flashover at negative LI and negative SI stress.

	$V_{50\%}$ (kV)	n	a	$m = n \times a$
-LI	351	124	0.2	24.8
-SI	308	134	0.2 – 0.3	26.8 – 40.2

4.4 V-t and V-N characteristics of internal bulk of solid insulators

Regarding the performance of internal bulk of solid insulators, the following three kinds of experimental data are available:

(1) Long-term V-t characteristics of solid insulators at AC stress,
(2) Influence of temperature and mechanical stress on the above V-t characteristics,
(3) V-N characteristics of solid insulators at LI and SI stresses.

4.4.1 Long-term V-t characteristics

Figure 4.4 shows the long-term V-t characteristics of solid insulators at room temperature using model solid insulators of eight different configurations made of epoxy [4.1]. The deterioration of insulation performance is basically given by Equation (4.1). The value of n is a specific constant for each insulation material and varies between 10 and 16.

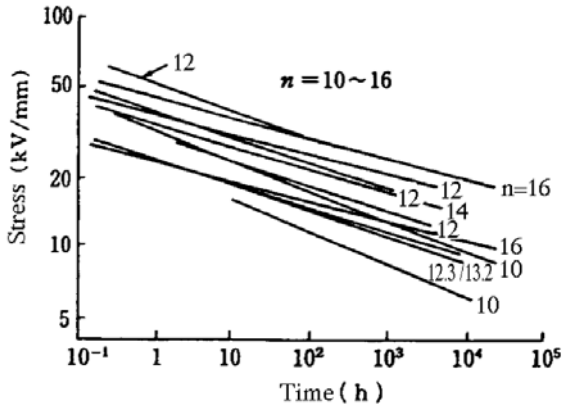

Fig. 4.4: Long-term V-t characteristics of solid insulators in GIS. Model epoxy insulators with alumina or silica filler of eight different configurations such as plane-plane, hemisphere-plane, hemisphere- hemisphere and coaxial configuration are tested. The numbers in the figure are the values of n in Eq.(4.1).

Similar V-t characteristics are reported in the recent CIGRE task force [4.5]. Lifetime data are experimentally gained by several constant field long-term tests with different stresses. For each stress, the experiments are performed using many test components such as real spacers, post insulators or material samples to get the scatter of the time to breakdown. Results of a few publications are complied in a common lifetime curve in Fig. 4.5. It is reported that the resulting value of n ranges from 10 to 20 with the median mainly being applied as n=15.

In Fig. 4.5, the data of full-sized real spacers under ambient temperature and sun exposure from –15 to +40 degrees Centigrade (closed triangles) are included and the details [4.6] are shown in Fig. 4.6. Two solid straight lines of 10% failure probability represent the value of n between 10

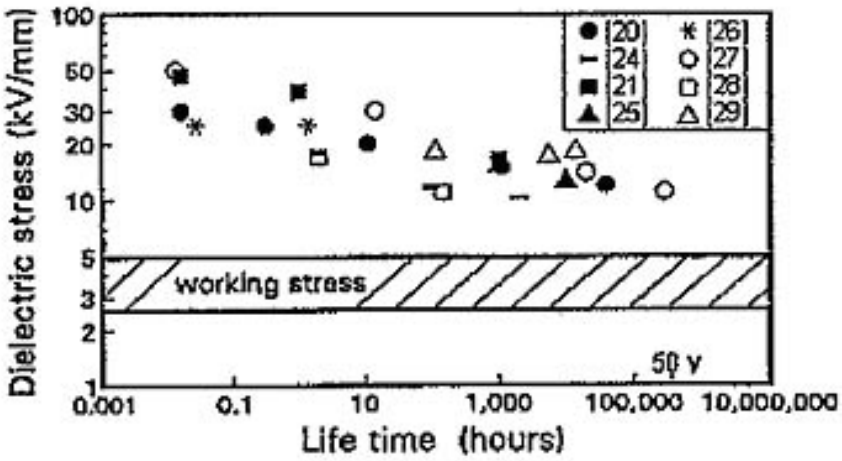

Fig. 4.5: Lifetime curves of epoxy resin gained by compiled published results. The related information is referred to Fig.4.13.

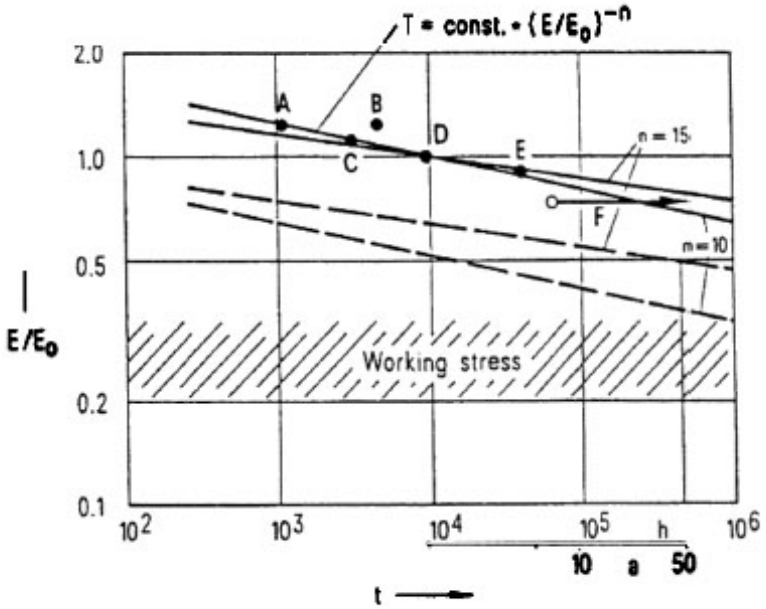

Fig. 4.6: Lifetime curves of post insulators. E/E_0: Maximum electric stress in p.u., E_0: Maximum stress in batch D. Solid line: 10% failure probability determined from batches A to F. Dashed line: 0.01% failure probability calculated by mathematical models.

to 15. And also, Figures 4.7 and 4.8 show the similar lifetime curves under ambient temperature and sun exposure from –20 up to more than +50 degrees Centigrade of real size post and disk insulators (mineral filled epoxy) and of real size operating rods and support insulators (fiber-reinforced epoxy tubes) with and without mechanical prestress, respectively [4.7]. The value of n is n=12 for both material types. The reference [4.7] also reports that the acceptable max. service stress for the mineral filled epoxy is approximately factor 2.5 higher than that for the fiber-reinforced epoxy.

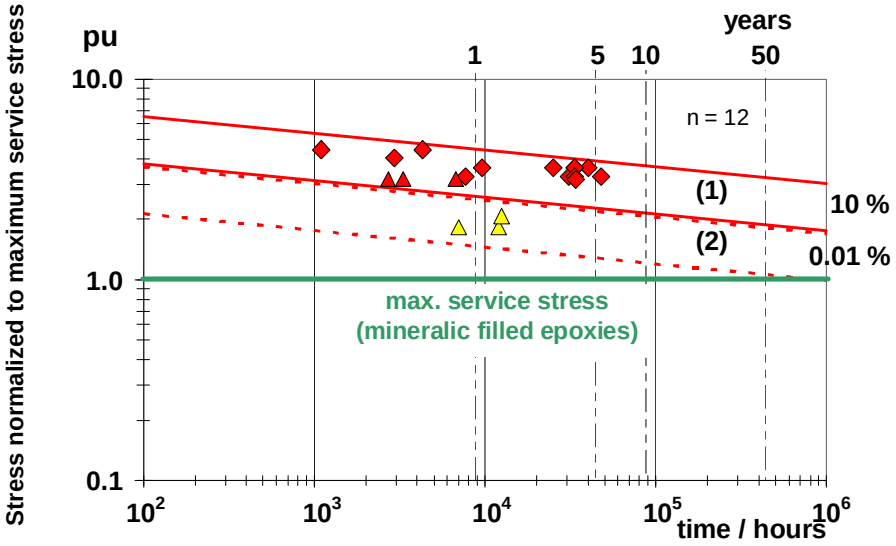

Fig. 4.7: Lifetime curves of post and disk insulators (mineral filled epoxy) normalized to maximum service stress.

(1): Range for 10 % failure probability (post insulators)
(2): Range for 0.01 % failure probability (post insulators)

Closed marks (red): small + medium volume
Open marks (yellow): large volume (lower service stress)

Rhombuses: post insulators Triangles: disk insulators

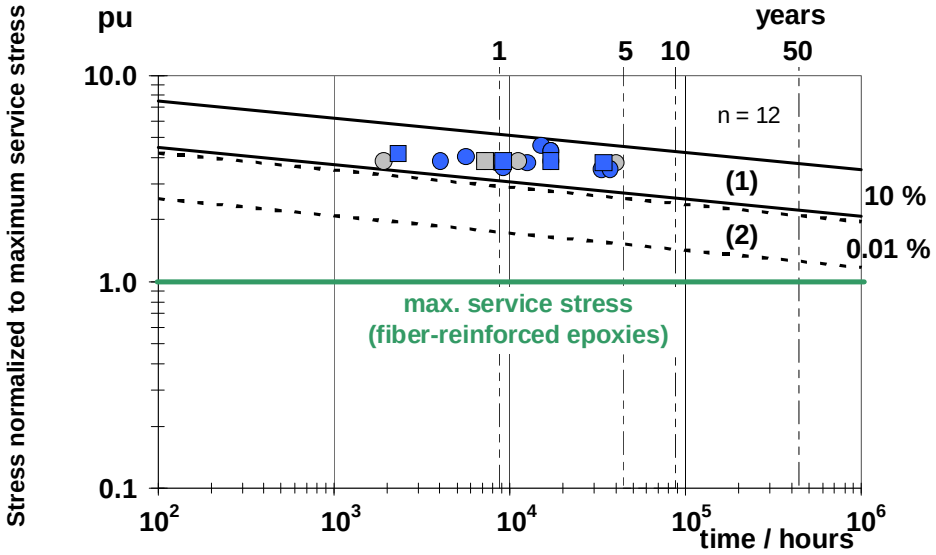

Fig. 4.8: Lifetime curves of operating rods and support insulators (fiber-reinforced epoxy tubes) normalized to maximum service stress.
(1): Range for 10 % failure probability (2): Range for 0.01 % failure probability

Closed marks (blue): without mechanical prestress
Open marks (grey): with in-service-comparable mechanical prestress of 1000 to 10000 CO (close-open) cycles in a circuit-breaker

Dots: operating rod samples Squares: support insulator samples

In the insulation design of a GIS, the puncture field after 30 - 50 years is basically considered and sufficient design margin from 2 to 3 is given. The puncture field E at room temperature is reported as the following equations [4.8][4.9].

$$E = E_{1m}\, t^{-1/n} \tag{4.9}$$

Here, E_{1m} is the puncture field at one minute in kVrms/mm. The values E_{1m} and n are given in the literature as follows.

$E_{1m} = 30$ and $n = 16$ (for alumina filled epoxy [4.8]) (4.10)
$E_{1m} = 30$ and $n = 12.3$ (for alumina filled epoxy [4.9]) (4.11)
$E_{1m} = 32$ and $n = 13.2$ (for silica filled epoxy [4.9]) (4.12)

Here, the test specimen of epoxy is referred to Figs. 4.11(a) and 4.10(a) for Equations (4.10) and (4.11) - (4.12), respectively. Note that the effective electrode area of the embedded electrode, which affects the puncture field, is large enough for a practical application of insulating spacers.

4.4.2 Influence of temperature and mechanical stress on the V-t characteristics

The influence of high temperature of 90- 105 degrees Centigrade to solid insulators on the V-t characteristics are reported in the references [4.8] and [4.9] and shown in Figs.4.9 and 4.10.

The figures suggest that the reduction of puncture field by high temperature would be below 10%. The values of n in Equation (4.1) and (4.9) are 16 and 15.4 and not so influenced by the high temperature compared with 16 and 12.3 - 13.2 at room temperature, respectively. In addition, considering the n value at ambient temperature and sun exposure from –20 up to more than +50 degrees Centigrade is n =12 [4.7], the temperature change from –20 up to +105 degrees Centigrade in an actual field operation would not affect the characteristics of the n value of solid insulators.

On the other hand, Figure 4.8 shows that there is no difference in the lifetime curves of operating rods and support insulators between with and without mechanical prestress up to 10000 CO cycles in a circuit breaker of a proper design. Therefore, the literature [4.7] concludes that mechanical prestress does not influence the long-term electrical performance of the insulators in an unacceptable way during the whole GIS lifetime.

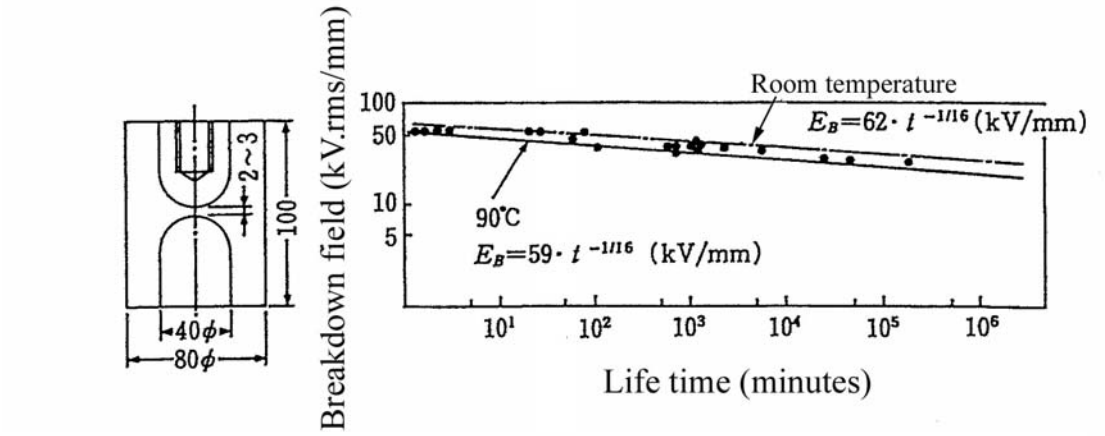

(a) Experimental model (b) Long-term insulation performance

Fig. 4.9: Influence of high temperature on long-term insulation performance of solid insulators in GIS. The temperature conditions are room temperature and 90 degrees Centigrade.

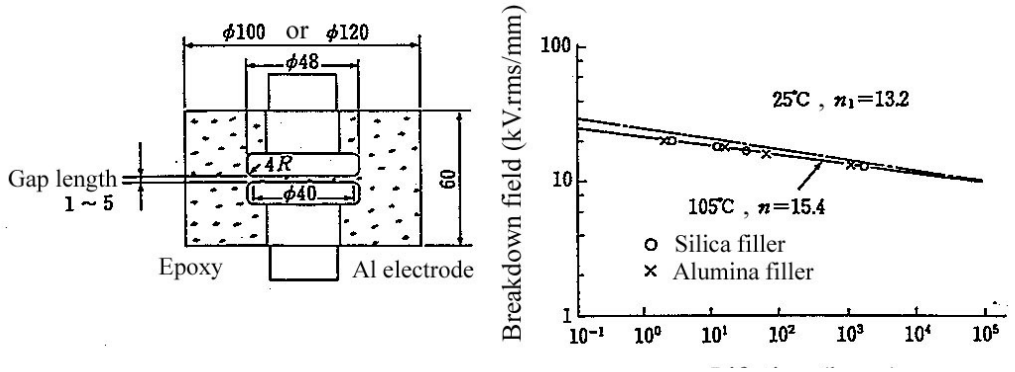

(a) Experimental model (b) Long-term insulation performance of solid insulator

Fig. 4.10: Influence of high temperature on long-term insulation performance of solid insulators in GIS. The temperature conditions are 25 and 105 degrees Centigrade.

4.4.3 V-N characteristics of internal bulk at LI and SI

In the literature [4.4], V-N characteristics of internal bulk of spacer model at LI and SI stresses are investigated in the similar process of the V-N characteristics of interface between insulator surface and SF_6 [4.3] introduced in the section 4.3.

The initial surface flashover probability $P(V)$ in terms of applied voltages V is investigated based on Equation (4.4). The shape parameter m in the equation is reported to be m=13.2 for LI and m=9.1 for SI voltages.

The V-N characteristics at LI and SI voltages are obtained as shown in Fig. 4.11. The value of n in Equation (4.5) is n=35.7 for LI and n=45.5 for SI voltages.

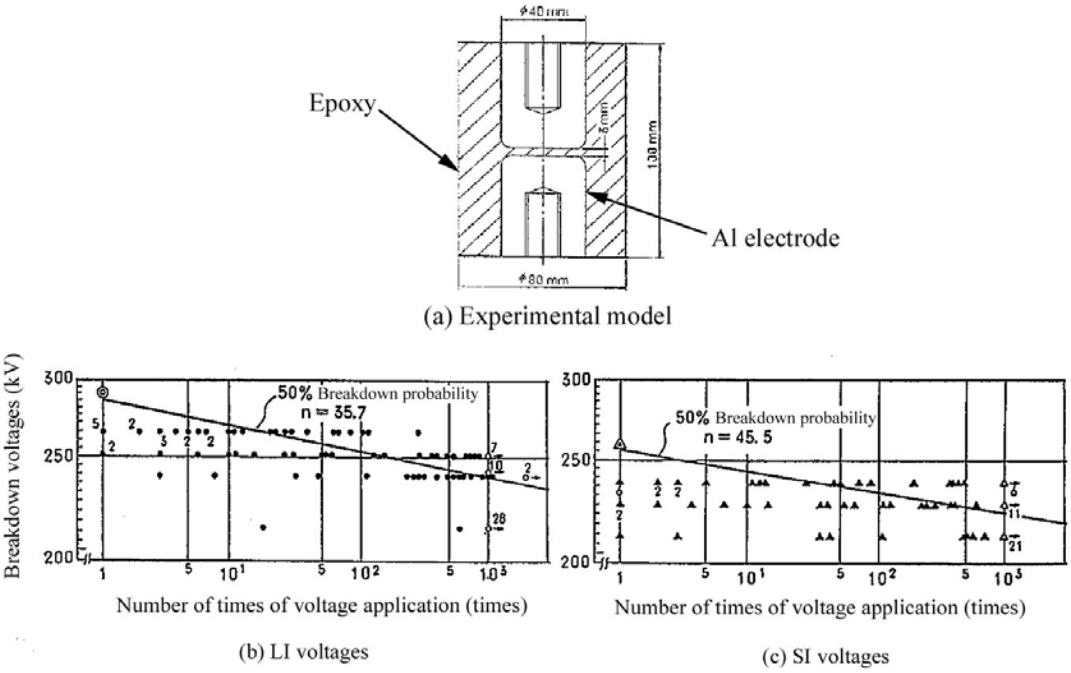

Fig. 4.11: V-N characteristics of internal bulk of spacer model at LI and SI stress.

The puncture probability $P(N)$ in terms of N at three kind of constant voltages is studied by Equation (4.6), giving the scale parameter a as a=0.37 - 0.53 for LI and as a=0.21 - 0.38 for SI voltages.

The experimental data are also analyzed based on the two-parameter Weibull distribution given in Equations (4.7) and (4.8). In this experiment, the values of m in Equation (4.4) are m=13.2 and m=9.1 for LI and SI voltages, respectively, while the values n x a in Equation (4.8) are 13.2 - 18.9 and 9.6 - 17.3 for LI and SI voltages, respectively. Therefore, m is nearly equal to n x a again, showing that the V-N characteristics can be well analyzed by the two-parameter Weibull distribution in Equations (4.7) and (4.8).

The statistical coefficients representing V-N characteristics are summarized in Table 4.3. The fact a<1 in Table 4.3 shows that the puncture properties are a teething fault. The reduction of insulation performance is within 10%, considering the value N of LI and SI application during the service life would be at most 50 and 100, respectively [4.4].

Table 4.3: Statistical coefficients that represent V-N characteristics of internal bulk of spacer model at LI and SI stress.

	$V_{50\%}$ (kV)	n	a	$m = n$ x a
LI	290	35.7	0.37 – 0.53	13.2 – 18.9
SI	261	45.5	0.21 – 0.38	9.6 – 17.3

4.4.4 Critical field for ageing

Critical field for ageing, that is AC stress deteriorating long-term insulation performance of epoxy insulator, is reported in the references.

In [4.10], the critical AC stress for long-term insulation performance of epoxy insulator is investigated, comparing the puncture field at LI voltage between before and after 30 years AC stress simulated by high-frequency accelerated AC voltage.

Fig. 4.12 shows the test specimen and the experimental results on residual insulating characteristics investigated by LI voltage application after ageing of 30 years. AC voltage at 2,300 Hz during 5,654 hours, which is comparable to about 30 years at 50Hz, is prestressed to the epoxy specimen. The puncture characteristics at LI voltages after 30 years AC stress are compared with those of the initial characteristics, since the ageing is more critical at LI voltage application rather than at AC stress only [4.10]. The test results show that the AC stress of 15kVrms/mm lowers the initial puncture voltage 324kV at LI to 298kV (8% reduction). However, the reduction rate of the LI puncture voltage is 4% and 2% for 12kVrms/mm and 9kVrms/mm stresses, respectively. The facts suggest that the critical field for ageing is 12kVrms/mm for 30 years operation.

CIGRE task force 15.03.07 reports the similar critical field for ageing [4.5]. Fig. 4.13 shows the distribution of puncture stress on unstressed (broken lines) and prestressed (unbroken lines) epoxy resin specimens of some millimeters thickness. The long-term prestresses between 15 and 20 kVrms/mm during 5,000 to 7,000 hours reduce the shape parameter m of Weibull distribution to the values between 4 and 6 of which the initial values are between 6 and 8. On the other hand, under the prestresses less than 12kVrms/mm, there is no influence on the shape parameter m. The result on critical field 12kVrms/mm for ageing is consistent with that by Fig. 4.12. The CIGRE task force also reports that no change of shape parameter m, which means no ageing, has to be

expected under service condition, since the maximum working stress in a GIS or a GIL ranges between 2.5 and 5 kVrms/mm under current technology for solid insulators as shown in Fig. 4.5.

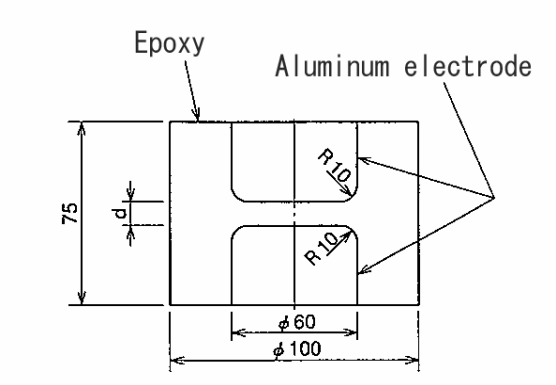

(a) Test specimen

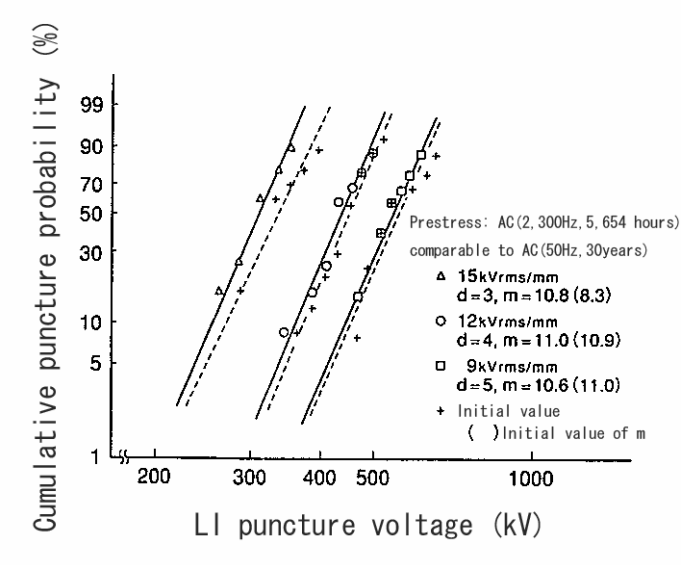

(b) Experimental results

Fig. 4.12: Test specimen and experimental results on residual insulating characteristics investigated by LI voltage application after aging of 30 years. AC voltage at 2,300 Hz during 5,645 hours, which is comparable to about 30 years at 50Hz, is applied to the test specimen followed by LI voltage application.

Another experiment in the literature [4.11] investigates the long-term deterioration characteristics of cast epoxy resin insulators by partial discharge (PD) measurements. Fig. 4.14 shows an example of the obtained results. The result of the investigations is that the epoxy resin degrades gradually even if the partial discharge level is small or undetectable. However, the continuous stress under service conditions is far below the critical stress for critical deterioration effects. Therefore, it can be also concluded that no ageing is expected under service conditions, as already mentioned above.

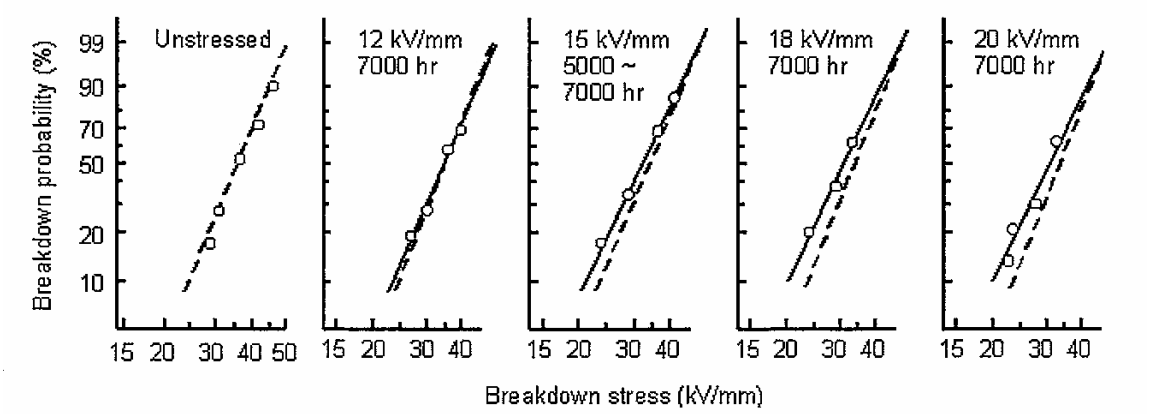

Fig. 4.13: Distribution of puncture stress on unstressed (broken lines) and prestressed (unbroken lines) epoxy resin specimens.

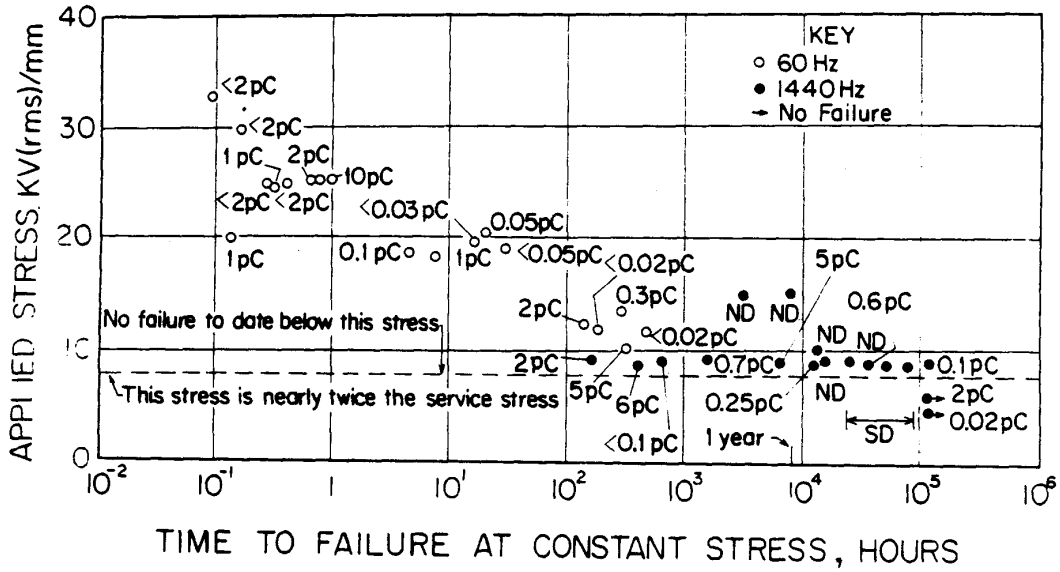

Fig. 4.14: Applied voltage versus time to failure for quartz filled cast epoxy resin (Diglycidyl Ether of Bisphenol A) with silver paint electrodes. Times to failure for 1,440 Hz are plotted as the equivalent time in 60Hz. ND: corona not determined, pC: picocoulomb, SD: tests with surface discharge (no paint).

4.5 Performance of combined and SF_6 impregnated dielectrics

This kind of dielectrics is used in SF_6 insulated instrument transformers for air insulated substations as well as for GIS-equipment, e.g. voltage transformers or bushings. In principle, several layers of an insulating foil, mostly impregnated with SF_6 and incorporated between two conductive layers form the combined dielectrics. Examples for these conductive layers are conductive films in the condenser of a bushing and wire-layers in a high-voltage coil. A variety of special insulating foils with different electrical and physical properties are used from different manufacturers.

In conventional condenser bushings, the electrical insulation of the condenser is in direct contact with the conductor and also acts as a thermal insulant. It is therefore directly heated by the conductor and applied to high temperatures which can exceed 100°C. Therefore, in IEC 60137, the thermal stability clause (clause 7.4) is written to cover the effects of conductor losses on the dielectric of the bushing condenser. How far this test is appropriate to cover or guaranty the long-term behavior of the bushing must be investigated. It must be mentioned that there are GIS-bushing designs available in which the condenser is not in direct thermal contact with the heated conductor, gas can circulate freely and therefore hot spots are avoided. In this case ageing due to a temperature effect can be neglected.

4.6 Influence of VFT on internal connections in GIS equipment

The quality of connections inside GIS equipment regarding very fast transient (VFT) must be considered as a possible ageing and failure mechanism. VFT in GIS has a typical rise time of about 5 ns and a main mono-frequency oscillation of approximately 300 kHz up to several tens of MHz. Due to the high frequency of VFT, low inductive connections are required, otherwise high voltage drops can occur. Depending on the design of the high-voltage equipment, these voltage drops can result in sparking, surface flashovers along insulating parts or even puncture of insulating materials. It was also observed that those events had been the origin of carbon dust, which was deposit on insulating spacers and created internal flashover.

4.7 Ageing of gas insulated equipment and switchgear after long-term service operation

In this section, the reports on ageing of an actual gas insulated equipment and switchgear after long-term service operation are introduced as the example of 245kV current transformer (CT), insulating spacer made of epoxy resin of 154kV and 72/84kV class and 123kV GIS.

4.7.1 Example of 245kV current transformer

Ageing and lifetime expectancy of a gas insulated instrument transformer for air insulated substations has been investigated in Germany [4.12]. The test object is a 245 kV CT with composite insulator manufactured in 1983, which was continuously in service for more than 17 years.

Fig. 4.15 shows the basic design of the internal insulation for the CT model. The main insulation is basically due to SF_6 gas except the insulation between the core housing on ground potential and the primary conductor on high-voltage potential. For this, the insulation medium consists of a dielectric film, impregnated with SF_6 gas, which is wrapped around the conductor and supports the core housing.

A repeated dielectric type-test according IEC 6044-1 was performed with the CT. The test had to be non-destructive, since the CT was intended to go in service again after passing all tests. To check the LI-withstand capability, five LI voltages of each polarity were applied. According to IEC the LI voltage was 80% of the specified 1050 kV.

The measured PD levels are listed in Table4.4. The basic noise level is 1 pC. The PD level of 5 pC at 460 kV is most probably due to external discharges in air. The results show that according to the design philosophy “to be free of PD up to the power frequency withstand voltage” there is no obvious ageing of the internal insulation. The results show that the dielectric performance of the 17 years old instrument transformer can be considered as that of a new one.

Other special tests performed to characterise the performance of a 17 years old composite polymer insulator are already published in [4.13]. The composite insulator also shows an excellent performance.

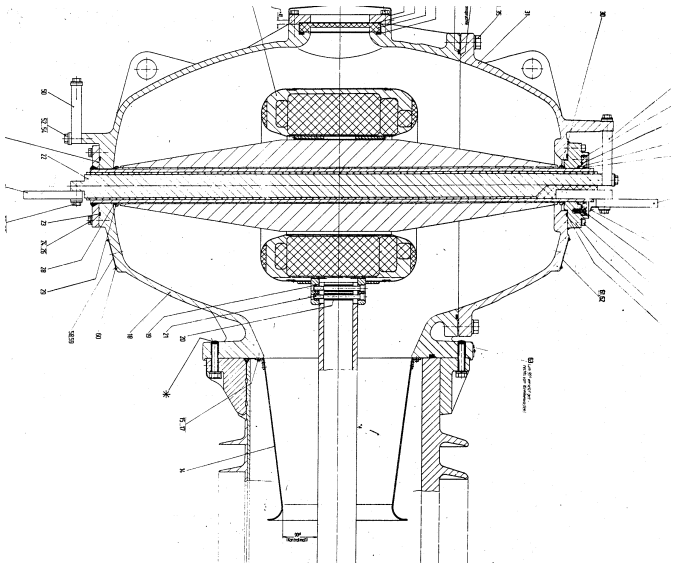

Fig. 4.15: Schematics of the internal insulation design of the investigated 245 kV CT.

Table 4.4: The measured PD levels for the 245 kV CT. The basic noise level is 1 pC.

	0 kV	141 kV	156 kV	173 kV	245 kV	294 kV	368 kV	460 kV
PD [pC]	1	1	1	1	1	1	1	5
PD [pC]	1	1	1	1	1	1	1	3

4.7.2 Example of epoxy spacer

Ageing and residual performance of insulating spacers made of epoxy resin are studied, using the actual spacers after long-term field operation in Japan [4.14][4.15].

The reference [4.14] reports the test results on the ageing of 154kV insulating spacer after 17 years operation since 1971. The cross-sectional view of the spacer is shown in Fig. 4.16. The verification tests by lightning impulse withstand voltage (LIWV), AC withstand voltage (ACWV) and PD measurement have been conducted based on the standard as shown in Table 4.5, which shows satisfactory insulating performance. Table 4.6 shows the comparison of breakdown voltages between unstressed spacer and 17 years old spacer at LI voltages. The test results also suggest that there is no deterioration during 17 years operation. The interface between high-voltage embedded electrode and epoxy resin is observed, reporting that no sign of deterioration is found at the interface.

The similar tests using 72/84kV epoxy spacers after 23 years operation are conducted in terms of the lifetime assessment [4.15]. Fig. 4.17 shows the half cross-section of 72/84kV GIS spacer tested and the example of epoxy resin surface observation at the position of the maximum electric field stress.

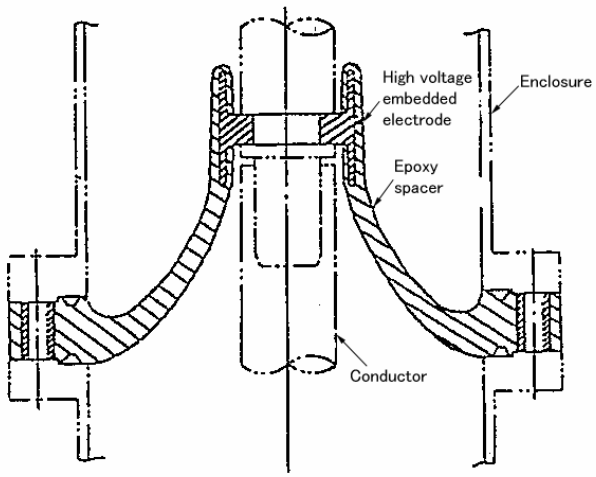

Fig. 4.16: Cross-sectional view of the tested 154kV insulating spacer after 17 years field operation.

Table 4.5: Withstand test results of 154kV insulating spacer.

	Testing voltages	Applied conditions	Test results
LIWV	750kV	One time application for each polarity	No breakdown
ACWV	325kVrms	One minute	No breakdown
PD measurement	194kVrms	Five minutes	No PD detection

Table 4.6: Comparison of breakdown voltages between unstressed spacer and 17 years old spacer at LI voltages.

	Unstressed spacer	17 years old spacer
Breakdown voltages (kV)	1,120 - 1,380	1,150 - 1,240

First, PD measurements at AC 128kVrms and AC withstand tests at 160kVrms for one minute are conducted at 0.4MPa for 12 spacers of 23 years old as shown in Table 4.7. No PD detection and no breakdown are confirmed.

Secondly, the ageing of the 23 years old spacers are accelerated by additional 1.5 times AC stress of operating voltage during 5.5 months, which corresponds to 67 years of operating voltage, considering Equation (4.1) and the value of n=12.3. After the AC voltage acceleration, PD measurements and breakdown tests at LI voltage are performed and no PD detection and no reduction of LI breakdown voltages are confirmed again as shown in Table 4.8.

Lastly, the interface between the high-voltage embedded electrode and the epoxy resin is observed in details as shown in Fig. 4.17(b). It is reported that there is no sign of ageing of epoxy

resin around the maximum electric field portion. Therefore, the series of the tests verified that the spacers have at least 90 years lifetime.

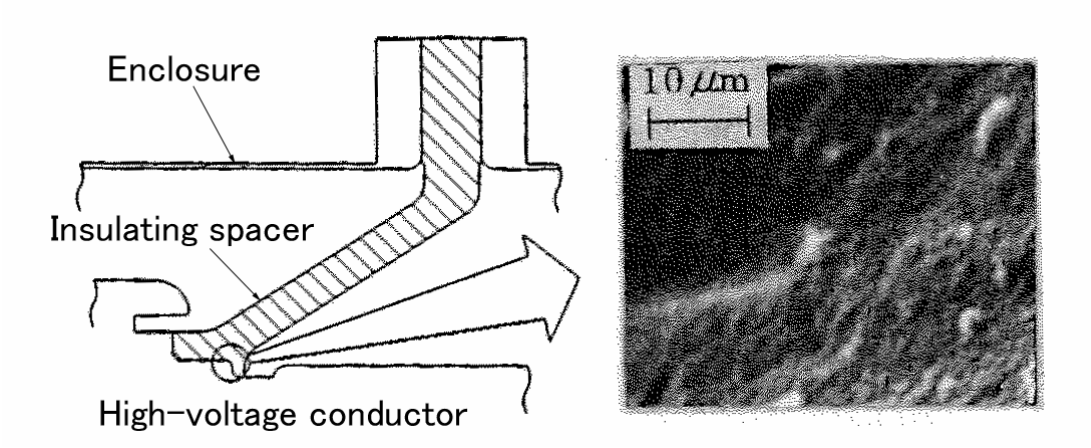

(a) Half cross-section of 72/84kV spacer

(b) Example of epoxy resin surface observation at maximum field stress (after AC stress equivalent to cumulative 90 years)

Fig. 4.17: Half cross-section of 72/84kV GIS spacer and example of epoxy resin surface observation at maximum electric field stress.

Table 4.7: Test results of 72/84kV spacer after 23 years field operation. The number of spacers tested is twelve and the gas pressure is 0.4MPa. The basic noise level is 1 pC.

	Testing voltages	Applied conditions	Test results
ACWV	160kVrms	One minute	No breakdown
PD measurement	128kVrms	Five minutes	No PD detection

Table 4.8: Test results of 72/84kV spacer after AC operating stress equivalent to cumulative 90 years (23 years field operation plus additional accelerated 67 years AC operating voltage). The number of spacers tested is ten and the gas pressure is 0.4MPa. The basic noise level is 1 pC.

	Testing voltages	Applied conditions	Test results
LIWV	400kV	Three times application for each polarity	No breakdown*
PD measurement	128kVrms	Five minutes	No PD detection

* The LI breakdown voltages are over 1.6 times of LIWV and there is no difference in the breakdown voltages between the unstressed spacer and the cumulative 90 years old spacers.

4.7.3 Example of 123kV GIS

The literature [4.5] reports that overall the entire sound insulation system does not exhibit an increase of the failure rate with time. Fig. 4.18 shows the failure rate of 123kV GIS in Germany since 1967 due to dielectric faults per 100 bays and year over the individual operation time until failure occurrence. The temporary increase and higher values of the failure rate after approximately 11 and 17 years were caused by some components which had been exchanged.

There is a general reduction of the failure rate with time, which proves that all further failures were caused by teething faults during the first 6 years of operation. However, Even after 25 up to 30 years of service no significant increase of the failure frequency is to be seen. Therefore, the literature [4.5] concludes that after 30 years of operation there is no general ageing which recognizably affects the long-term performance.

4.8 Insulation performance after 50 years GIS service life

The long-term performance of insulation system in GIS during the 50 years service life is summarized in Table 4.9, using the two parameter Weibull distribution together with the statistical coefficients representing the V-t and V-N characteristics. The insulation performance after 50 years operation is also estimated by each ageing factor.

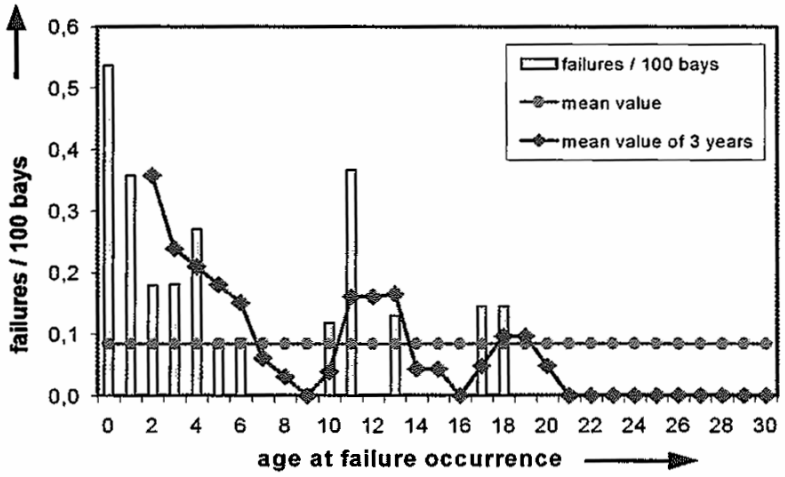

Fig. 4.18: Failure rate of 123kV GIS in Germany due to dielectric faults.

The shape parameter a is very important to evaluate whether there is a critical ageing of insulation system in GIS [4.5]. All the values of the shape parameter a in Table 4.9 are $a<1$. The fact shows that the failure rate decreases with the time t or number of times N and the failure is considered to be caused by teething faults.

As to the insulating performance after the service life of 50 years, the reduction rate is large for the internal bulk of insulators. The puncture field E_{50y} after 50 years operation is calculated by Equation (4.9), applying E_1m=30kVrms/mm in Equation (4.10) and (4.11) as a severe condition and also n=13 and 15 as the median in the references [4.1] and [4.5], respectively.

Considering other reduction of performance such as high temperature (10%), V-N characteristics (LI: 10%, SI: 10%), cumulative puncture field E_{c50y} after 50 years operation is estimated as follows.

E_{c50y} = 8.1 x 0.9 x 0.9 x 0.9 = 5.9 kVrms/mm (for n=13) (4.13)

E_{c50y} = 9.6 x 0.9 x 0.9 x 0.9 = 7.0 kVrms/mm (for n=15) (4.14)

The value E_{c50y} of 5.9 - 7.0 kVrms/mm are larger than the maximum working stress 5 kVrms/mm in Fig. 4.5, which shows that epoxy insulators would have enough performance even after 50 years operation. The enough insulation performance is also confirmed by the facts that the critical field for ageing is 12kVrms/mm during a long-term operation as described in the section 4.4.4.

Regarding the performance of interface between insulator surface and SF_6 gas, the reduction rate during 50 years is negligibly small, since the value is at most 6% for both LI and SI voltage application.

As to the long-term performance of SF_6 gas under clean and particle contamination, the reduction rate of 20% and 22% is not critical again, since in the case of AC stress the reduction could be covered by the design margin s generally defined as the following Equation:

s = (minimum breakdown electric field of the system) / (design electric field). (4.15)

The above evaluation shows that even if considering various reduction of insulation performance during the service life of 50 years, a GIS insulation system still has enough design margins.

Furthermore, it is verified that the GIS components such as epoxy insulators and CTs after the operation from 17 to 23 years had enough dielectric performance as explained in the section 4.7, which proves that the components have enough design margins and/or there is not a significant ageing. The field failure data of 123kV GIS suggest that after 30 years of operation there is no general ageing which recognizably affects the long-term performance of the GIS.

Therefore, it is noted that a GIS insulation system of a proper design has a service life of 50 years even if considering various reduction of insulation performance and no significant ageing is recognized in the actual GIS after long-term operations.

However, in a practical GIS, some other aspects such as metallic particles generation from the contacts, mechanical/thermal performance and gas seal performance should also be considered.

4.9 Conclusion

The long-term performance of a GIS has been reviewed in terms of V-t and V-N characteristics of SF_6 insulation system. The long-term field experience of a GIS and the key components is introduced and the insulation performance after the 50 years service life is evaluated.

(1) A GIS insulation system of a proper design has a service life of 50 years even if considering various reduction of insulation performance.
(2) No significant ageing is recognized in the actual GIS after long-term operations in the recent reports.
(3) However, some other aspects such as metallic particles generation from the contacts, mechanical/thermal performance and gas seal performance should also be considered in a practical GIS.

Table 4.9: Summary of statistical coefficients representing V-t and V-N characteristics of SF_6 insulated system in GIS at AC, LI and SI stress. Puncture field and reduction of insulation performance after 50 years service life are estimated.

Long-term insulation performance			Stress	*n*-value[*1]	*a*-value[*1]	Puncture field E_{50y} or Reduction rate after 50 years	References
Internal bulk of insulators	Room temperature	V-t	AC	13 [*5]	No data	8.1 kVrms/mm[*2]	[4.1]
				15 [*5]	0.4 -0.53, 0.9 [*4]	9.6 kVrms/mm[*2]	[4.5]
	90 - 105 degrees Centigrade			15.4 - 16	No data	10 % reduction from room temperature	[4.8],[4.9]
	Room temperature	V-N	LI	35.7	0.37 - 0.53	10 %[*3]	[4.4]
			SI	45.5	0.21 - 0.38	10 %[*3]	
Interface between insulator surface and SF_6 gas	Room temperature	V-N	-LI	124	0.2	3 %[*3]	[4.3]
			-SI	134	0.2 - 0.3	3 %[*3]	
SF_6 gas	under clean condition	V-t	AC	78[*5]	0.25 - 0.50	20 %[*3]	[4.1] [4.2]
	with metallic particles within quality control level			30 (< 10minutes)	0.88 - 0.98	-	
				69 (> 10minutes)	0.4 - 0.46	22%[*3]	

[*1] The values of *n* and *a* are the statistical coefficients representing V-t and V-N characteristics based on two parameter Weibull distribution given in the following equations:

$$P(V,t) = 1-\exp[-(V/V_s)^m(t/t_s)^a] \quad \text{or} \quad P(V,N) = 1-\exp[-(V/V_s)^m(N/N_s)^a], \quad m = n \times a.$$

Here, $P(V,t)$ and $P(V,N)$ are the cumulative breakdown probability dependent on breakdown voltages V and time to breakdown t or number of voltage application N. The values of m and a are the shape parameters of V and t or N, respectively. The value of n gives the gradient $-1/n$ of V-t and V-N characteristics.

[*2] Puncture field E_{50y} after 50 years operation: $E_{50y} = E_{1m}t^{-1/n}$, here E_{1m} =30kVrms/mm (puncture field at 1 minute) [4.8] [4.9], t=50 years = 60x24x365x50 minutes. Considering other reduction of performance such as high temperature (10%), V-N characteristics (LI: 10%, SI: 10%), cumulative puncture field E_{c50y} after 50 years operation is estimated as E_{c50y}=8.1x0.9x0.9x0.9=5.9 kVrms/mm (for n=13) and E_{c50y}=9.6x0.9x0.9x0.9=7.0 kVrms/mm (for n=15). Therefore, E_{c50y}=5.9 - 7.0 > 5 kVrms/mm (maximum working stress in Fig. 4.5 [4.5]).

[*3] V-N characteristics: Reduction rate = $[1-(N/N_0)^{-1/n}]$ x 100 (%), here N=50 at LI, N=100 at SI, N_0 = 1. V-t characteristics: Reduction rate = $[1-(t/t_0)^{-1/n}]$ x 100 (%), here t=50 years = 60x24x365x50 minutes, t_0 = 1 minute.

[*4] a=0.4 - 0.53 under service condition between 2.5 and 5.0 kVrms/mm, a=0.9 under high stress between 15 and 30 kVrms/mm.

[*5] Median of *n*-value. The variation of *n*-value is 10 to 16 [4.1], 10 to 20 [4.5] and 74 [4.2] to 82[4.1], respectively.

REFERENCES of Chapter 4

[4.1] Investigation R&D Committee Chaired by Prof. T. Kawamura, "Properties on Electrical Insulation Related to Testing Voltages and Power Equipment", *Technical Reports by IEE Japan*, No.518 (1994) (in Japanese).

[4.2] C.M.Cooke, CIGRE document 15-76(WG-03).

[4.3] S.Okabe, T.Ohno, E.Zaima, K.Kobayashi, T.Yamagiwa and F.Endo, "Surface Insulation Characteristics of a GIS Spacer Model for Repeated Impulse Voltages", *T. IEE Japan*, Vol. 115-B, No.2, pp.187-193 (1995) (in Japanese).

[4.4] S.Okabe, T.Ohno, E.Zaima, H.Aoyagi, H.Murase and I.Oshima, "Deterioration Characteristics of Insulating Spacer Model toward Repeating Impulse Voltage", *T. IEE Japan*, Vol. 115-B, No.8, pp.978-984 (1995) (in Japanese).

[4.5] CIGRE Task Force 15.03.07 of Working Group 15.03, "Long-term Performance of SF_6 Insulated System", *CIGRE Session 2002*, Report 15-301.

[4.6] A.Diessner, G.Luxa and W.Neyer, "Electrical Aging Tests on Epoxy Insulators in GIS", *IEEE Trans. Electrical Insulation*, Vol.24, No.2, pp.277-283 (1989).

[4.7] K.Juhre and E.Kynast, "Long Term Performance under High Voltage of Mineralic Filled and Fiber-reinforced Epoxy Insulators Used in GIS", *14th ISH*, Beijing, Paper No.O11.C-07 (2005).

[4.8] H.Aoyagi et al., *Technical Report in Electrical Insulation Materials of IEE Japan*, EIM-77-14 (1979) (in Japanese).

[4.9] K.Nakanishi et al., "Dielectric Performance of Epoxy Insulators at AC Voltages", *Technical Report of Mitsubishi Electric Corp.*, Vol.54, No.3, pp.187-191 (1980) (in Japanese).

[4.10] S.Okabe, E.Zaima, K.Inami, K.Sasamori and S.Sakuma, "Deterioration Characteristics of Model of Insulating Spacer for GIS under AC and Impulse Voltage", *T. IEE Japan*, Vol. 115-B, No.1, pp.30-35 (1995) (in Japanese).

[4.11] T.W.Dakin and S.A.Studniarz, "The Voltage Endurance of Cast Epoxy Resins", *IEEE International Symposium on Electrical Insulation G7*, pp.216-221 (1978).

[4.12] U.Prucker, "Information on the Breakdown Behaviour of SF_6 and SF_6/N_2 Mixtures and the V-t Characteristics", 33-02 (TF13-13) 02 IWD, Paris Meeting (2002).

[4.13] H.Janssen and R.Hennings, "Lifetime of Composite Polymer Insulators for HV Outdoor Applications: Today's Knowledge", *Proc. 2001 Word Insulator Congress*, Shanghai (2001).

[4.14] T.Yorozuya, N.Takasuga, T.Yamazaki, M.Nakayama, Y.Hashimoto and Y.Murayama, "Tests on Ageing of Insulating Spacer after Long-term Field Operation", *1990 National Convention Record IEE Japan*, No.1279 (1990) (in Japanese).

[4.15] T.Hakari, H.Tanpo, Y.Shimizu, H.Hama and K.Sasamori, "Lifetime Assessment of GIS Insulating Spacer after Long-term Field Operation", *1998 Annual conference Record IEE Japan at Kansai Branch*, No.G136 (1998) (in Japanese).

5. INFLUENCE OF PRESTRESS VOLTAGE ON INSULATION WITHSTAND OF GIS

In this chapter, the experimental results on insulation characteristics under LI and VFT voltages superimposed to AC or DC voltages are presented in the sections 5.1 and 5.2. The influence of AC and DC prestress on insulation performance of GIS applying IEC 62271-203 is discussed in the section 5.3, using the above experimental results.

5.1 Insulation characteristics under impulse voltages superimposed to AC voltages

In the actual field, power equipment is subject to impulse voltage stresses superimposed AC operating voltage. It is essential to clarify the insulation characteristics under impulse voltages superimposed to AC voltages, especially when LIWV is reduced at higher voltage class and the ratio of AC operating voltage to LIWV increases.

Fig. 5.1 shows three kinds of test samples for lightning impulse breakdown experiments superimposed to AC voltages to investigate the characteristics of (a) sparkover, (b) surface flashover and (c) puncture, respectively [5.1]. The unit of length in the figure is millimeter.

Fig. 5.2 shows the relation between the sparkover voltages (total voltages to ground at sparkover) and the values of applied AC component in the case of sparkover test sample in Fig. 5.1 (a). The figure suggests that the insulation characteristics at LI voltages superimposed to AC voltages are comparable to those at LI voltages without AC prestress when the ratio of AC prestress to LI sparkover voltages is within about 60%.

The literature [5.1] also reports that the same tendency is observed for the experiments on Fig. 5.1 (b) and (c), which will be explained in the section 5.3.

On the other hand, the similar test results on the insulation performance of SF_6 insulated component under impulse overvoltages superimposed with AC stress show that the reduction of impulse strength is not observed unless very large metallic particles are involved [5.2].

5.2 Insulation characteristics under impulse voltages superimposed to DC voltages

The stress condition of overvoltages superimposed to a DC voltage could occur due to operation of disconnecting switch (DS) even for AC GIS [5.2]. When switching on or off busbar sections of a GIS by a DS, the operation causes a number of restrikes between the contacts, leading to VFT overvoltage. Furthermore, a DC voltage due to a residual charge is left on the open side after opening the DS. Consequently, when closing the DS, the stress to ground on the load side is characterized by a VFT superimposed to a residual DC prestress applied for a relatively long time.

The literature [5.2] reports the following points from the test results.

(1) Large reduction of the impulse strength may be caused by the presence of the DC prestress. Important reductions were observed only in the condition of DC and impulse voltage having opposite polarity as shown in Fig. 5.3.

(2) As shown in Fig. 5.3, the large reduction of the strength is not caused by the presence of spacers from the tests with and without spacers in extremely clean conditions. They are mainly related to the presence of free particles.

(3) The reduction is present for all impulse types of SI, LI and VFT. Particular tests have shown that the strength under VFT may be well represented by that with LI, also in the presence of a DC prestress as shown in Fig. 5.4.

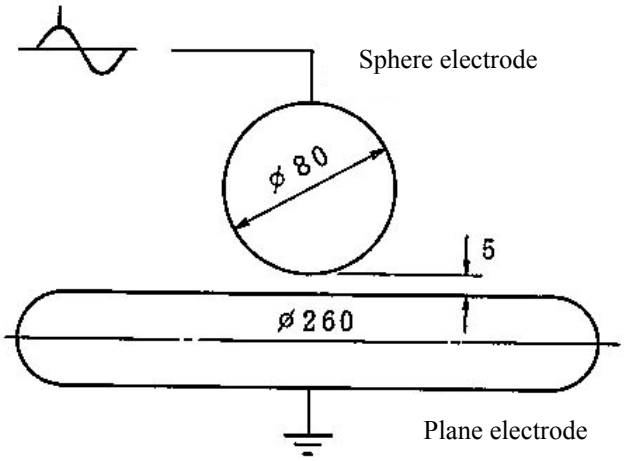

(a) Sample for sparkover tests

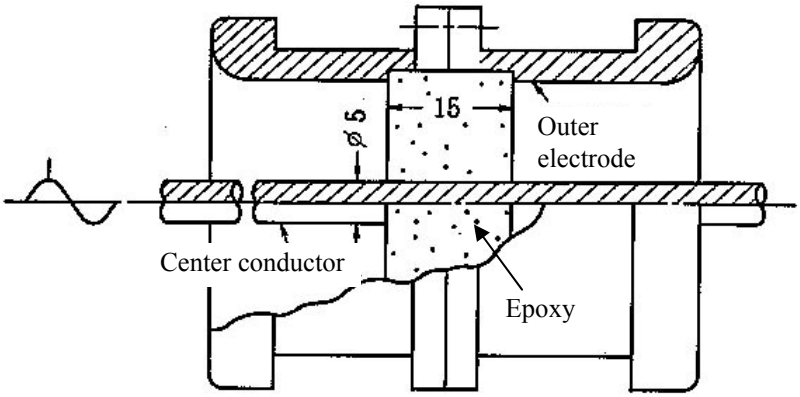

(b) Sample for surface flashover tests

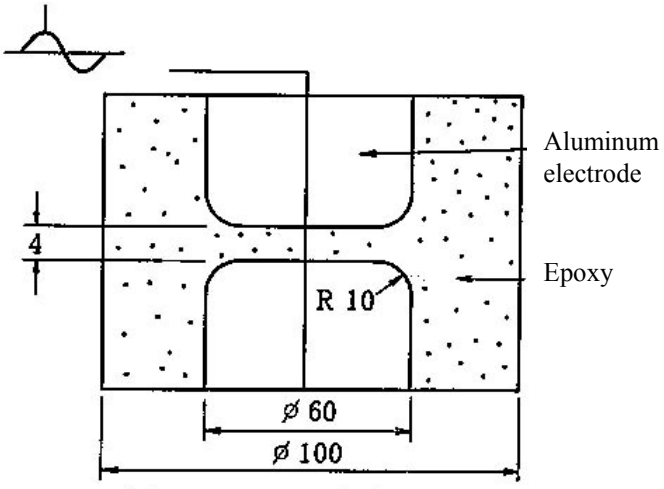

(c) Sample for puncture tests

Fig. 5.1: Test samples for LI breakdown experiments superimposed to AC voltages.

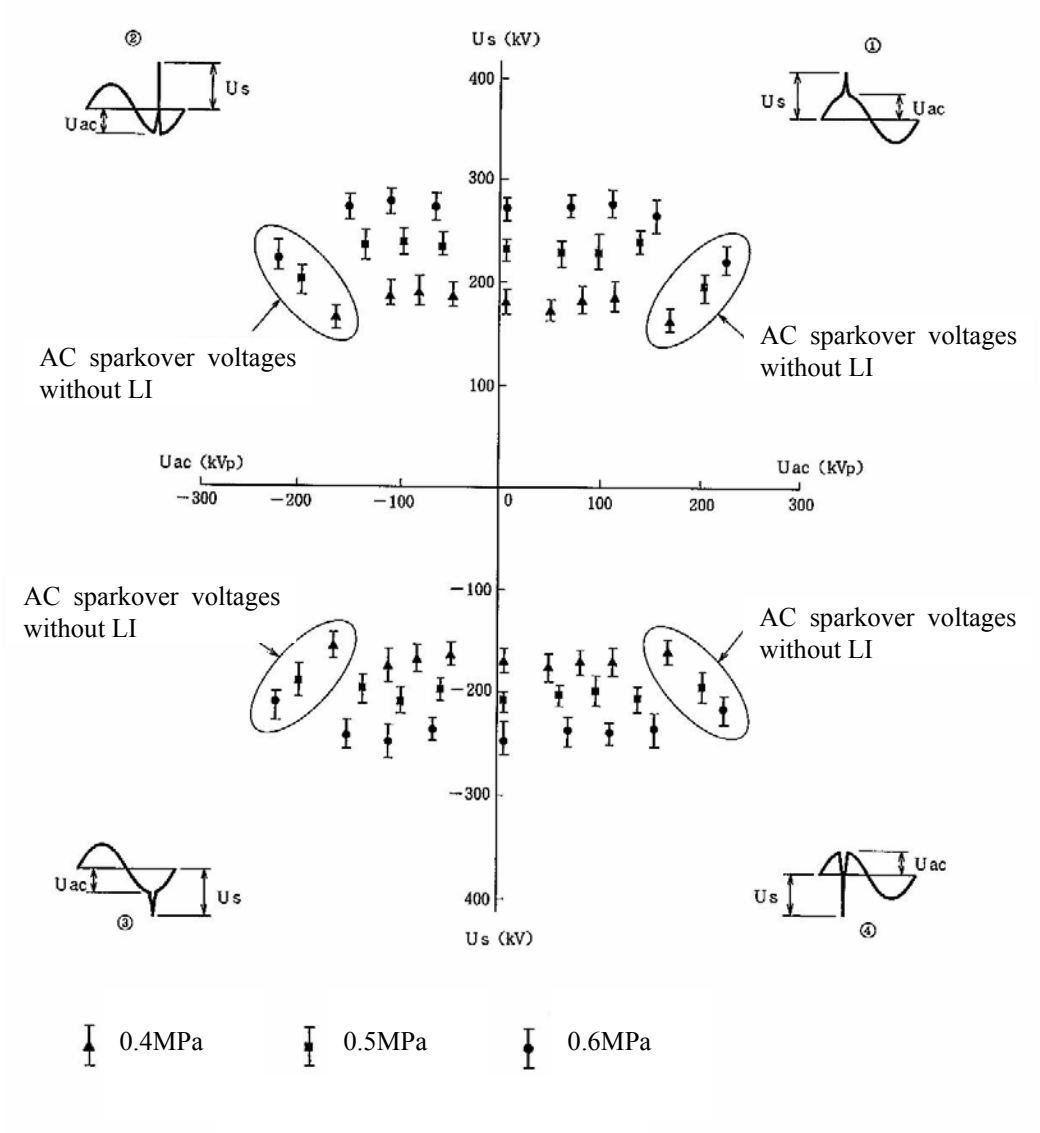

Fig. 5.2: Relation between sparkover voltages (total voltages to ground at sparkover) and values of applied AC component in the case of sparkover test sample in Fig.5.1 (a).

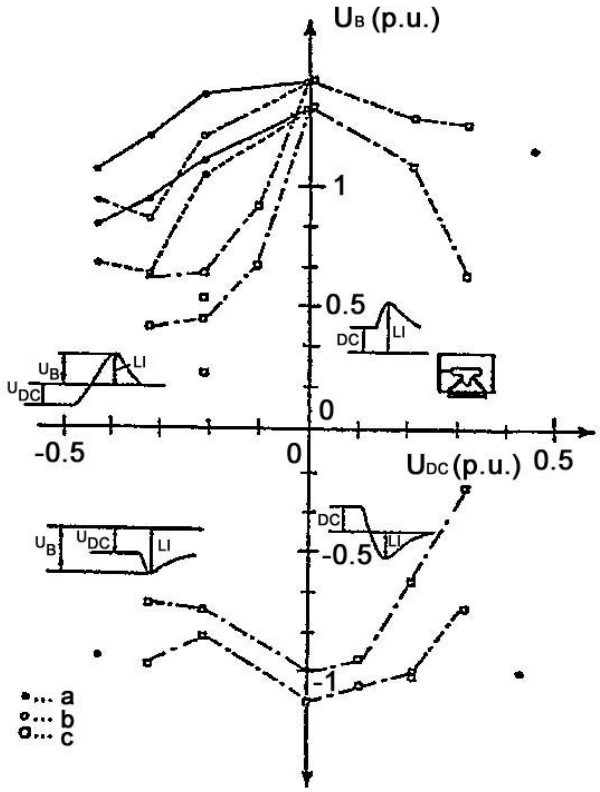

Fig. 5.3: Tests with composite stress (LI+DC). Breakdown voltage (total voltage to ground at breakdown) versus the value of the applied DC component (1p.u.: minimum observed breakdown voltage under negative LI without DC prestress).
a – Clean condition with preconditioning,
b – Clean condition without preconditioning,
c – With particles (1g weight, 0.5mm maximum length, aluminum) without preconditioning.

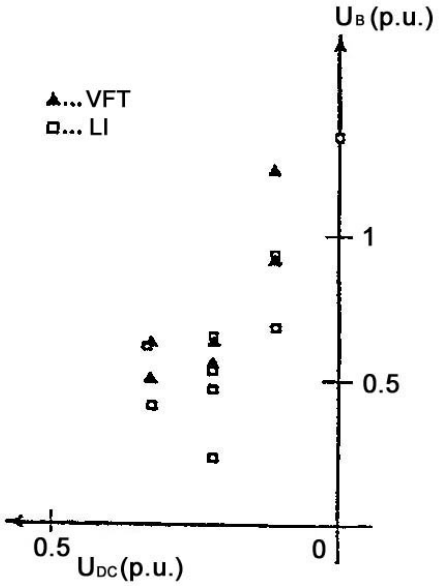

Fig. 5.4: Tests with composite stress. Breakdown voltage with VFT (total voltage to ground at breakdown) versus the value of the applied DC component. Comparison with results obtained with LI (1p.u.: minimum observed breakdown voltage under negative LI without DC prestress).

The references [5.2][5.3] also represent the test data to evaluate the influence of the above DC prestress for the insulation performance of GIS, considering the stress condition related to DS switching of capacitive currents.

Fig. 5.5 shows the lowest limit curve measured with composite voltages of LI + DC on industrial clean conditions, which are taken as representative of all GIS. The tests are conducted for various GIS with many testing arrangements. The limit curve is obtained with a duration of the DC prestress sufficiently long to be at least comparable to the duration occurring when closing a DS in presence of a trap charge left by a previous opening operation. The references [5.2][5.3] suggest that the reduction of LI strength with a DC prestress could be caused by small particles, which may not be fully avoided, and their presence may not even be checked by usual dielectric and partial discharge tests. The references note that the strength under composite voltage of the type VFT + DC is very important in design and may constitute a limit when thinking of compact solutions.

On the other hand, the experimental results focused on the effect of DC prestress on impulse flashover characteristics of insulator model is reported in a reference [5.4], while the above references [5.2][5.3] suggest that the large reduction of the strength caused by DC prestress is not caused by the presence of spacers.

Fig. 5.6 shows the insulation model to measure the effect of DC prestress on LI flashover characteristics. The model consisted of a post-type spacer and electrodes. Each spacer is set between a plane grounded electrode and a cylindrical high voltage (HV) electrode with a hollow. There is a small gap between the spacer surface and the end of the HV electrode. The gap is 1mm in length and the position of the gap is about the center of the spacer surface. The pressure of SF_6 gas is 0.5MPa.

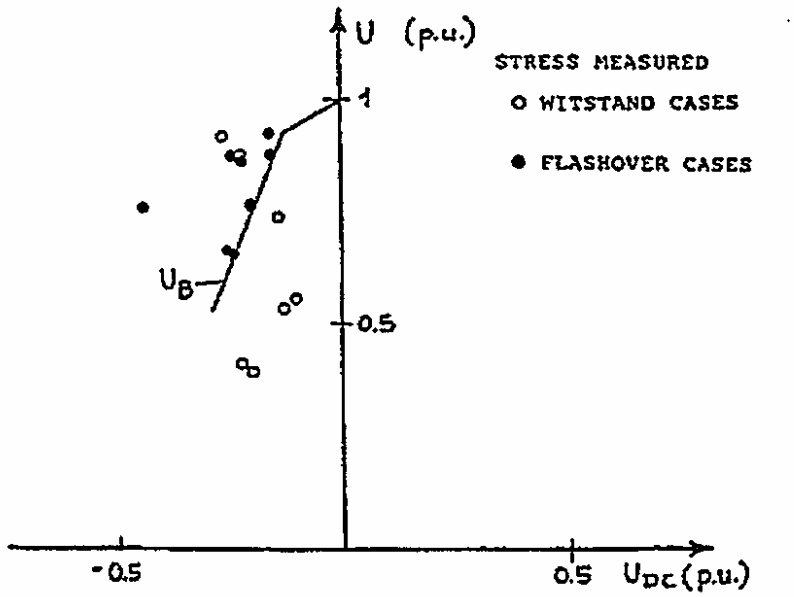

Fig. 5.5: Tests with composite stresses (LI+DC). Minimum observed breakdown voltages (total voltage to ground at breakdown) obtained after a large number of test repetitions versus the value of the applied DC component (1 p.u. = minimum observed breakdown voltage under negative LI without DC prestress at the examined pressure).

Fig. 5.7 shows the effect of DC prestress (U_{DC}) on LI flashover voltage (U_{LI}). In the figure, $U(=U_{DC} + U_{LI})$ is shown as the flashover voltage, and the polarities of U_{DC} and U_{LI} are determined that U_{DC} and U_{LI} are positive when the HV electrode are positive. The two groups of the data surrounded by ellipses show the DC flashover voltages without U_{LI}. The flashover voltage U decreases when the polarity of U_{LI} is opposite to that of U_{DC}, compared with the value under simple impulse. Especially the voltage U decreases about 30% when U_{DC} is +130kV, while U does not decrease when the polarity of U_{LI} is the same as U_{DC}.

The influence of DC prestress is explained by the effect of surface charge on dielectric strength. Fig. 5.8 shows the effect of surface charge on dielectric strength. When positive charges are accumulated on the spacer surface with positive DC prestress, the direction of the electric field caused by negative U_{LI} is the same as that caused by the accumulated charges. Therefore, the field is enhanced and the flashover voltage decreases. On the other hand, since the direction of the field caused by positive U_{LI} is opposite to that caused by the accumulated charges, the field is not enhanced and the flashover voltage does not decrease. The phenomena with negative U_{DC} can be explained in a similar way.

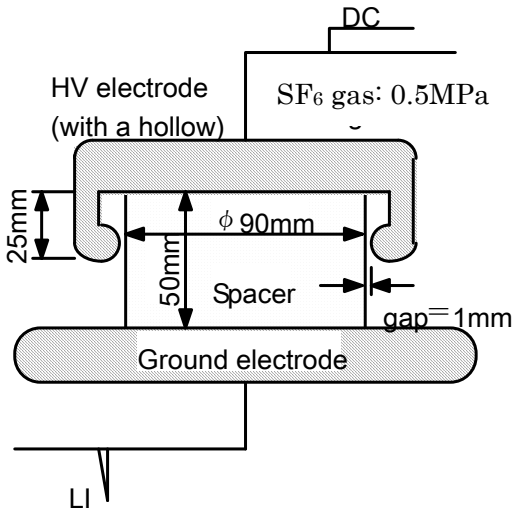

Fig. 5.6: Insulator test sample for investigating effect of DC prestress on LI breakdown voltages. The SF_6 gas pressure is 0.5MPa.

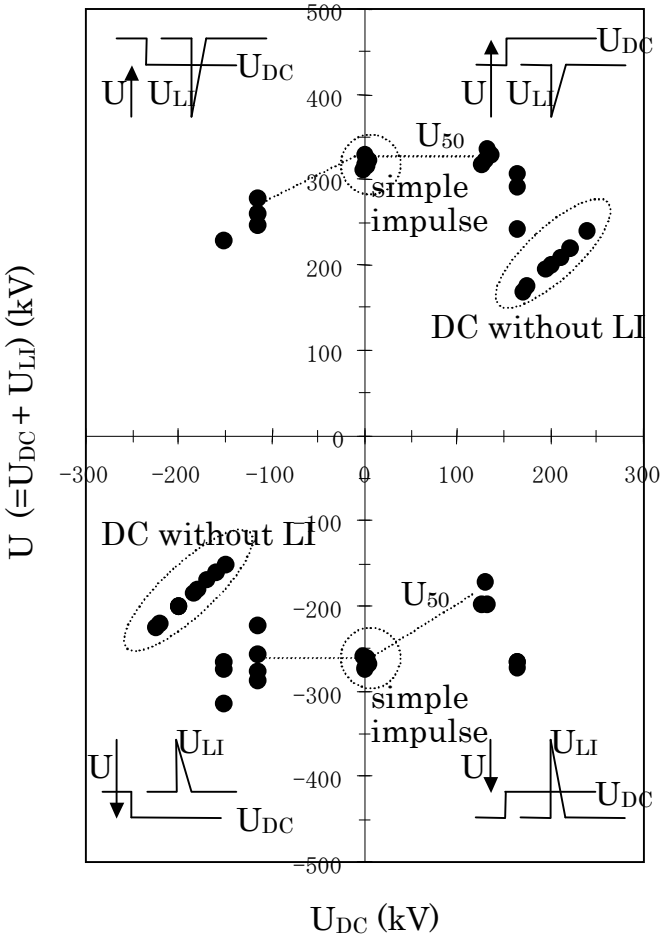

Fig.5.7: LI flashover voltage *U* superimposed on DC prestress U_{DC}.

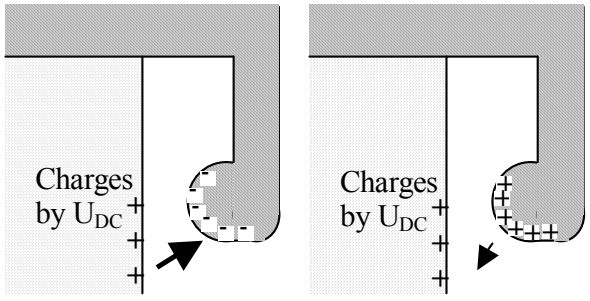

Accumulated charges enhance electric field.

(a) U_{DC}: positive
U_{LI} : negative

Accumulated charges do not enhance electric field.

(b) U_{DC}: positive
U_{LI} : positive

Fig. 5.8: Effect of surface charge on dielectric strength.

5.3 Influence of AC and DC prestress on GIS insulation performance

The influence of AC prestress on GIS insulation performance is discussed in the reference [5.1]. Fig. 5.9 summarizes the test results with composite stresses (LI+AC) and influence of AC prestress on insulation performance, using the three kinds of test samples in Fig. 5.1. Here, U_s and U_{ac} correspond to the composite breakdown voltages normalized by the simple 50% LI breakdown voltages and the applied AC peak values normalized by the simple 50% LI breakdown voltages, respectively. The peak value of rated voltage normalized by LIWV is also indicated in the figure. The rated voltages up to 800kV in the figure are referred to IEC 62271-203, while the rated voltage of 1100kV with 2250kV in LIWV is applied to UHV equipment in Japan.

	Test sample	Positive 50% LI breakdown voltages (kV)
○	Sparkover tests	230
×	Surface flashover tests	139
△	Puncture tests	365

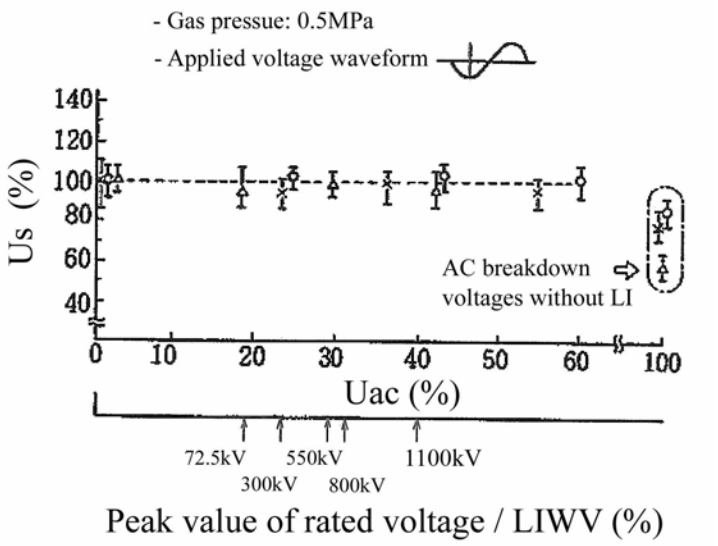

Fig. 5.9: Test results with composite stresses (LI+AC) and influence of AC prestress on insulation performance at three different test samples in Fig.5.1 (a), (b) and(c). The rated voltages up to 800kV in the figure are referred to IEC 62271-203, while the rated voltage of 1100kV with 2250kV in LIWV is applied to UHV equipment in Japan.

It is obvious that reduction of LI breakdown voltage is not observed when the superimposed AC component is within 70% of AC breakdown voltage (about 60% of LI breakdown voltage) for the three kinds of samples of sparkover, surface flashover and puncture. Therefore, there is no need to consider the influence of AC prestress on a GIS insulation performance under good quality control conditions up to the voltage class of 800kV and also UHV.

As for the influence of DC prestress on GIS insulation performance, the literature [5.3] reports the comparison between limit withstand curves under composite stresses in Fig. 5.5 and overvoltage levels due to DS operation for different system ratio between LIWV and system voltage levels. Referring to the literature [5.3], the similar study has been conducted as follows.

Fig. 5.10 shows the comparison between the minimum breakdown curves U_{min} (solid curves) under composite stresses of VFT+DC with small particles contamination under industrial clean conditions and the overvoltage levels U_{max} (broken line) by DS operation for different rated voltage.

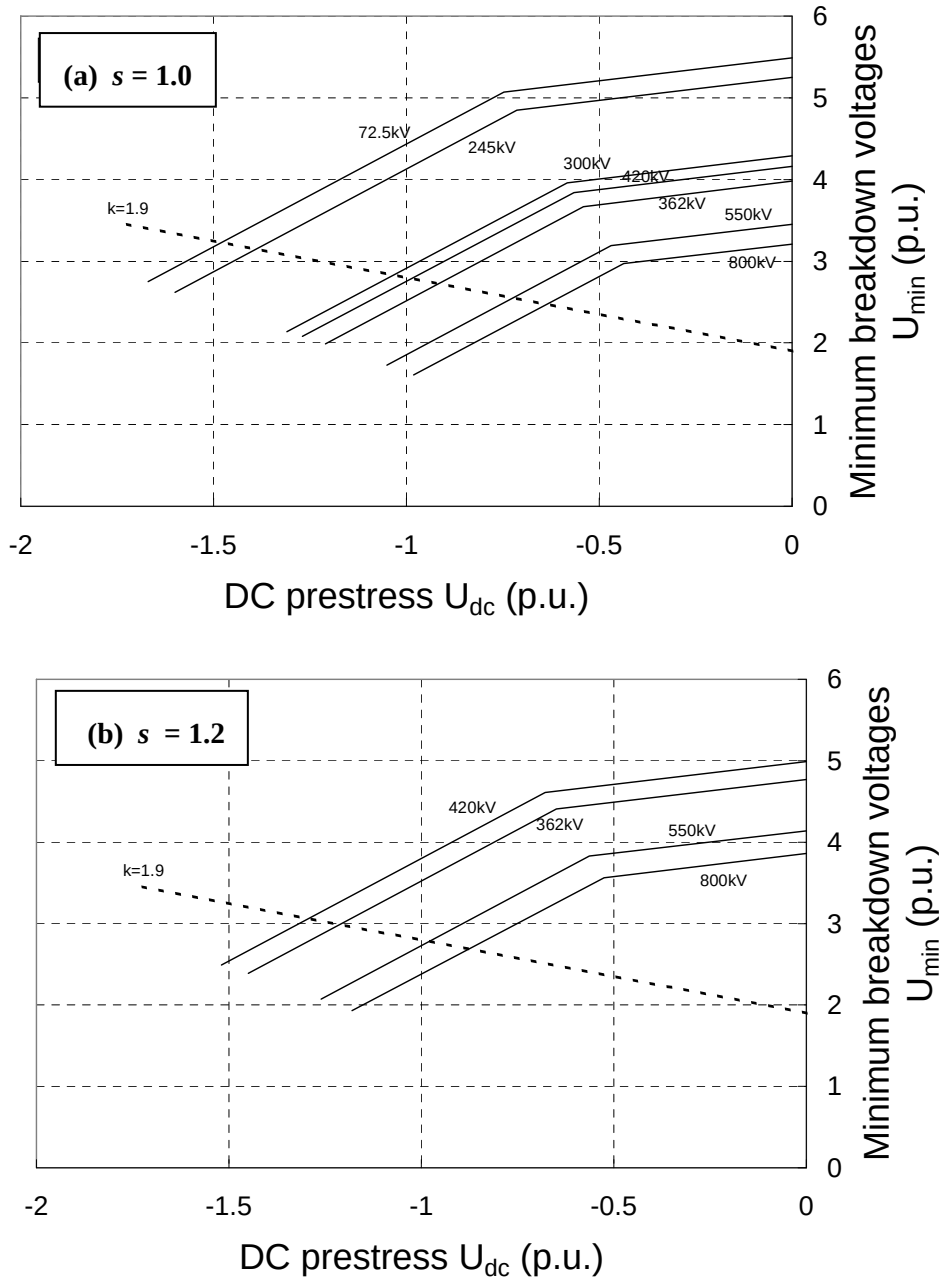

Fig. 5.10: Comparison between the minimum breakdown curves U_{min} (solid curves) under composite stresses of VFT+DC with small particles contamination under industrial clean conditions and the overvoltage levels U_{max} (broken line) by DS operation for different rated voltage in the IEC 62271-203. The value of *s* corresponds to the insulation design margin defined as *s* = (minimum breakdown electric field of the system) / (design electric field).

The curves are derived from Fig. 5.5 assuming the minimum breakdown voltage under negative LI equal to the LIWV in IEC 62271-203. And also, the minimum breakdown voltages at VFT are considered to be the same as the minimum LI breakdown voltages, referring the results in Fig. 5.4.

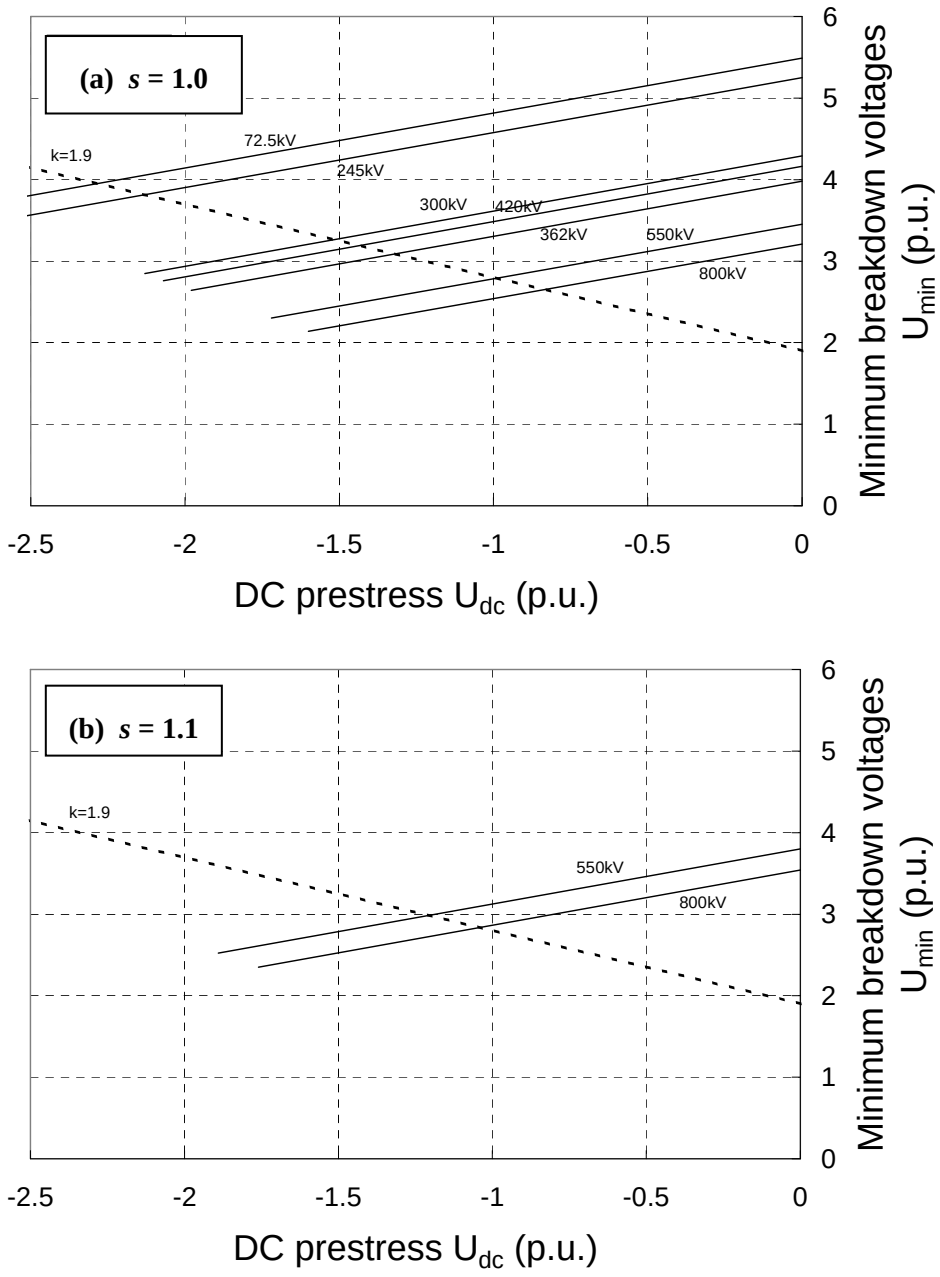

Fig. 5.11: Comparison between the minimum breakdown curves U_{min} (solid curves) under composite stresses of VFT+DC with charge accumulation on spacer surface for various rated voltages and the overvoltage levels U_{max} (broken line) by DS operation for different rated voltage in the IEC 62271-203.

For the rated voltage U_r, the minimum breakdown voltage U_{min} is obtained as,

$$U_{min} = \text{LIWV} / (U_r \cdot \sqrt{2} / \sqrt{3}). \quad \text{(p.u.)} \tag{5.1}$$

With the presence of a trapped charge left by a previous opening operation, the voltage difference at DS terminals before restrikes is equal to the phase voltage plus the trapped charge U_{dc} at the first restrike. The maximum overvoltage levels U_{max} in p.u. by DS closing operation are calculated by the following equation [5.3].

$$U_{max} = (1 - U_{dc}) \cdot k + U_{dc} \quad \text{(p.u.)} \tag{5.2}$$

Where k is the overvoltage factor that depends on the substation layout at the moment of DS operation. The value of k is referred to a literature [5.5] that reports maximum overvoltage levels U_{max} is 2.8p.u. in actual substations, which leads to the value of k of 1.9 using Equation (5.2).

Fig. 5.11 also shows the similar comparison between the minimum breakdown curves U_{min} (solid curves) under composite stresses of VFT+DC with charge accumulation on spacer surface based on Fig. 5.7 and the overvoltage levels U_{max} (broken line) by DS operation.

In an actual insulation design for a GIS, a design margin is considered to guarantee the required performance of the GIS according to the specifications as discussed in the section 4.8. The insulation design margin s, which is defined by the Equation (4.15), is varied between 1.0 and 1.2 to study the influence of DC prestress in Figs. 5.10 and 5.11.

Using the design margin s, the minimum breakdown curves U_{min} are calculated as $s \cdot U_{min}$ by Equation (5.1).

In the case of the design margin s=1.0, the overvoltage level U_{max} at the trapped charge U_{dc} =1.0, which corresponds to the practical maximum value, exceeds the minimum breakdown curves U_{min}, when the rated voltages are above 300kV in Fig. 5.10 (a) with small particles contamination under industrial clean conditions and also above 550kV in Fig. 5.11 (a) with charge accumulation on spacer surface. Considering the design margin s, the minimum curves U_{min} become larger than the overvoltage U_{max} at U_{dc} =1.0 at the rated voltages up to 550kV at s=1.2 in Fig. 5.10 (b) and up to 800kV at s=1.1 in Fig. 5.11 (b). However, an additional measure would be needed for the GIS of rated voltages 800kV and above, since the design margin s up to a level of 1.2 cannot completely cover the dielectric performance of the GIS with small particles contamination under industrial clean conditions.

As mentioned above, the reduction of LI strength with a DC prestress in Fig. 5.5 is considered to be caused by small particles, which may not be fully avoided, and their presence may not even be checked by usual dielectric and partial discharge tests. It seems that the small particles could levitate from an inner surface of GIS enclosure under DC prestress, which would cause a firefly phenomena [5.6][5.7] and reduce the dielectric performance of GIS when LI or VFT voltages are applied. Therefore, inhibiting the particle levitation is one of the effective measures to prevent the reduction of LI strength with a DC prestress.

The literature [5.6] reports the effect of a dielectric coating on inner surface of GIS enclosure to inhibit particle levitation for a high voltage DC GIS. Fig. 5.12 shows the enhancement of particle levitation field strength E_L by dielectric coating for 10mm long/0.2mm diameter aluminum particles. Here, coat A and coat B are epoxy resin and phthalic acid ester resin, respectively. At DC voltages, the particle levitation field for the dielectric coated enclosure is 1.5MV/m and about three times higher than that of 0.5MV/m for the bare enclosure. The levitation field reaches 0.7MV/m for the dielectric coated enclosure from 0.5MV/m for the bare enclosure at AC voltages.

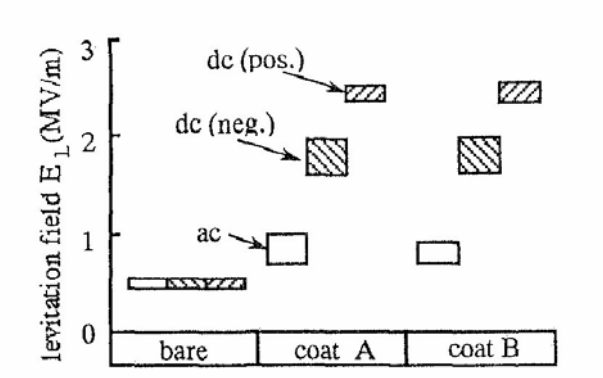

Fig. 5.12: Enhancement of particle levitation field strength by dielectric coating for 10mm long/0.2mm diameter aluminum particles. Coat A: epoxy resin, Coat B: phthalic acid ester resin.

The actual GIS will mechanically vibrate when circuit breakers and DS are operated. Such vibration gives particles an accelerated velocity, which causes to start levitation at field strength lower than E_L for a static condition. Figure 5.13 shows the dependency of E_L on the accelerated velocity of enclosure vibration for the dielectric coated enclosure [5.6]. The dielectric coating is epoxy resin of 40 μm thickness. Aluminum particles of 3mm long and 0.25mm diameter are used for the experiment. Negative DC voltages are applied after the prestress of positive DC voltages. The literature [5.6] reports that without the prestress no particles levitate even at 6G at the field strength of 0.7MV/m on the enclosure, although the levitation field decreases as increasing the accelerated velocity. And also, since the maximum accelerated velocity of vibration at an actual DS operation is around 0.5G, particle levitation would be prevented by the coating up to 0.7MV/m of which value is 1.4 times higher than that for bare enclosure.

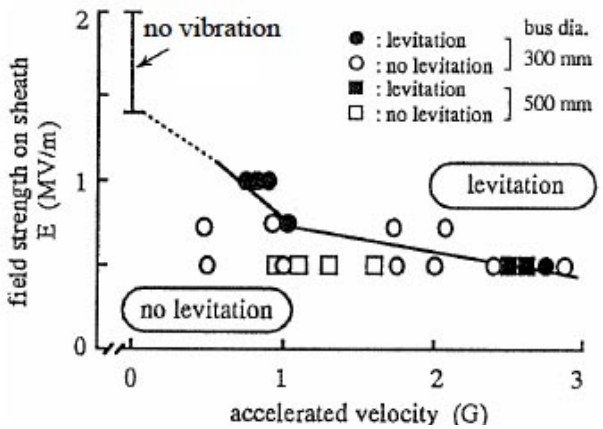

Fig.5.13: Dependence of levitation field strength on accelerated velocity of enclosure vibrations for dielectric coated enclosure. Aluminum particles of 3mm long/0.25mm diameter are used in the experiment.

The literature [5.7] reports the similar effect of a thin dielectric coating (phthalic acid ester resin) on inner surface of GIS enclosure to prevent particle levitation for a high voltage DC GIS.

The experiments on particle levitation are conducted using an actual busbar at DC voltage application. The particles are made of aluminum and the size is 3mm in length and 0.2mm in diameter. The thickness of the dielectric coating is 30 μm. An impulsive force that simulates the accelerated velocity by circuit breakers and DS operations is given to the enclosure when measuring particle levitation field strength. It is reported that the levitation field for the dielectric coated enclosure is 0.72kV/mm and 2.4 times higher than that for the bare enclosure of 0.3kV/mm.

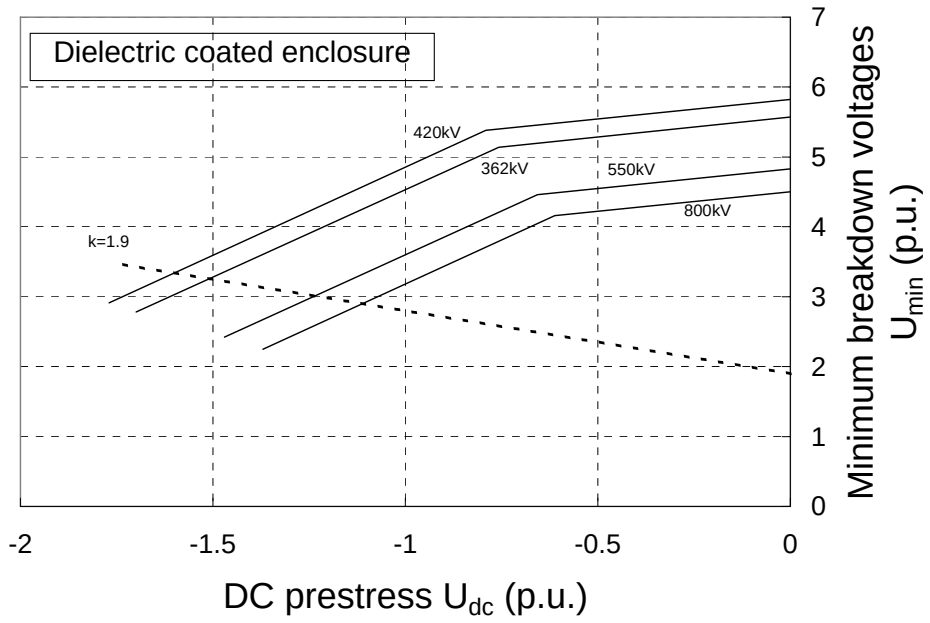

Fig.5.14: Comparison between the minimum breakdown curves U_{min} (solid curves) under composite stresses of VFT+DC with small particles contamination under industrial clean conditions and the overvoltage levels U_{max} (broken line) by DS operation for different rated voltage in the IEC 62271-203, when dielectric coated enclosure is applied.

The above experimental results of [5.6] and [5.7] suggest that the levitation field for the dielectric coated enclosure is 1.4 to 2.4 times higher than that for bare enclosure and also that the values 1.4 to 2.4 could correspond to the insulation design margin *s* defined in Equation (5.3).

Considering the minimum value of 1.4 as the insulation design margin *s*, the above results in Fig. 5.10 is calculated again for a dielectric coated enclosure. Figure 5.14 shows the similar comparison between the minimum breakdown curves U_{min} (solid curves) under composite stresses of VFT+DC with small particles contamination under industrial clean conditions based on Figs.5.5 and 5.4 and the overvoltage levels U_{max} (broken line) by DS, when dielectric coated enclosure is applied. It is noted that even at the rated voltage of 800kV, the minimum breakdown curve U_{min} exceeds the overvoltage level U_{max} at the trapped charge U_{dc} =1.0 which corresponds to the practical maximum value.

The influence of DC prestress on a GIS insulation performance is summarized in Fig. 5.15 (a) and (b) based on the results of Figs 5.10, 5.11 and 5.14, which shows the negative critical DC trapped charges U_{dc} that could lower the dielectric strength of a GIS. The figure suggests the following three points.

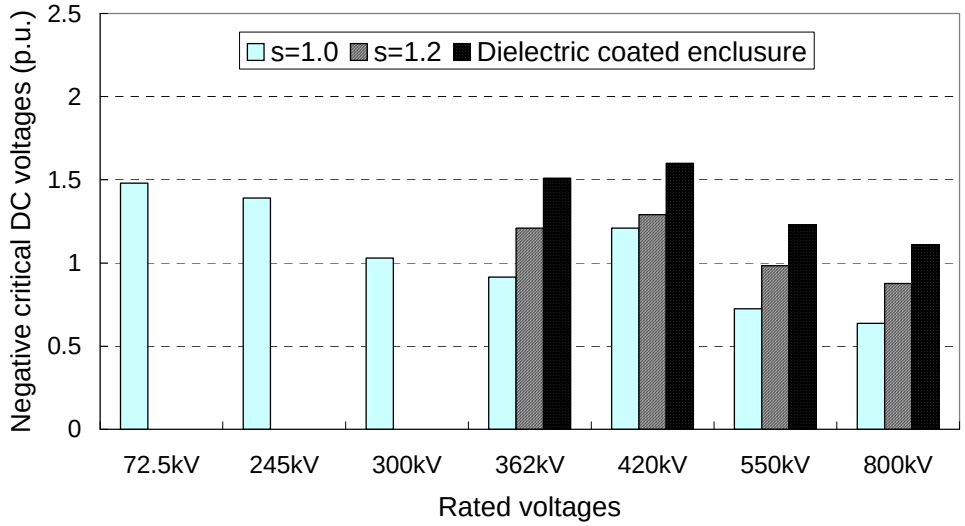

(a) With small particles contamination under industrial clean conditions

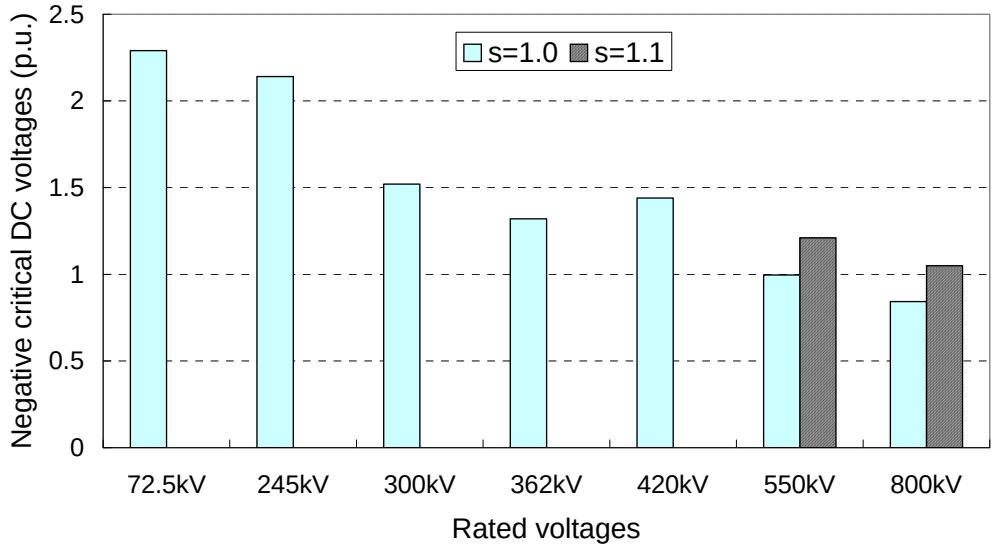

(b) With charge accumulation on spacer surface

Fig.5.15: Negative critical DC trapped charges that lower the dielectric strength of GIS.

The effect of small particles contamination under industrial clean conditions is greater than that of charge accumulation on spacer surface in terms of the influence of DC prestress on a GIS performance. The influence of DC prestress with charge accumulation on spacer surface could be neglected if an appropriate insulation design margin is taken for a GIS. On the other hand the influence of DC prestress with small particles contamination under industrial clean conditions could be prevented by applying a thin dielectric coating such as epoxy resin and phthalic acid ester resin on the inner surface of GIS enclosure.

5.4 Conclusion

The influence of AC and DC prestress on insulation performance of GIS applying IEC 62271-203 is discussed using the experimental results on insulation characteristics under LI and VFT voltages superimposed to AC or DC voltages.

(1) There is no need to consider the influence of AC prestress on a GIS insulation performance under good quality control conditions up to the voltage class of 800kV and also UHV.

(2) In terms of the influence of DC prestress on a GIS performance, the effect of small particles contamination under industrial clean conditions is greater than that of charge accumulation on spacer surface.

(3) The influence of DC prestress with charge accumulation on spacer surface could be neglected if an appropriate insulation design margin is taken for a GIS. On the other hand the influence of DC prestress with small particles contamination under industrial clean conditions could be prevented by applying a thin dielectric coating on the inner surface of GIS enclosure.

REFERENCES of Chapter 5

[5.1] Investigation R&D Committee Chaired by Prof. T. Kawamura, "Properties on Electrical Insulation Related to Testing Voltages and Power Equipment", *Technical Reports by IEE Japan*, No.518 (1994) (in Japanese).

[5.2] G.Luxa, E.Kynast, W.Boeck, H.Hiesinger, A.Pigini, A.Bargigia, S.Schlicht, N.Wiegart and L.Ullrich, "Recent research activity on the dielectric performance of SF_6 with special reference to very fast transients", *1988 CIGRE general session report*, 15-06.

[5.3] A.Bargigia, A.Porrino, B.Mazzoleni, W.Mosca and G.Rizzi, "Performance of metal-clad disconnector and its impact on the insulation design of gas insulated substations", *1988 CIGRE general session report*, 35-15.

[5.4] S.Okabe, T.Okada, S.Yuasa, T.Utsumi, F.Endo and K.Saitoh, "Effect of pre-stress on dielectric characteristics of an insulator in SF_6 gas", *12th ISH*, 4-30, pp.351-354 (2001).

[5.5] Investigation R&D Committee Chaired by Prof. T. Kawamura, "Very Fast Transient Overvoltages and Insulation Issues on GIS", *Technical Reports by IEE Japan*, Part II, No.324 (1990) (in Japanese).

[5.6] T.Hasegawa, K.Yamaji, M.Hatano, F.Endo, T.Rokunohe and T.Yamagiwa, "Development of insulation structure and enhancement of insulation reliability of 500kV DC GIS", *IEEE Trans. Power Delivery,* Vol.12, No.1, pp.194-202 (1997).

[5.7] M.Shikata, K.Yamaji, M.Hatano, E.Tsuchie, H.Takeuchi and K.Inami, "Development and design of DC-GIS", *T. IEE Japan*, Vol.117-B, No.5 (1997) (in Japanese).

6. TEST CONVERSION FACTORS IN SF_6 AND N_2/SF_6 GAS MIXTURES

In this chapter, V-t characteristics are investigated and breakdown voltages between LI, SI and AC voltages are compared to determine the test conversion factors in SF_6 and N_2/SF_6 gas mixtures. Most critical stress in SF_6 and N_2/SF_6 gas mixtures is discussed using the above data.

6.1 Breakdown properties at LI, SI and AC voltages in SF_6

6.1.1 Properties under quasi-uniform field

For the high pressure region, the discharge inception voltage in SF_6 can be calculated by means of the following streamer criterion.

$$N = \int_0^{x_c} \left(\alpha(x) - \eta(x)\right) dx \geq 18...20 \tag{6.1}$$

$$\frac{\alpha - \eta}{p} = 28\,kV \left[\frac{E(x)}{p} - \left(\frac{E}{p}\right)_{\lim} \right]$$

$$\left(\frac{E}{p}\right)_{\lim} = 89\ kV(cm\,bar)^{-1} \tag{6.2}$$

$$for: \quad 50\,\frac{kV}{cm\,bar} \leq \left(\frac{E}{p}\right)_{\lim} \leq 150\,\frac{kV}{cm\,bar}$$

For times longer than several microseconds, the V-t characteristics of quasi-uniform gaps are relatively flat for both polarities, whereas the breakdown voltage for negative polarity is always lower than that for positive polarity.

Table 6.1: Ratio of breakdown voltages between LI, SI and AC at coaxial electrode system. The gas pressure is between 0.1 and 0.41 MPa.

Configuration (mm)	Absolute pressure [kg/cm²(MPa)]	LI/AC(rms)		SI/AC(rms)		SI/LI	
		+LI	−LI	+SI	−SI	+SI/+LI	−SI/−LI
38/200	1 (0.10)	—	—	1.51	—	—	—
	2 (0.20)	1.92	1.70	1.84	1.36	0.95	0.80
	3 (0.31)	2.14	1.61	1.78	1.36	0.90	0.81
	4 (0.41)	2.22	1.91	—	1.32	—	0.69
100/200	1 (0.10)	1.63	1.63	1.63	1.47	1.0	0.9
	2 (0.20)	1.95	1.81	1.87	1.51	0.97	0.84
	3 (0.31)	2.19	1.88	1.74	1.51	0.80	0.80
	4 (0.41)	2.29	1.70	—	1.47	—	0.80
100/320	1 (0.10)	1.61	1.61	1.85	1.47	1.15	0.92
	2 (0.20)	1.99	1.71	2.01	1.56	1.01	0.90
	3 (0.31)	2.19	1.78	2.12	1.58	0.97	0.89
	4 (0.41)	2.26	1.80	2.15	1.58	0.95	0.88
100/540	1 (0.10)	1.74	1.65	1.78	1.43	1.02	0.86
	2 (0.20)	1.99	1.78	1.81	1.43	0.87	0.80
	3 (0.31)	2.18	1.85	—	1.43	—	0.77
200/540	1 (0.10)	1.91	1.77	—	—	—	—
	2 (0.20)	2.14	1.81	—	—	—	—
	3 (0.31)		1.82	—	—	—	—

The data on breakdown properties under quasi-uniform field especially at coaxial electrode system are essential to study the practical test conversion factors. Table 6.1 shows the ratio of breakdown voltages[6.1] - [6.3], that is V_{LI}/V_{ACrms}, V_{SI}/V_{ACrms} and V_{SI}/V_{LI}. Here, V_{LI}, V_{SI} and V_{ACrms} are breakdown voltages at LI, SI and AC rms value, respectively. The experiments are carried out using the different five kinds of coaxial electrode systems. The gas pressure is varied between 0.1 to 0.41 MPa.

In the literature [6.3], the empirical equations of 50% breakdown fields $E_{50\%}$ at pressure P at LI, SI and AC voltages at negative polarity are given as follows.

$$E_{50\%}/P = 66.3 + 33.7/P - 1.85P \ \ (\mathrm{kV/cm/kg/cm^2}) \ \text{at negative LI} \tag{6.3}$$

$$E_{50\%}/P = 55.1 + 55.5/P - 1.61P \ \ (\mathrm{kV/cm/kg/cm^2}) \ \text{at negative SI} \tag{6.4}$$

$$E_{50\%}/P = 40.6 + 40.8/P - 0.78P \ \ (\mathrm{kV/cm/kg/cm^2}) \ \text{at negative AC (Crest value)} \tag{6.5}$$

Here, the diameter of inner conductor and outer enclosure is 50 mm and 96 mm, respectively. The values of V_{LI}/V_{ACrms}, V_{SI}/V_{ACrms} and V_{SI}/V_{LI} are calculated based on the above Equations from (6.3) to (6.5) and summarized in Table 6.2.

Table 6.2: Ratio of breakdown voltages between LI, SI and AC at coaxial electrode system. The gas pressure is between 0.51 and 0.71 MPa.

Absolute gas pressure	−LI/AC(rms)	−SI/AC(rms)	−SI/LI
5kg/cm²•abs(0.51MPa)	2.01	1.84	0.91
6kg/cm²•abs(0.61MPa)	2.01	1.81	0.90
7kg/cm²•abs(0.71MPa)	2.01	1.80	0.89

In the literature [6.4], an empirical formula is proposed to calculate the breakdown field of a technical electrode surface in a nearly homogeneous coaxial electric field for negative polarity. As further discussed in paper [6.4], a higher dielectric strength can be achieved with decreasing electrode roughness.

$$E_b = E_d \ p^z \tag{6.6}$$

$$\text{for } E_d = \begin{Bmatrix} 84\dfrac{kV}{cm\,bar} & for & BIL \\ 75\dfrac{kV}{cm\,bar} & for & SIL \\ 65\dfrac{kV}{cm\,bar} & for & AC \end{Bmatrix} \qquad z = \begin{Bmatrix} 0.71 & for & BIL \\ 0.69 & for & SIL \\ 0.73 & for & AC \end{Bmatrix}$$

p : pressure in bar

The breakdown fields in SF_6 for a technical electrode surface and different voltage waveforms calculated with Equation (6.6) are shown in Fig.6.1.

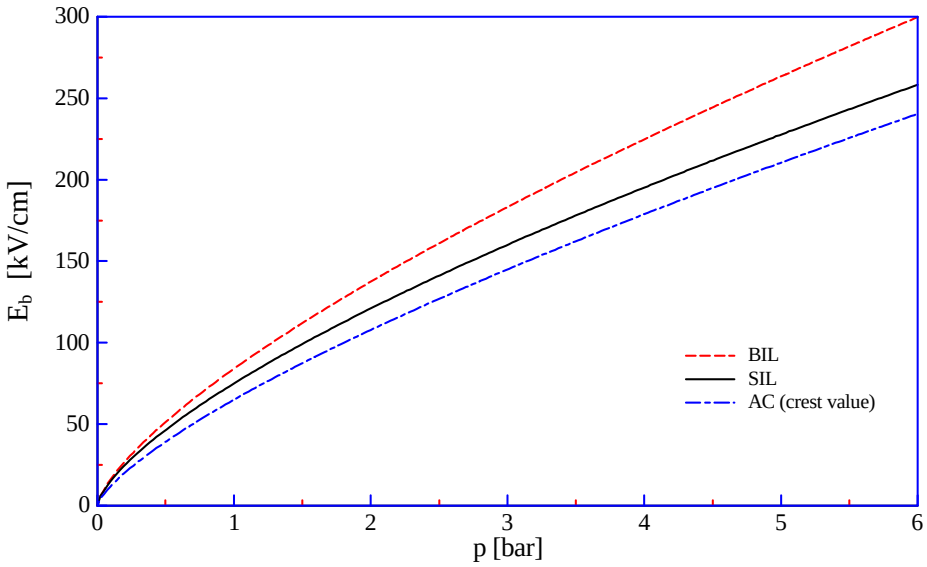

Fig.6.1: Breakdown fields in SF_6 for a technical electrode surface and different voltage waveforms calculated by Equation (6.6).

Further values of E_d and z are given in [6.4] in dependence of the electrode preparation. A higher dielectric strength can be achieved with decreasing electrode roughness. Electrode material and surface preparation have an influence on the breakdown voltage in compressed gases when the electric field is of the order 10-20 MV/m. In this range, Paschen's law is no longer satisfied and the breakdown voltage is lower than the theoretical value. This effect is mainly attributed to field enhancement at micro protrusions which cause field emission of electrons at the cathode. Polishing of the electrode surface reduces the number of field emission sites and therefore increases the breakdown voltage in pure SF_6.

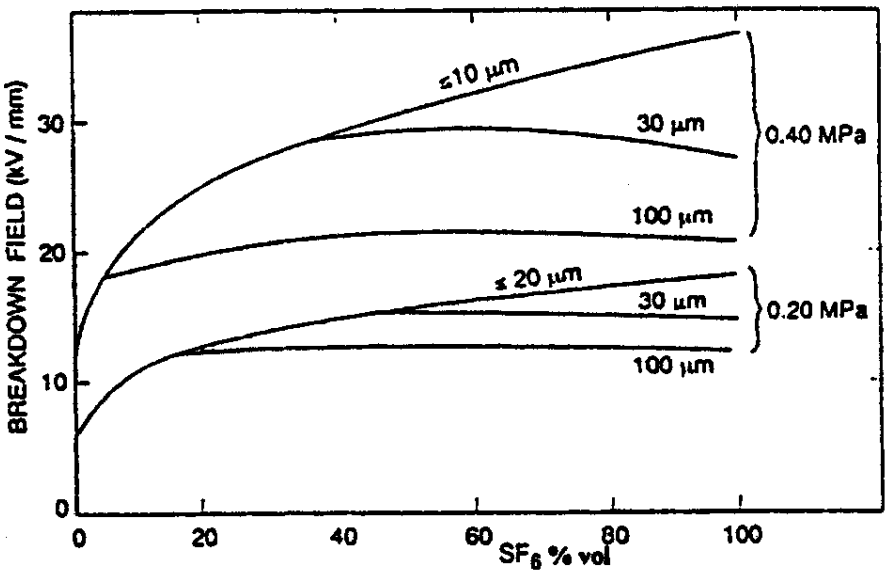

Fig.6.2: Breakdown field versus SF_6 content. The value of the surface roughness indicates the dimensions of the investigated protrusions.

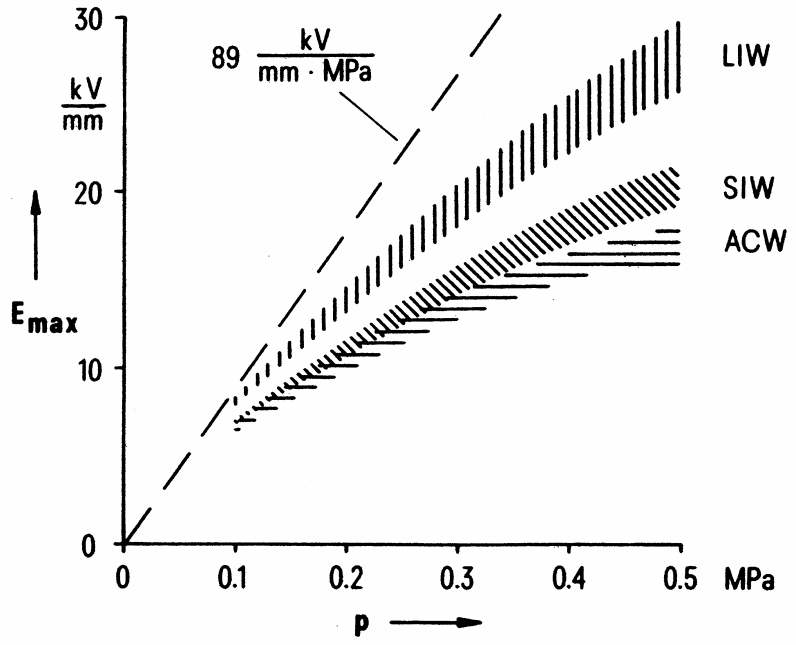

Fig.6.3: Ranges of maximum electric fields for withstand voltages of industrial GIS units at factory tests. The broken line corresponds to the theoretical breakdown field. E_{max}: maximum electric field, P: SF_6 gas pressure, LIW: LI withstand voltage, SIW: SI withstand voltage, ACW: AC withstand voltage (crest value).

According to [6.5], a number of studies have shown that SF_6/N_2 mixtures are less sensitive to electrode surface roughness and particle contamination than pure SF_6 at the low gas pressure range of around 0.4MPa or lower. The effect of electrode surface roughness on the calculated breakdown field is shown in the next Fig. 6.2 taken from the literature [6.5].

Insulation characteristics of industrial GIS components are introduced in [6.6]. The reference reports that in numerous development and type tests it was found that the maximum electric field is a decisive factor for the withstand voltage in SF_6 in quasi homogeneous fields. Fig. 6.3 shows the typical ranges of the maximum electric field versus the SF_6 pressure at different withstand voltages for various industrial GIS components. The broken line corresponds to the theoretical breakdown field. The figure gives the spreading of breakdown fields caused by the difference of industrial GIS components.

The literature [6.7] shows V-t characteristics of 84kV bus system with epoxy cone-type spacers. The experimental setup is shown in Fig.6.4 (a) and the spacers are varied between one and seven in the experiment. Fig. 6.4 (b) shows the example of electric field analysis around cone-type spacer in the bus system of Fig. 6.4 (a). The V-t characteristics of the bus system with one spacer and with seven spacers at 0.3 MPa are shown in Figs. 6.5 (a) and (b), respectively. The applied voltages are negative polarity for both cases. The computed V-t curves by electric field analysis are compared with the experimental data in the figures.

Another aspects that must be considered in GIS are VFT, e.g. due to DS. VFT occurring in GIS has a very short rise time in the order of 10 nanoseconds. Therefore, the V-t characteristic for times shorter than 1 μs is of special interest in the case of GIS.

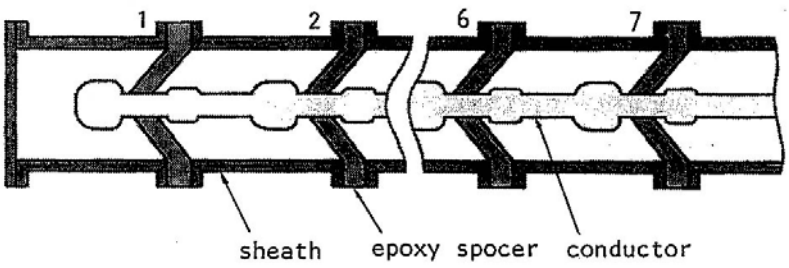

(a) 84kV bus system with cone-type spacer

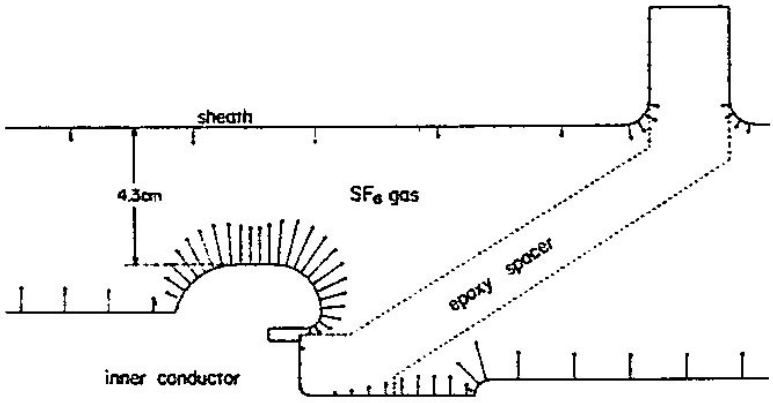

(b) Example of electric field analysis around cone-type spacer

Fig.6.4: Experimental setup and electric field analysis around cone-type spacer.

For times longer than several microseconds, the V-t characteristics of quasi-uniform gaps are relatively flat for negative and positive polarity. The breakdown voltage of negative polarity is always lower than that of positive polarity. For times shorter than 1 μs, the V-t curve for negative polarity rises more steeply with decreasing time than that for positive polarity [6.8] as shown in Fig.6.6. Thus the positive breakdown voltage becomes lower than the negative one. The reversing phenomenon is more pronounced with increasing gas pressure and field non-uniformity. The author notes that "generally negative V-t characteristics have been regarded as the decisive basis for the insulation design of GIS, however it seems to be necessary to consider both polarities, i.e. negative polarity in the time range longer than around one microsecond, and positive polarity for shorter times". Thus the V-t characteristics of negative polarity must be considered to be the dimensioning curve in the long-term region, while the positive polarity is the dimensioning one in the short-term region.

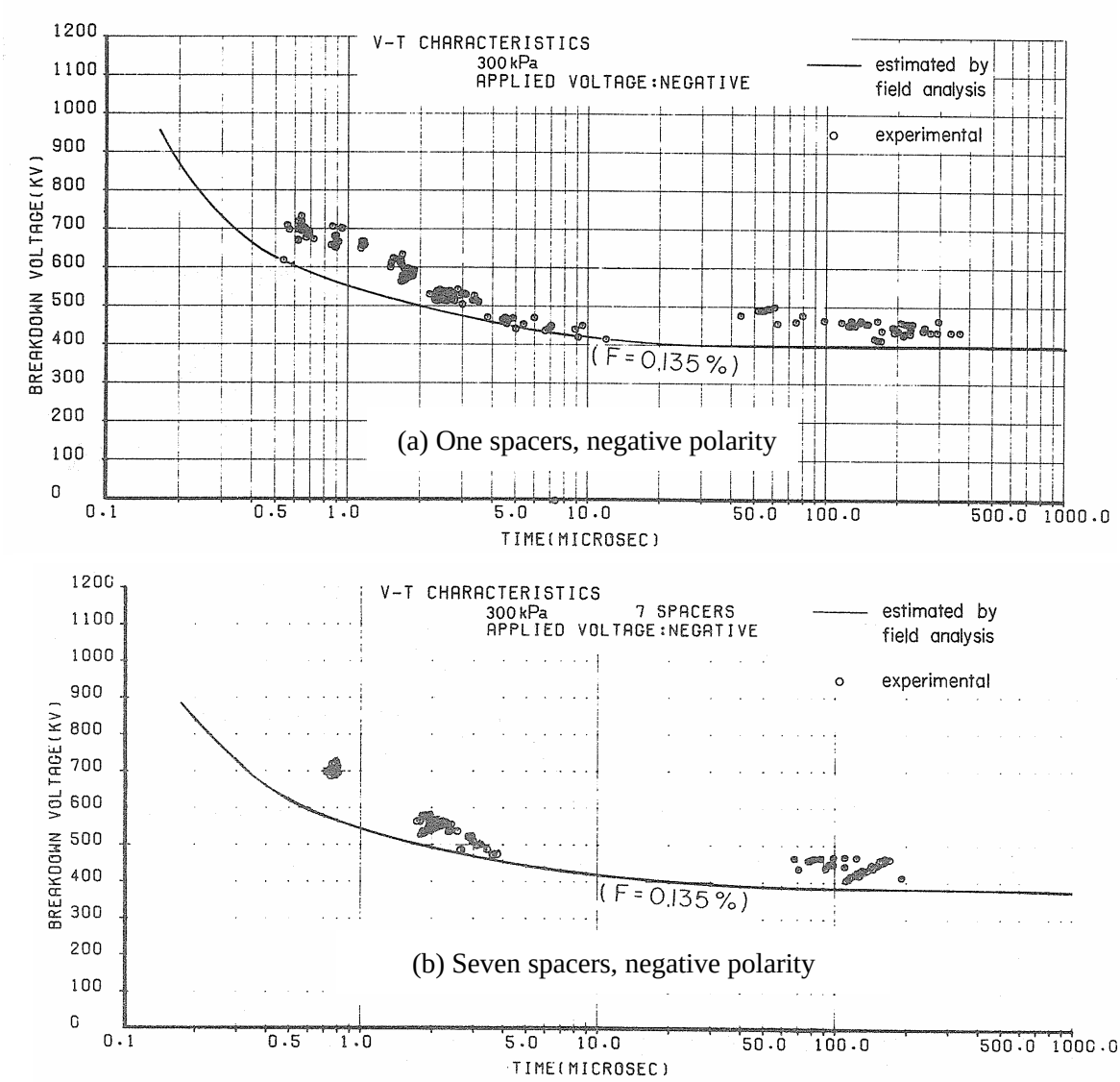

Fig.6.5: Computed V-t curves of 0.135% breakdown probability based on electric field analysis of Fig. 6.3 compared with experimental data.

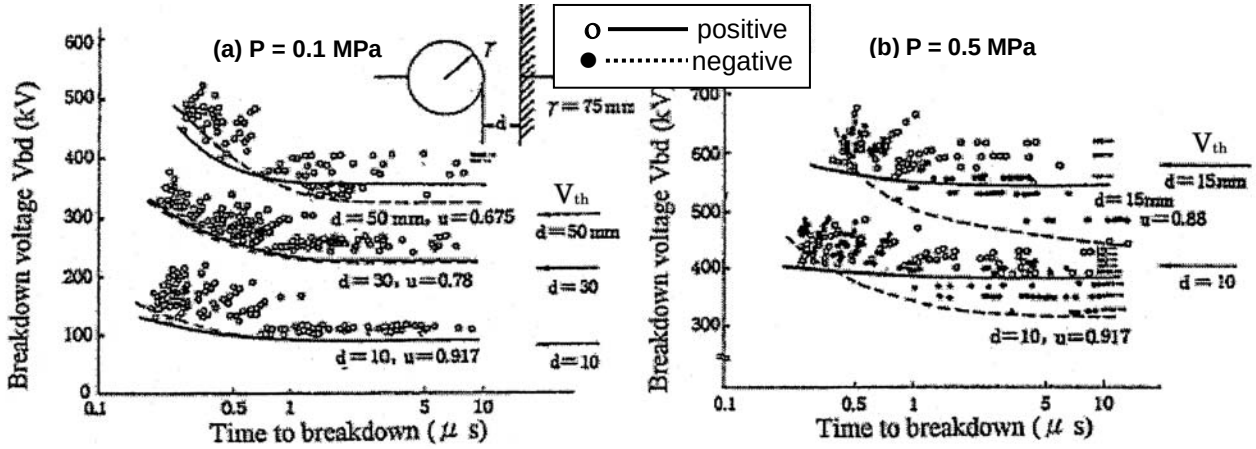

Fig.6.6: V-t characteristics of a quasi-uniform sphere-plane gap. The sphere radius is 75mm.

6.1.2 Properties under non-uniform field

The Dielectric performance of a GIS is sometimes influenced by the existence of metallic particle contaminated in the GIS or a local field concentration at a triple junction at which a solid insulator meets a metallic electrode in SF_6 gas even under clean condition.

In this section, breakdown properties under non-uniform field, that is triple junction initiated surface flashover properties and also particle initiated sparkover and surface flashover properties are introduced to study the V-t characteristics and to compare the breakdown voltages between LI, SI and AC voltages. As to particle initiated sparkover properties, the V-t characteristics at non-uniform field of rod-rod gap configuration are introduced first and followed by the V-t characteristics initiated by a particle of submillimeter diameter.

Fig. 6.7 shows a half cross-sectional view of model spacer system for surface flashover experiments initiated from the triple junction [6.9][6.10]. The material of the spacer is alumina filled epoxy and the relative permittivity is 6.2. The high-voltage and grounded sheath are coated by anodized aluminum (Al_2O_3), while the grounded ring-shape electrodes on both sides of the spacer are bare or coated by dielectric materials of Polytetrafluoroethylene or Al_2O_3.

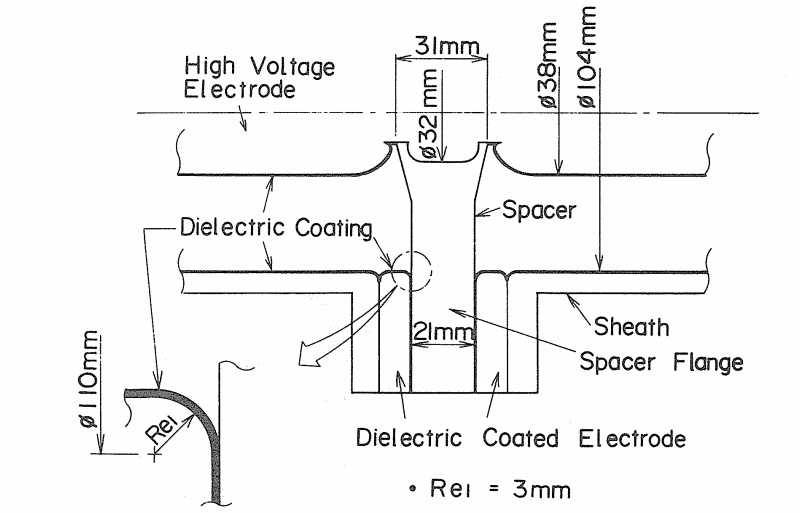

Fig.6.7: Half cross-sectional view of model spacer system for surface flashover experiments initiated from the triple junction.

Fig. 6.8 shows the influence of applied voltage waveform on the surface flashover characteristics initiated from the triple junction at the sheath side at 0.59MPa. Here, the polarity such as +LI, -LI, +SI and -SI in the figure is for the sheath side and the illustrations of applied waveform are for the high-voltage conductor. The surface flashover voltages at +LI are nearly equal to those at +SI, while the flashover voltages at AC are lower than those at +SI and SI polarity reversal. The phenomenon is explained by the polarity reversal at every half cycle of AC voltages, which causes charge accumulation on the insulator surface. The accumulated charge enhances the local field concentration at the triple junction and reduces the AC flashover voltages.

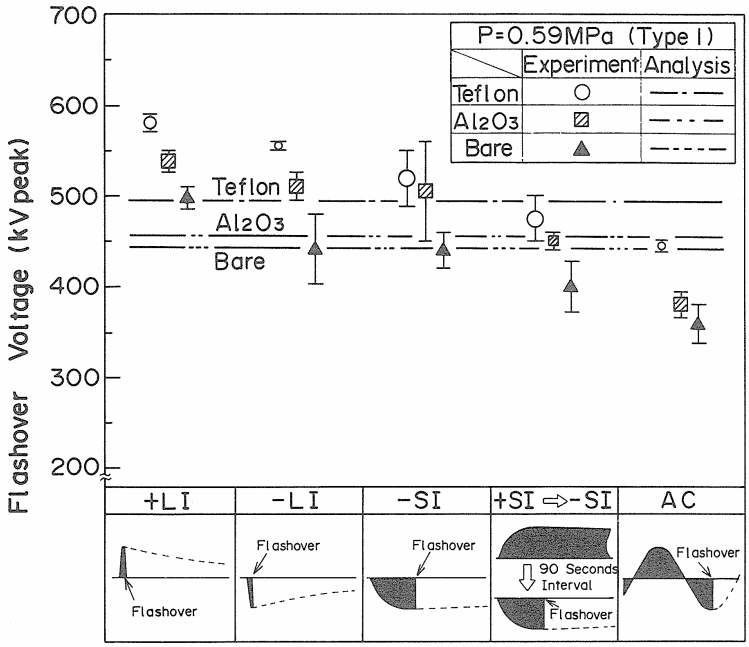

Fig.6.8: Influence of applied voltage waveform on surface flashover characteristics initiated from the triple junction at the sheath side at 0.59MPa.

In [6.8], the V-t characteristics at non-uniform field of rod-rod gap configuration are discussed. It is considered to be that of a strong non-uniform gap as shown in Fig.6.9. The diameter of the rod is 10mm. The V-t characteristics become V-shaped for negative polarity as shown in Fig.6.9 (b). The V-shaped form is more pronounced at higher gas pressures. Whereas the breakdown voltages are nearly independent on polarity for nearly homogeneous electric fields (negative polarity is slightly lower), the sparkover voltages are higher for negative polarity and lower pressure.

Fig. 6.10 shows the V-t characteristics of coaxial electrode system initiated from a metallic particle of sub-millimeter diameter with positive impulse voltages at 0.45MPa [6.11]. The diameters of the inner and outer electrode are 42 mm and 150 mm, respectively. The metallic particle diameter is 0.25mm and the length is varied between 1, 3, 5 and 10mm. The particle is fixed at the high-voltage electrode. The positive sparkover voltages are lower than the negative ones and U-shaped V-t characteristics are observed at positive polarity. These data show that the sparkover voltages at SI are much higher than those at LI, since corona stabilization effect at the tip of a particle is stronger at SI than at LI.

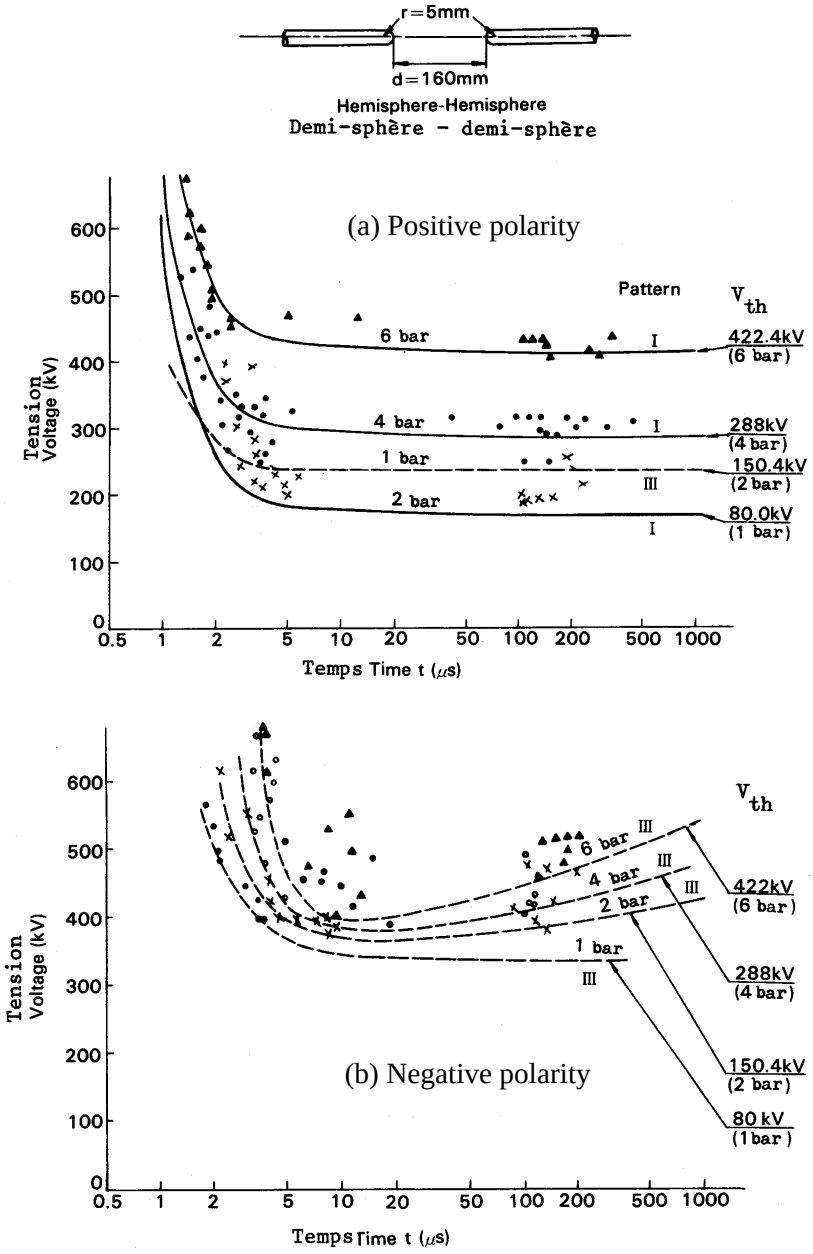

Fig.6.9: V-t characteristics of strong non-uniform electric field of rod-rod gap configuration.

At AC voltages, free metallic particles that move between high-voltage conductor and inner enclosure have different characteristics, compared with fixed particles in a gas gap. In the literature [6.12] [6.13], the breakdown properties by a fixed particle at LI voltages and by free particles at AC voltages are introduced using an actual bus system.

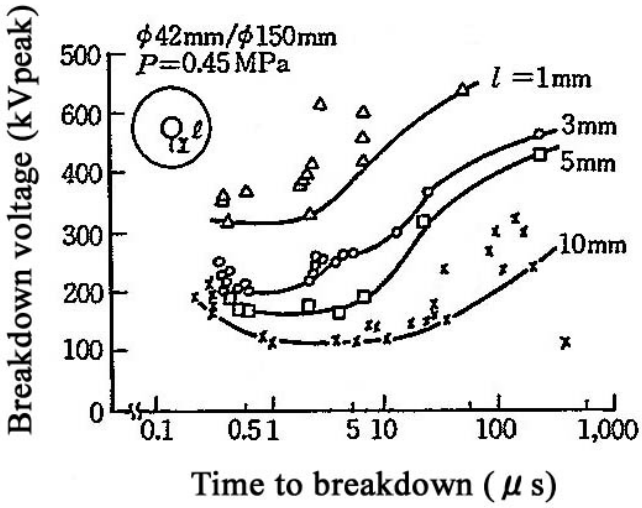

Fig.6.10: V-t characteristics of coaxial electrode system initiated from metallic particle with positive impulse voltages at 0.45MPa. The diameters of the inner and outer electrode are 42 mm and 150 mm, respectively.

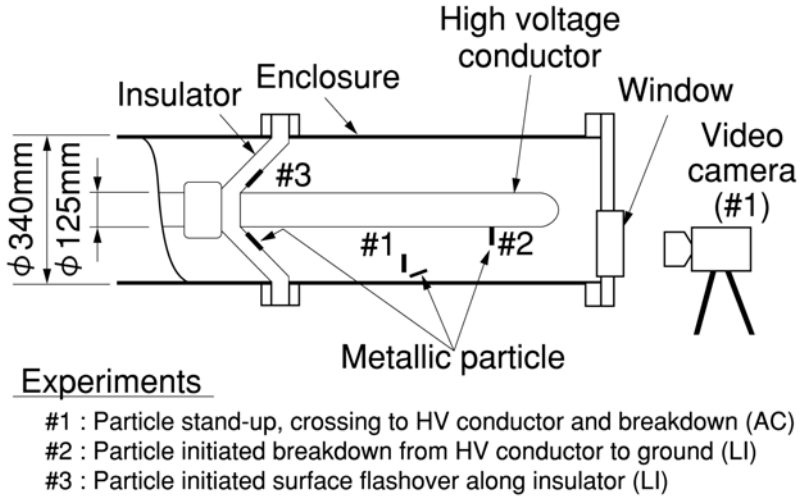

Fig.6.11: Experimental setup for three kinds of measurements under metallic particle contamination in SF_6 and N_2/SF_6 gas mixtures using an actual bus.

Fig. 6.11 shows the experimental setup for the measurements under metallic particle contamination in SF_6 and N_2/SF_6 gas mixtures using an actual bus. The diameter and length of metallic particle is 0.2 mm and 3 mm, respectively. The 50% breakdown voltages initiated by the particle at positive LI as a function of gas pressure of SF_6 and N_2/SF_6 gas mixtures due to the (#2) experiment in Fig. 6.11 are shown in Fig. 6.12. Fig. 6.13 shows time dependent breakdown properties of the actual bus initiated by free metallic particles in pure SF_6 and N_2/SF_6 gas mixtures at AC voltages due to (#1) experiment in Fig. 6.11. Here, for the experimental conditions, three combinations of SF_6 content and design gas pressure, which have the equal dielectric performance with pure SF_6 at 0.4MPa, are chosen from the results of the trial design of 550kV GIB, which will be explained later in Table 6.6.

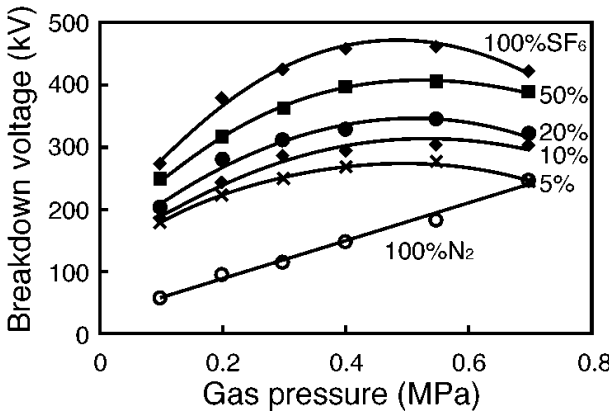

Fig.6.12: 50% breakdown voltages initiated by wire particle at positive LI as a function of gas pressure of SF_6 and N_2/SF_6 gas mixtures due to the (#2) experiment in Fig.6.11.

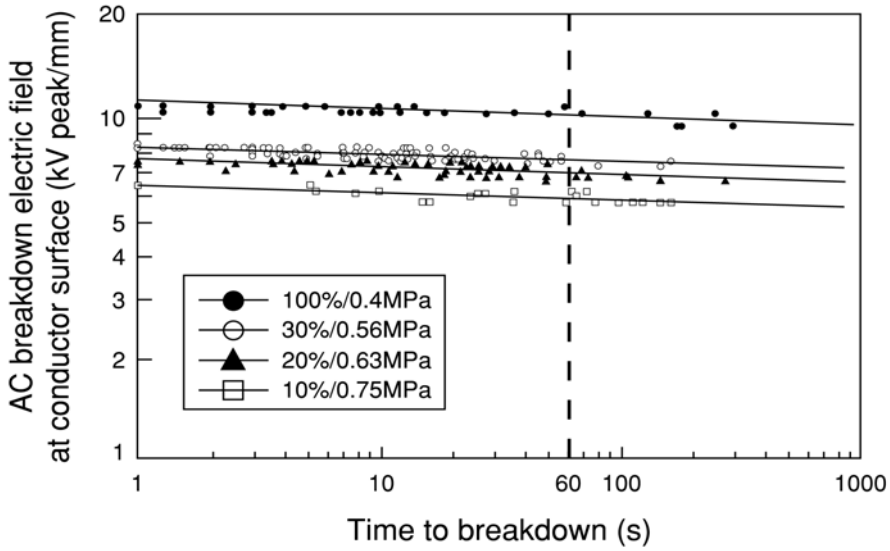

Fig.6.13: Time dependent breakdown properties of an actual bus initiated by free metallic particles in pure SF_6 and N_2/SF_6 gas mixtures at AC voltages.

In the references [6.14] and [6.15], the lift-off voltage as a function of the electric field is investigated using bare and dielectric coated electrodes. It is reported that the lift-off field does not depend on the particle length and gas pressure but depends on the particle material density and the particle shape as shown in Fig.6.14 [6.14]. The induced surface charge acquired by the particle increases linear with the length of the particle. The lift-off voltage seems to be independent of the electrode system. For the parameters investigated in [6.14], the lift-off field is between 4-15 kV/cm for aluminum and 7-27 kV/cm for copper particles in dependence of the particle shape.

In [6.15], the lift-off field is found in the range of 6-8 kV/cm for an aluminum particle of 0.27 mm in diameter and 6 mm in length and a coated electrode system. An increase of the coating thickness improves the dielectric strength but only to a certain limit; further increase in coating thickness does not produce any appreciable improvement. For thin coatings of up to 200 µm, the lifting field is dependent upon the coating thickness [6.16].

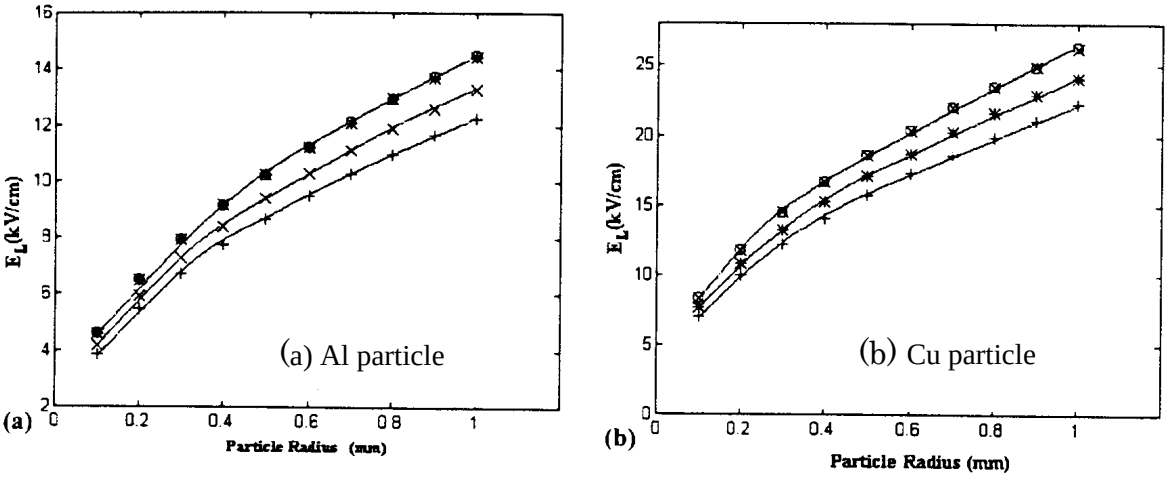

Fig.6.14: Lift-off field in dependence of the particle radius. Four kinds of plot marks in the figures are estimated lift-off field calculated by different models in [6.14]. (O Felici's model, + Indira's model, * Asano's half-cylinder model, × Asano's full-cylinder model)

A metallic particle attached to an insulator surface sometimes causes surface flashover. The surface flashover characteristics initiated by the metallic particles are reported in the references [6.1] and [6.17].

Fig. 6.15 shows the relation between particle diameter and surface flashover voltages at 4 bar [6.1]. The experimental setup is illustrated in the figure. Eight particles are attached to the insulator surface and the length of the particles is 5mm. The surface flashover voltages at LI are nearly constant for the particle diameter between 0.2 and 0.8 mm, while the flashover voltages at AC are strongly influenced by the particle diameter. As decreasing the particle diameter, the flashover voltages increase due to corona stabilization effect at the tip of the particle.

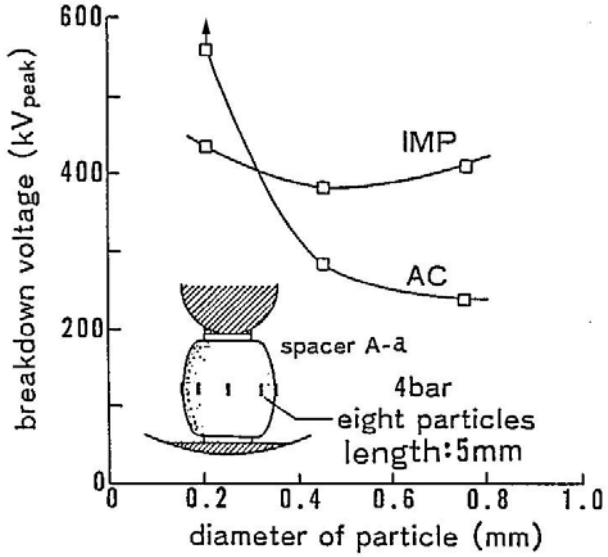

Fig.6.15: Relation between wire particle diameter and surface flashover voltages at 4 bar.

The influence of voltage waveform and applied method on the surface flashover properties and the V-t characteristics at 4 bar are shown in Figs.6.16 [6.17] and 6.17 [6.1], respectively. The experimental setup is the same as Fig.6.15.

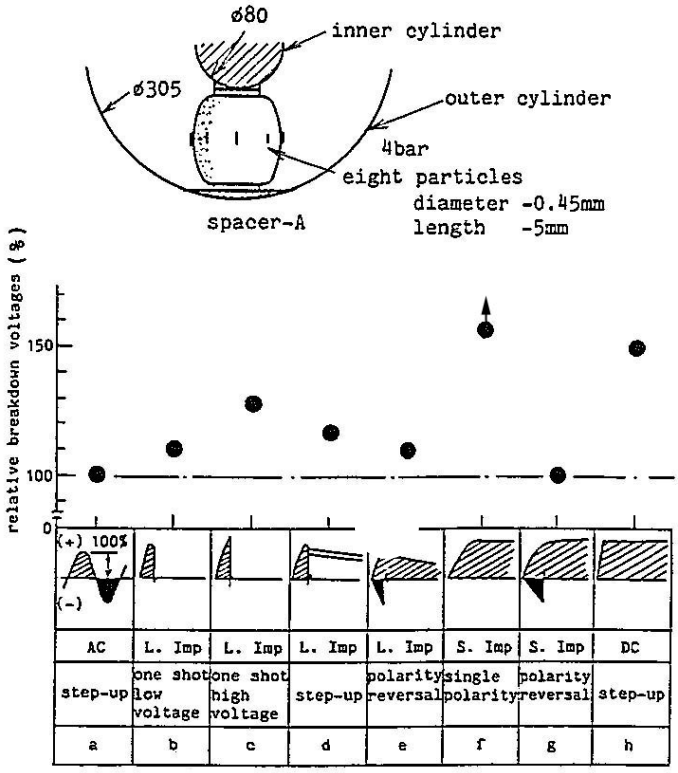

Fig.6.16: Influence of voltage waveform and applied method at 4 bar.

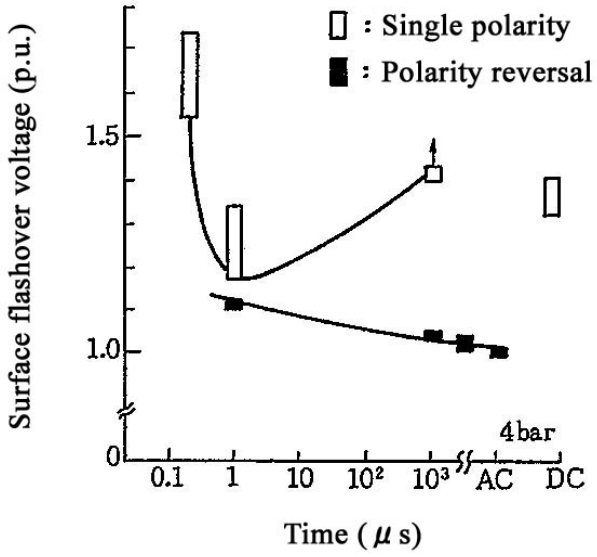

Fig.6.17: V-t characteristics of surface flashover initiated by wire particles at 4 bar.

The particle diameter and length is 0.45mm and 5mm, respectively. The flashover voltages at SI are much higher than those at LI, which shows the same tendency as the particle initiated sparkover properties in Fig.6.10. The flashover voltages at AC are the lowest among LI, SI and AC voltages. The phenomenon at AC voltages is similar to that at the triple junction as shown in Fig.6.8. The repetitive polarity reversal at AC voltages produces charge accumulation on the spacer surface, which enhances the local field at the tip of particle and reduces the flashover voltages.

6.1.3 Test conversion factors in SF_6

Using the data in the sections 6.1.1 and 6.1.2 and also those in IEC [6.18] and CIGRE [6.19], the test conversion factors under quasi-uniform field and non-uniform field in SF_6 are calculated and summarized in Table 6.3 (a) and (b), respectively. Generally, the test conversion factors under non-uniform field are not defined even in IEC and The Institute of Electrical Engineers of Japan (IEEJ). However, the factors are calculated to discuss what kind of voltage tests is effective to find out the defect such as a metallic particle and a local field concentration at triple junction. The discussion will be presented in the section 6.3.1.

The test conversion factors under quasi-uniform field investigated by IEC, IEEJ and CIGRE are shown and compared in the table. Here, the conversion factors by IEEJ are obtained from the values between 0.41 and 0.71MPa in Tables 6.1 and 6.2. The values of V_{LI}/V_{SI} and V_{ACrms}/V_{SI} scatter between 1.10 and 1.45 and between 0.54 and 0.76, respectively, whose mean values of 1.28 and 0.65 are adopted in Table 6.3 (a). Comparing the above conversion factors, there is not a significant difference between IEC, IEEJ and CIGRE.

The values of V_{LI}/V_{SI} and V_{ACrms}/V_{SI} derived from the data by 84kV GIS bus system and by the empirical equation are within the scatter of the IEEJ data between 1.10 and 1.45 and between 0.54 and 0.76, respectively.

The V-t characteristics under non-uniform field are quite different from those under quasi-uniform field. The tendency of the conversion factors V_{SI}/V_{LI} and V_{ACrms}/V_{LI} under non-uniform field are different between “Triple junction” and “Particle contamination” as shown in Table 6.3 (b). The V-t characteristics of “Triple junction” are flat at the time range between LI and SI. However, the breakdown voltages at SI are higher than those at LI regarding “Particle contamination”. It should be also noted that the value of V_{ACrms}/V_{LI} depends strongly on the particle diameter in the case of “Insulator surface”, that is, a thin wire particle smaller than 0.3mm diameter has the higher V_{ACrms}/V_{LI} value, while a thick particle has the lower value.

Table 6.3 (a): Test conversion factors under quasi-uniform field in SF_6.

Conditions		Items		Conversion factors			Experimental conditions				References
				LI	SI	AC (rms)	P (MPa)	Polarity *1	Configuration (Inner/Outer diameter)	Particle (Diameter/Length)	
Quasi-uniform	Clean	Range I ≦ 245kV	IEC	1.25	1.0	0.99/√2=0.7	No data	Negative	Coaxial electrode	None	[6.18]
		Range II >245kV	IEC	-	1.13x√2=1.6	1.0	No data		Coaxial electrode		
			IEEJ	-	1.09x√2=1.54	1.0	0.41-0.71		Coaxial electrode*2		[6.1]
		IEEJ		1.28	1.0	0.92/√2=0.65	0.41-0.71		Coaxial electrode*2		
		CIGRE		1.0	0.75	0.64/√2=0.45	0.4-0.8		Coaxial electrode		[6.19]
				1.37	1.0	0.83/√2=0.59	0.5		Coaxial electrode		[6.6]
		84kV GIS bus system		1.37	1.0	0.98/√2=0.69	0.2		Φ160/Φ255mm *3		[6.7]
				1.37	1.0	0.96/√2=0.68	0.2		Φ160/Φ255mm *4		
		Empirical equation		1.16	1.0	0.93/√2=0.66	0.4-0.7		Coaxial electrode		[6.4]

*1 Voltage polarity that shows lower breakdown voltages.
*2 Configuration: Φ38/Φ200mm, Φ100/Φ200mm, Φ100/Φ320mm, Φ100/Φ540mm, Φ200/Φ540mm, Φ32/Φ96mm, Φ50/Φ96mm.
*3 84kV Bus system with one spacer. The sparkover occurs between high voltage electrode and enclosure.
*4 84kV Bus system with seven spacers. The sparkover occurs between high voltage electrode and enclosure.

Table 6.3 (b): Test conversion factors under non-uniform field in SF_6.

Conditions		Items		Conversion factors			Experimental conditions				References
				LI	SI	AC (rms)	P (MPa)	Polarity *1	Configuration (Inner/Outer diameter)	Particle (Diameter/Length)	
Non-uniform	Clean	Triple junction		1.0	1.0	0.81/√2=0.57	0.59	Positive	Φ38/Φ104mm Disk-type spacer *2	None	[6.9]
	Particle contamination	Gas gap	Fixed to electrode	1.0	2.27	-	0.45	Positive	Φ42/Φ150mm	Φ0.25/3mm	[6.1] [6.11]
				1.0	2.56	-				Φ0.25/5mm	
			Free	(1.0) *3	(>1.0) *3	1.35/√2=0.96	0.4	No data	Φ125/Φ430mm	Φ0.2/3mm	[6.12][6.13]
		Insulator surface		1.0	(>1.0)	1.27/√2=0.90	0.4	Positive	Φ80/Φ305mm Post-type spacer	Φ0.2/5mm	[6.1] [6.17]
				1.0	>1.13	0.80/√2=0.57				Φ0.45/5mm	

*1 Voltage polarity that shows lower breakdown voltages.
*2 Surface flashover occurs from the triple junction at the earth side.
*3 Using the breakdown field data in the case of "Fixed to electrode" as a reference.

6.2 Breakdown properties at LI, SI and AC voltages in N_2/SF_6 gas mixtures

6.2.1 Properties under quasi-uniform field

Equation (6.1) is also valid for SF_6 gas mixtures when substituting $(E/p)_{lim\ SF6}$ by $(E/p)_{lim\ mix}$. For SF_6/ N_2 gas mixtures, $(E/p)_{lim\ mix}$ can be calculated according to [6.20]:

$$\left(\frac{E}{p}\right)_{\lim.\,mix.} = 40\left(\frac{\chi}{\%}\right)^{0.17} \quad \frac{kV}{cm\ bar} \tag{6.7}$$

for χ = ratio of SF_6 to N_2 and $\chi \geq 0.5\%$.

This simple formula is in very good agreement with sophisticated computer simulations based on impact models. A list of measured and/or calculated $(E/p)_{lim}$ values can be found in the references [6.20] and [6.21].

Fig. 6.18 [6.22] shows critical field strength of N_2/SF_6 mixture as a function of SF_6 percentage. It should be noted that the sold line in the figure is completely consistent with the value calculated by the above Equation (6.7).

Fig. 6.19 shows the normalized values of the intrinsic dielectric strength E^0_{cr}, the required pressure p^0 for mixtures of equal intrinsic dielectric strength, and the resulting total amount and leakage rate q^0 of SF_6 [6.23]. The example shows that a mixture with a low SF_6 content of 20% has 69% of the dielectric strength of pure SF_6; that a modest pressure increase of only 45% is necessary to achieve the same strength as pure SF_6; and that the required SF_6 amount and the resulting leakage rate is considerably reduced, by 71%.

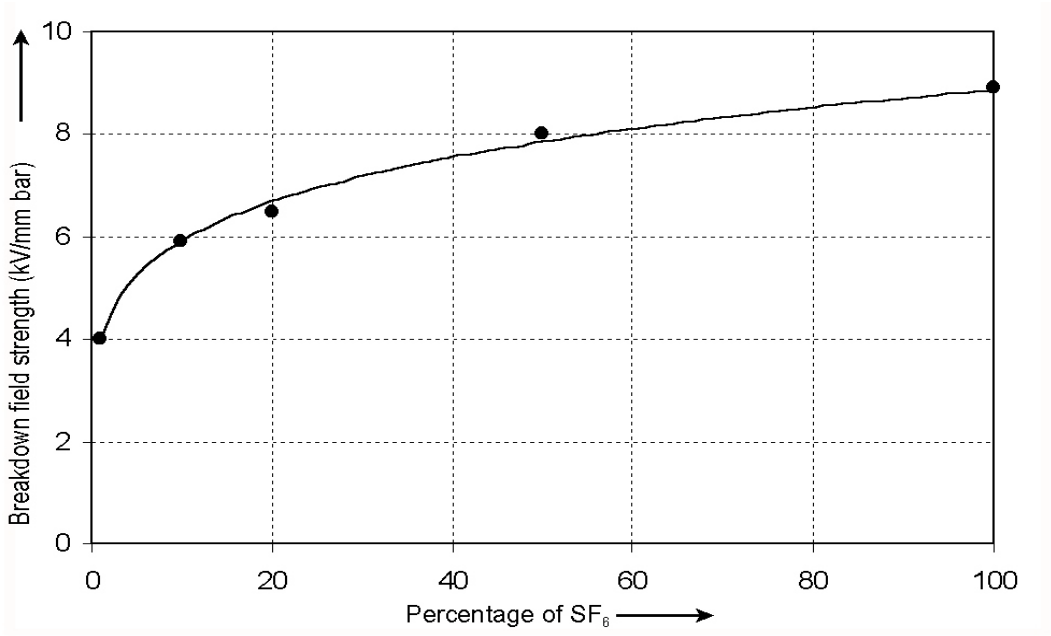

Fig.6.18: Critical field strength of N_2/SF_6 mixture as a function of SF_6 percentage.

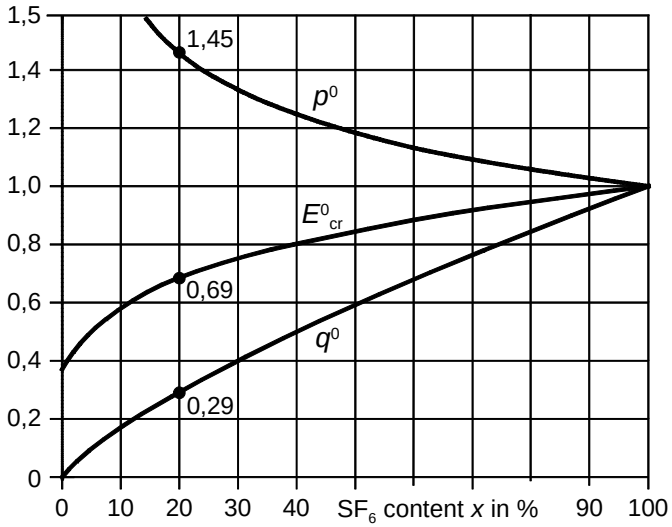

Fig.6.19. Normalized intrinsic dielectric strength E^0_{cr}, normalized pressure p^0 required for equal dielectric strength and resulting normalized quantity or leakage rate q^0 of SF_6 as a function of the SF_6 content x.

Regarding breakdown properties at LI, SI and AC voltages in N_2/SF_6 gas mixtures under quasi-uniform field, the following data are available.

Fig. 6.20 (a) shows experimental setup for breakdown voltage measurements in N_2/SF_6 gas mixtures using an actual bus system [6.13]. The electrodes tested are made of aluminum alloy whose diameter and length are 240mm and 100mm, respectively. The distance between each electrode is set to 150mm to avoid the interference with each other. The utilization factor of the test electrode system is around 0.59 equivalent to an actual bus. The number of the electrodes is changed between one and twelve to investigate area effect of breakdown electric fields.

The pressure dependence of the minimum field $E_{0.1\%}$ at positive and negative LI and AC voltages when the effective electrode area is infinitely large are shown in Fig.6.20 (b) [6.13]. The SF_6 content of the gas mixtures is 10 and 20%. The minimum field $E_{0.1\%}$ increases as raising the gas pressure. However, the pressure dependence at AC voltages seems to be weaker than that at LI voltages. The tendency suggests that the area effect of breakdown would be more prominent at AC voltages rather than at LI voltages.

Fig. 6.21 shows the ratio V_{LI}/V_{AC} as a function of the gas pressure [6.13] [6.24]. Using the data in Fig.6.20 (b), the minimum breakdown voltages considering the area effect are taken into account for the values of V_{LI} and V_{AC} in AC crest value. The values of V_{LI}/V_{AC} reported in the literature applying actual GIL [6.25] - [6.27] and GIB [6.28], whose utilization factors are between 0.56 and 0.6, are also plotted in the figure. The values V_{LI}/V_{AC} including those in the literature increase as raising the gas pressure and are approximately expressed by a solid line regardless of the SF_6 content between 5 and 20%. The tendency can be explained by the weak pressure dependence of the V_{AC} compared with the V_{LI} due to the area effect of breakdown. As the example of IEC 517 and IEC 62271-203 at the rated voltage of 550kV, both cases of LIWV/ACWV ratio are calculated and plotted by the dotted lines in Fig.6.21. Here, the ACWV is a crest value in the calculation of LIWV/ACWV ratio. It should be noted that ACWV is more critical withstand voltages than LIWV over 0.8MPa for IEC 517, while over 0.53MPa for IEC 62271-203, respectively.

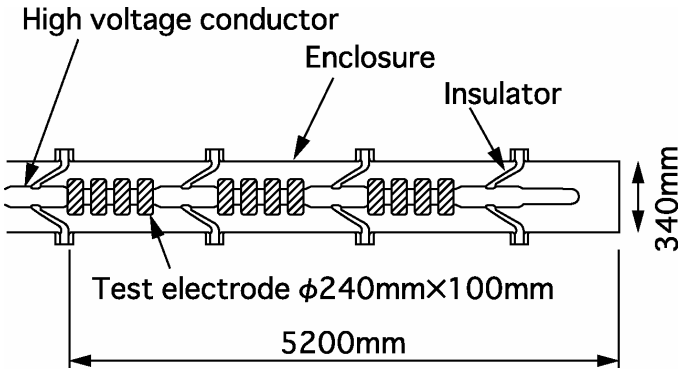

(a) Experimental setup for breakdown measurements using an actual bus.

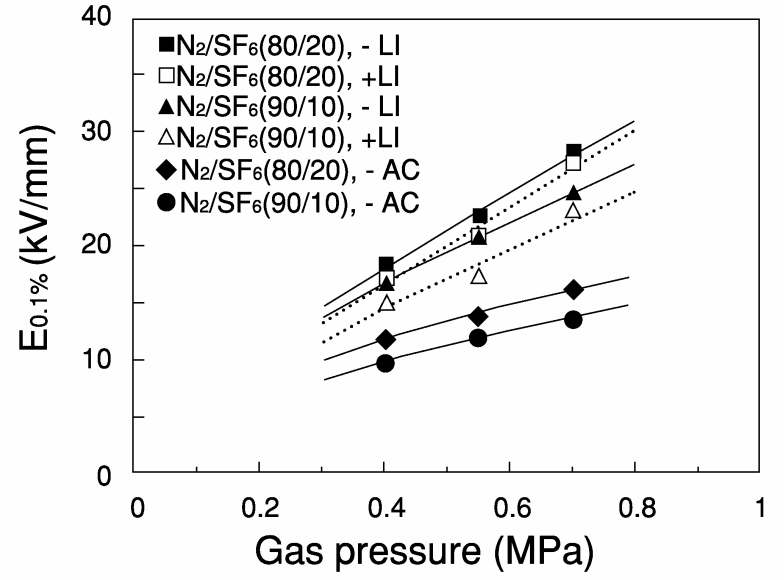

(b) Dependence of minimum breakdown field $E_{0.1\%}$ of 0.1% breakdown probability of Weibull distribution on gas pressure at LI and AC voltages (crest values) when effective electrode area is infinitely large.

Fig.6.20: Experimental setup and pressure dependent minimum breakdown field $E_{0.1\%}$.

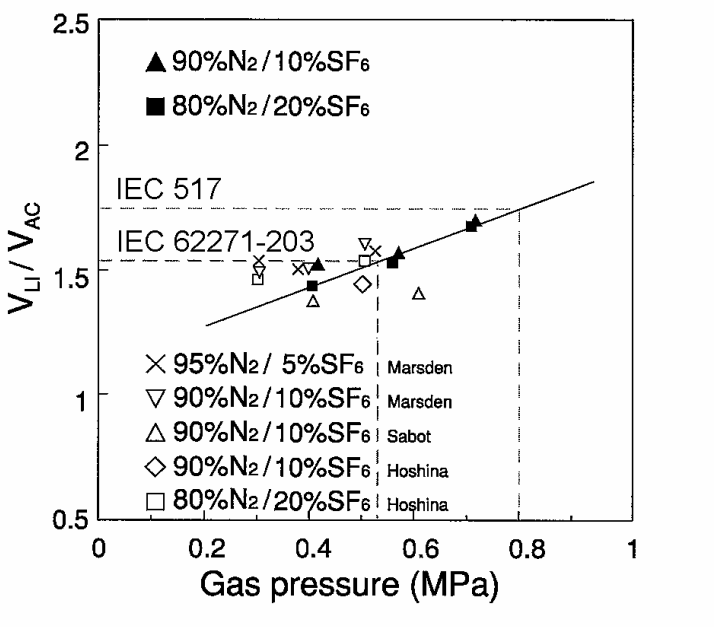

Fig.6.21: Pressure dependence of impulse ratio V_{LI}/V_{AC}. (V_{AC} : crest value)

The boundaries of dominant withstand voltages are shown in Fig.6.22 [6.24] for the insulation design regarding LIWV and ACWV at the standards of IEC, IEEE Std C37.122-1993 and also JEC-2350-2005 [6.29]. The curves in the figure are derived from the solid line in Fig.6.21, showing pressure dependent AC breakdown voltages when LI breakdown voltages V_{LI} are set to be constant and equal to the rated LIWV. The rated ACWV for the standards is plotted in the curves.

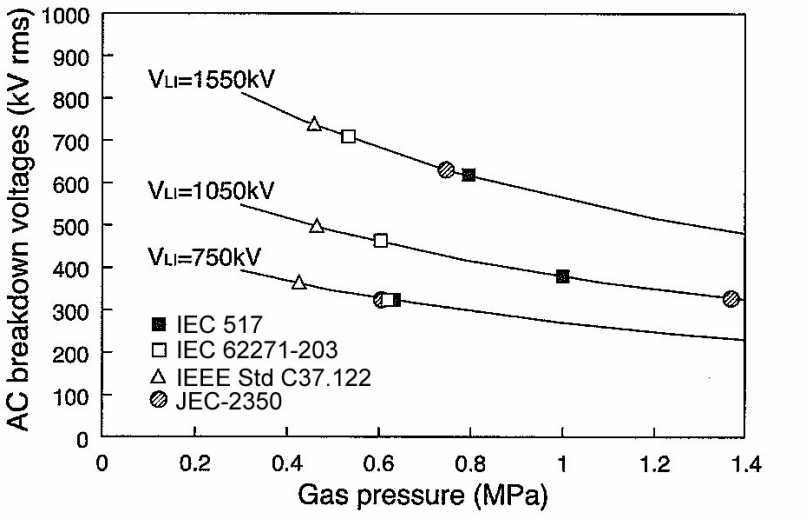

Fig.6.22: Boundary of dominant withstand voltages for the insulation design regarding LIWV and ACWV at the four kinds of standards.

Table 6.4: Test conversion factor between AC and LI.
Reference number in the table is referred to the literature [6.22].

Ref	Ratio	Pressure (kPa)	SF_6 percentage in gas mixtures								
			0%	5%	10%	15%	20%	30%	40%	60%	100 %
[20]	$K_{tPF/LI}$	400-800									0.64
[31]	$K_{tPF/LI}$	400									0.76
[21]	$K_{tPF/LI}$	450							0.73	0.72	0.72
[32]	$K_{tPF/LI}$	500									0.62
[31]	$K_{tPF/LI}$	600									0.70
[32]	$K_{tPF/LI}$	600									
[36]	$K_{tPF/LI}$	600					0.77				
[21]	$K_{tPF/LI}$	620					0.71		0.71	0.70	0.69
Mean value		$K_{tPF/LI}$					0.74		0.72	0.71	0.69
Note: In the present table peak voltages are considered for calculation, while in chapter 6 PF rms											

Table 6.5: Test conversion factor between SI and LI.
Reference number in the table is referred to the literature [6.22].

Ref	Ratio	Pressure (kPa)	SF_6 percentage in gas mixtures								
			0%	5%	10%	15%	20%	30%	40%	60%	100 %
[20]	$K_{tSI/LI}$	400-800									0.75
[21]	$K_{tSI/LI}$	450							0.76	0.79	0.81
[22]	$K_{tSI/LI}$	500									0.72
[21]	$K_{tSI/LI}$	520					0.71		0.75	0.79	0.81
[36]	$K_{tSI/LI}$	600					0.77				
[32]	$K_{tSI/LI}$	600	*>0.80*			*0.75*					
[21]	$K_{tSI/LI}$	620					0.70		0.74	0.75	
Mean value		$K_{tSI/LI}$					0.73		0.75	0.77	0.77

Therefore, the breakdown voltages at LIWV are equal to those at ACWV at the plotted points.

The values in IEC 62271-203 and IEEE Std C37.122 are located between 0.4 and 0.6MPa, while those in IEC 517 and JEC-2350 over 0.6MPa. Therefore, the reference [6.24] notes that for the insulation design using low SF_6 content and highly pressurized gas mixtures, ACWV is severer than LIWV when the standards with high ACWV levels such as IEC 62271-203 and IEEE Std C37.122 are applied.

The conversion factors in N_2/SF_6 gas mixtures at industrial configuration are reported by recent CIGRE Working Group [6.22],[6.30] - [6.32]. Tables 6.4 and 6.5 show the conversion factors between AC and LI and between SI and LI, respectively. From the practical point of view, the data of the gas mixtures of SF_6 content of 60% or lower and at high gas pressure around 600kPa are selected in the tables.

In [6.32], the breakdown properties of low SF_6 content and highly pressurized N_2/SF_6 gas mixtures are investigated at LI, SI and AC voltages using an actual bus system. Fig. 6.23 shows the experimental setup of a coaxial electrode for the investigation. The outer diameter of the conductor and the inner diameter of the enclosure are 120mm and 400mm, respectively.

The Comparison of the maximum withstand values of LI, SI and AC voltages for N_2-insulation with small amount of SF_6 admixed at a total pressure of 0.6MPa is shown in Fig.6.24. The literature [6.32] reports that no significant difference was recognized between the SI values and the crest values of the AC voltages, with the result that both voltage types could be combined in one scattering range.

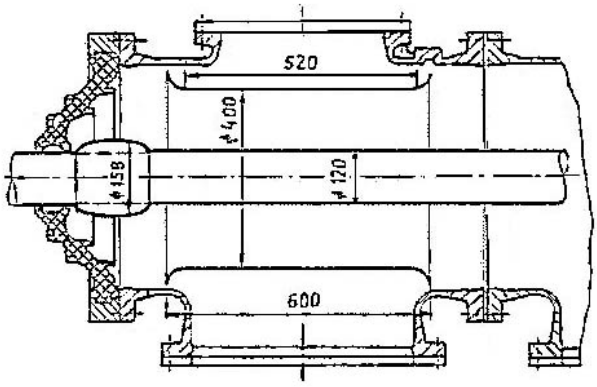

Fig.6.23: Test setup for investigation of N_2/SF_6 gas mixtures.

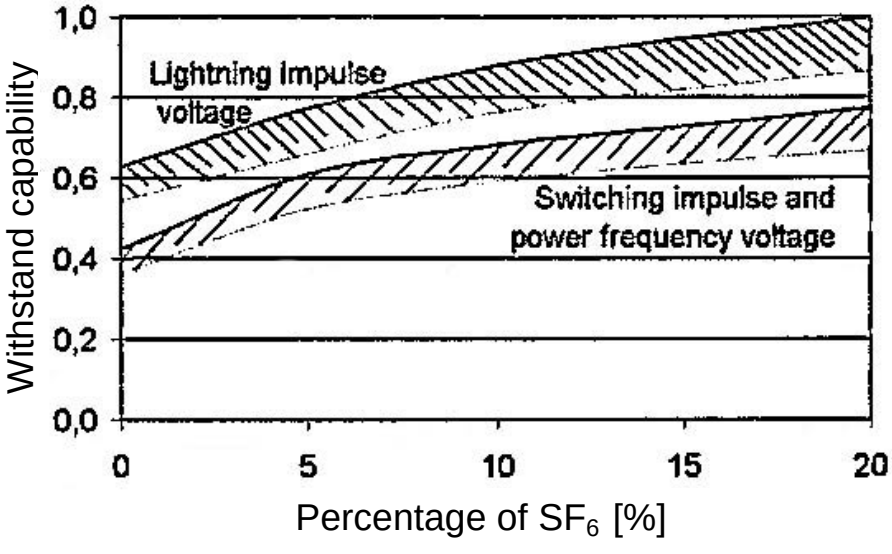

Fig.6.24: Comparison of the maximum withstand values of lightning impulse, switching impulse and AC voltage for N_2-insulation with small amount of SF_6 admixed at a total pressure of 0.6MPa.

6.2.2 Properties under non-uniform field

In the references [6.5] and [6.33], it is reported that at equal gas pressure, SF_6/N_2 gas mixtures are less sensitive to insulation defects than undiluted SF_6 and that SF_6/N_2 mixtures are less sensitive to particle contamination than pure SF_6.

On the other hand, the research on low-SF_6-content and high-pressure N_2/SF_6 gas mixtures has been conducted to apply the gas mixtures to GIL and GIB to reduce SF_6 use and emission to the atmosphere, since SF_6 is identified as one of the potent green house gases [6.23].

The references [6.12] and [6.13] study a trial design of 550kV/8kA GIB applying N_2/SF_6 gas mixtures. Table 6.6 shows the combination of SF_6 content and design pressure which has the equal dielectric performance with pure SF_6 at 0.4MPa as the results of the trial design. Dielectric performance of the gas mixtures under metallic particle contamination is compared with that of pure SF_6, using the experimental setup shown in Fig. 6.11.

Fig. 6.25 shows the comparison of dielectric performance of the GIB against metallic particles in the gas conditions in Table 6.6 [6.13] [6.23]. The 50% breakdown voltages are normalized by those in pure SF_6 at 0.4MPa. For three cases of crossing at AC voltages (#1), fixed to the high-voltage conductor at positive LI (#2) and attached to the insulator at positive LI (#3) in Fig.6.11, the breakdown voltages decrease as lowering SF_6 content and increasing gas pressure. Here, AC breakdown voltages at the #1 experiment are the values at 60 seconds in Fig.6.13 which corresponds to the time duration specified in the rated ACWV of IEC 62271-203. Therefore, the references [6.13] and [6.23] note that a metallic particle lowers the dielectric performance of the gas mixtures as reducing SF_6 content and increasing the gas pressure at positive LI and AC.

Table 6.6: Combination of SF_6 content and design pressure which has the equal dielectric performance with pure SF_6 at 0.4MPa as the results of the trial design of 550kV/8kA GIB.

SF_6 content	100%	30%	20%	10%
N_2 content	0%	70%	80%	90%
Design pressure	0.4MPa	0.56MPa	0.63MPa	0.75MPa

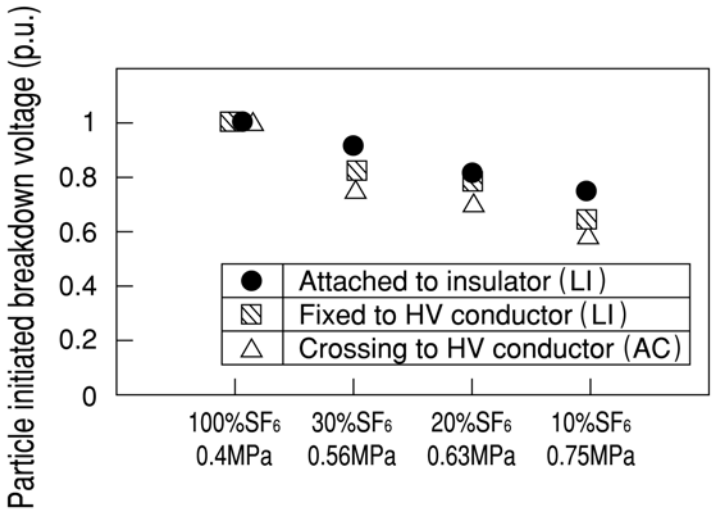

Fig.6.25: Comparison of dielectric performance of the GIB against metallic particles in four gas conditions in Table 6.6. In the case without particles, the dielectric performance of the gas mixtures is identical to pure SF_6 at 0.4MPa.

6.2.3 Test conversion factors in N_2/SF_6 gas mixtures

The test conversion factors V_{LI}/V_{SI}, V_{ACrms}/V_{SI} and V_{LI}/V_{ACrms} under quasi-uniform field are calculated based on the data explained in section 6.2.1 and are summarized in Table 6.7. The breakdown voltages at low SF_6 content of 20% or lower and at high gas pressure from 0.52 to 0.7 MPa are used to obtain the test conversion factors from the practical point of view of the equipment applying the N_2/SF_6 gas mixtures.

The test conversion factors V_{LI}/V_{SI} and V_{LI}/V_{ACrms} in N_2/SF_6 gas mixtures under quasi-uniform field are higher than those in SF_6. Assuming that SI breakdown voltages V_{SI} are nearly equal to AC breakdown voltages V_{AC} in crest value based on the data in [6.30] and [6.32], the V_{LI}/V_{SI} value in N_2/SF_6 gas mixtures is between 1.30 and 1.66, while the value in SF_6 is between 1.10 and 1.45 as described in section 6.1.3.

6.3 Most critical stress in SF_6 and N_2/SF_6 gas mixtures

6.3.1 Most critical stress in SF_6

Applying the test conversion factors given in Tables 6.3 (a) and (b), the voltages calculated by the conversion factors are compared with the rated withstand voltages and the most critical withstand voltage is discussed. Here, the rated withstand voltages are LIWV, switching impulse withstand voltage (SIWV) and ACWV.

Figures 6.26 (a)-(d) show the comparison between the rated withstand voltages for GIS and the voltages calculated by the test conversion factors of V_{LI}/V_{SI} and V_{AC}/V_{SI} under quasi-uniform field. Note that V_{AC}/V_{SI} instead of V_{ACrms}/V_{SI} are used to calculate the voltages by the crest value of AC. The values of LIWV, SIWV and ACWV are referred to IEC 62271-203. The rated voltages are 550kV, 300kV, 245kV and 72.5kV, respectively.

Under quasi-uniform field condition, it is recognized that LIWV is basically the most critical stress to a GIS, while some data show that SIWV stress is the most critical in the Range II of 300kV or higher of IEC 62271-203. On the other hand, in the case of the Range I, LIWV is basically the most critical stress.

Figures 6.27 (a) and (b) show the comparison between LIWV, SIWV and ACWV and the voltages calculated by the conversion factors of V_{SI}/V_{LI} and V_{AC}/V_{LI} under non-uniform field in SF_6.

The figures show that LIWV is the most critical stress if the field is non-uniform by the defect such as a fixed particle, a particle attached to insulator surface and local field concentration at triple junction. However, it is obvious that ACWV is the most critical stress if a free moving particle is contaminated in GIS, since a particle cannot move during stressing LI and SI voltages, and AC-voltage test cannot be substituted by LI and SI tests. Therefore, under non-uniform field condition, LI- and AC-voltage tests are essential to find out a defect in GIS, while SI-voltage test could be eliminated, since the local field concentration at a defect is relaxed by corona stabilization effects.

Table 6.7: Test conversion factors under quasi-uniform field in N_2/SF_6.

Conditions		Items	Conversion factors			Experimental conditions					References
			LI	SI	AC (rms)	P (MPa)	SF_6 content	Polarity *1	Configuration (Inner/Outer diameter)	Particle (Diameter/Length)	
Quasi-uniform	Clean	Coaxial electrode	1.58x$\sqrt{}$ 2=2.23	-	1.0	0.6	5-20%	*2	Φ 240/Φ 340mm	None	[6.24]
			1.66x$\sqrt{}$ 2=2.35	-	1.0	0.7					
			1.41	1.0	-	0.52	20%	Negative	Φ 89/Φ 226mm		[6.30]
			1.43	1.0	1.01/$\sqrt{}$ 2=0.71	0.62					
			1.33	1.0	-	0.6	15%	*3	Φ 185/Φ 400mm		[6.31]
			1.30	1.0	1.0/$\sqrt{}$ 2=0.71	0.6	20%	*3	Φ 120/Φ 401mm		[6.32]

*1 Voltage polarity that shows lower breakdown voltages.
*2 LI: Positive, AC: Negative
*3 LI: Positive, SI and AC: No data

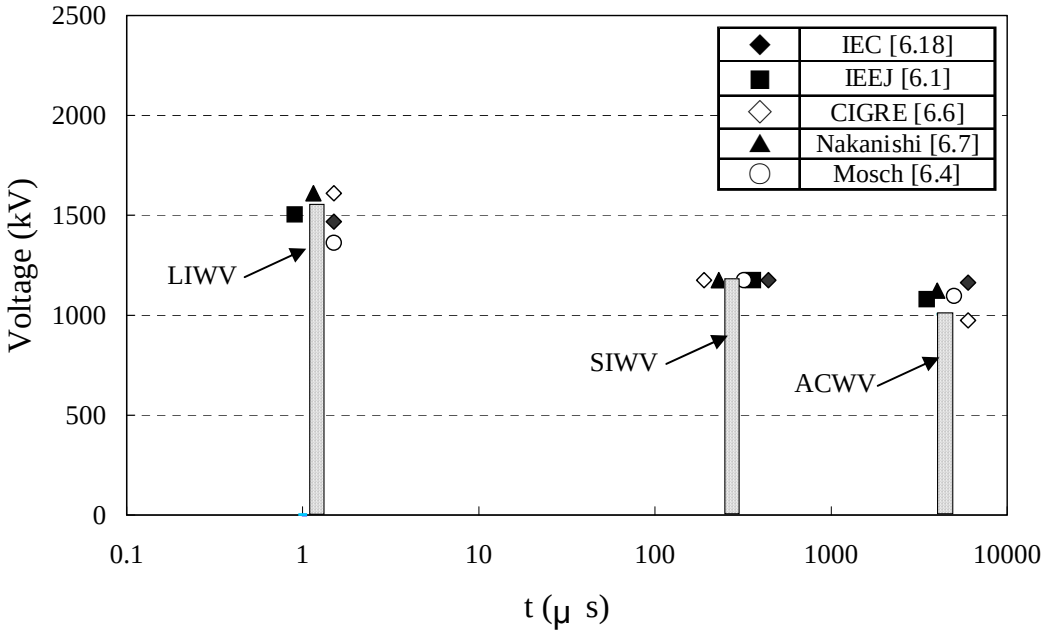

(a) Rated voltage 550kV (Range II)

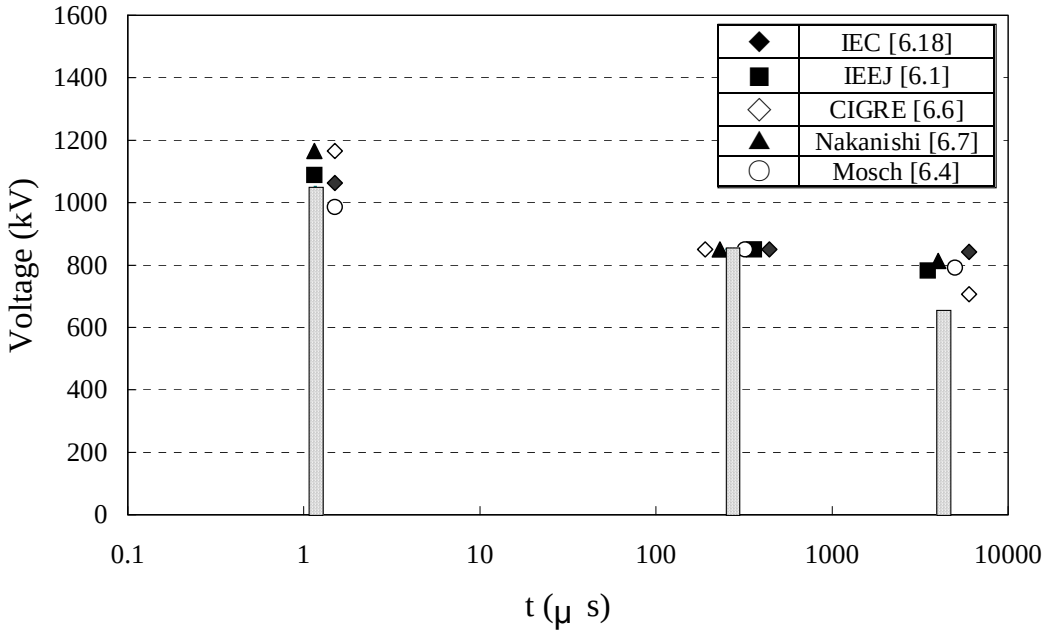

(b) Rated voltage 300kV (Range II)

Fig.6.26: Comparison between the rated withstand voltage (LIWV, SIWV and ACWV) for GIS and the voltages calculated by the conversion factors of V_{LI}/V_{SI} and V_{AC}/V_{SI} under quasi-uniform field in SF_6. The values of LIWV, SIWV and ACWV are referred to range I and II of IEC 62271-203.

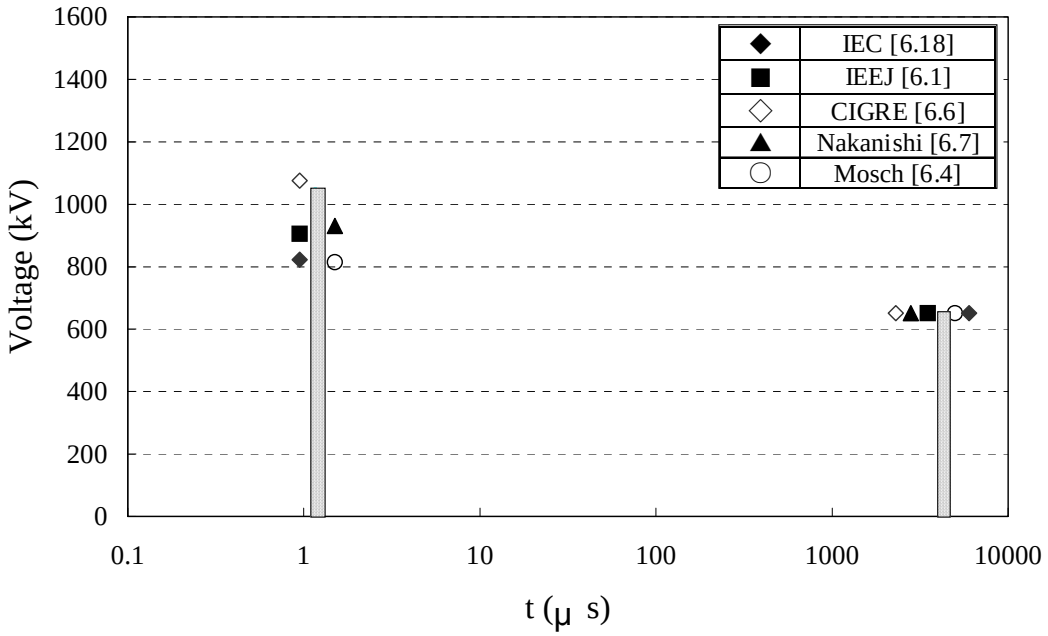

(c) Rated voltage 245kV (Range I)

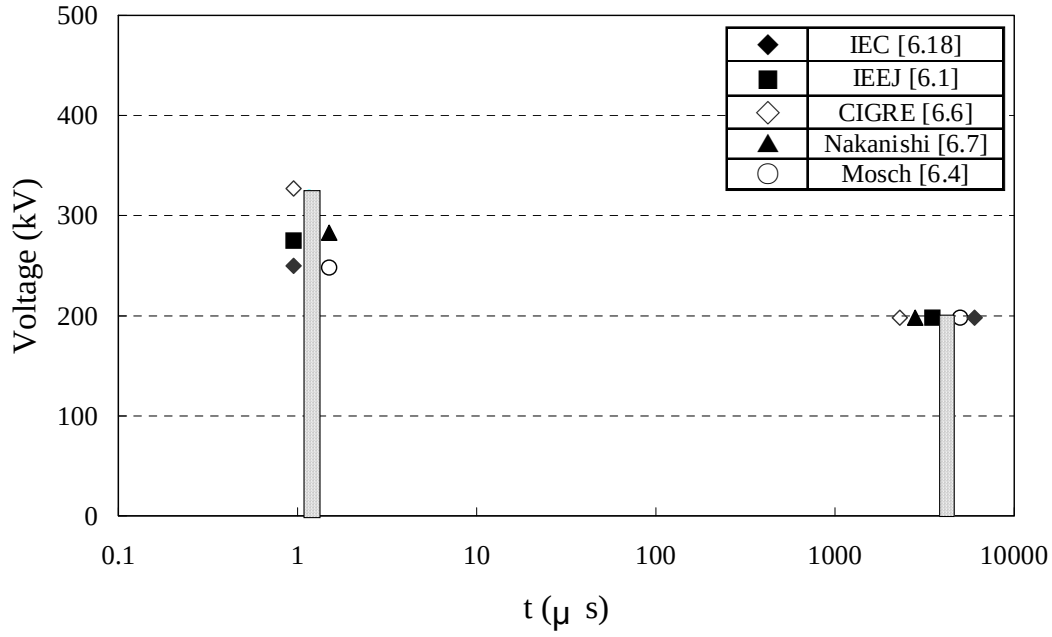

(d) Rated voltage 72.5kV (Range I)

Fig.6.26: Comparison between the rated withstand voltage (LIWV, SIWV and ACWV) for GIS and the voltages calculated by the conversion factors of V_{LI}/V_{SI} and V_{AC}/V_{SI} under quasi-uniform field in SF_6. The values of LIWV, SIWV and ACWV are referred to range I and II of IEC 62271-203.

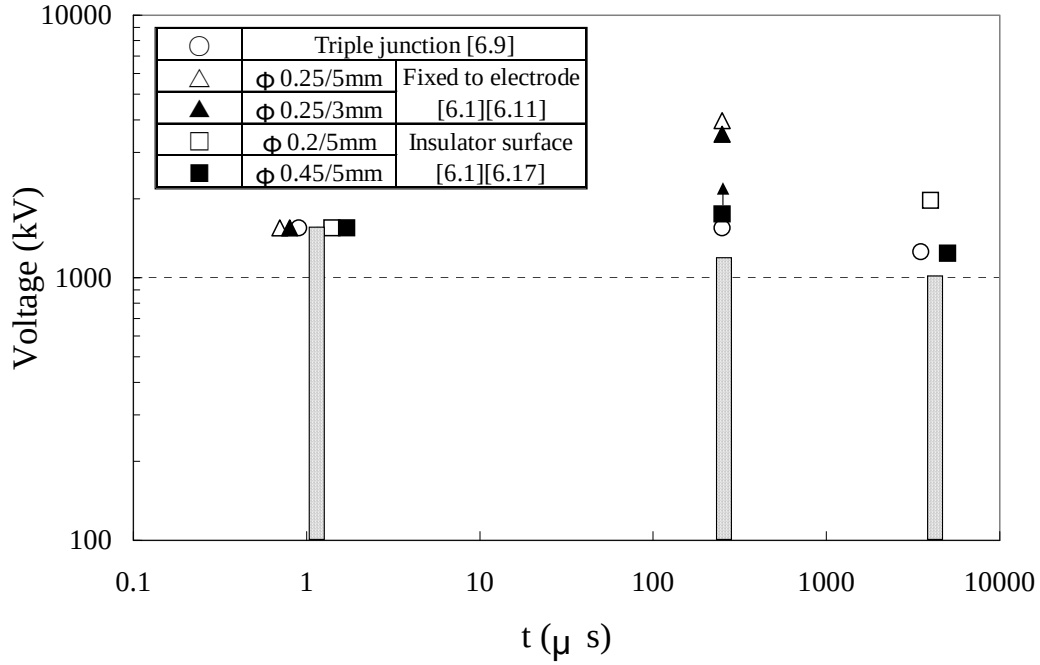

(a) Rated voltage 550kV (Range II)

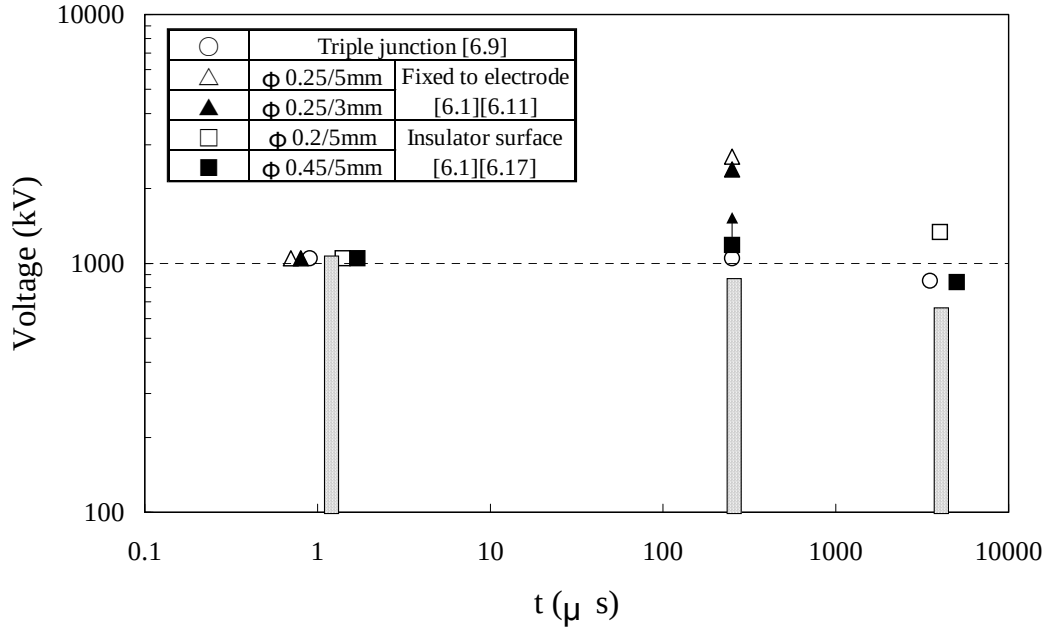

(b) Rated voltage 300kV (Range II)

Fig.6.27: Comparison between LIWV, SIWV and ACWV and the voltages calculated by the conversion factors of V_{SI} / V_{LI} and V_{AC}/V_{LI} under non-uniform field in SF_6. The values of LIWV, SIWV and ACWV are referred to range I and II of IEC 62271-203.

6.3.2 Most critical stress in N_2/SF_6 gas mixtures

The voltages calculated by the test conversion factors in Table 6.7 are compared with the rated withstand voltages, discussing again the most critical stress in N_2/SF_6 gas mixtures.

Figures 6.28 (a)-(d) show the comparison between LIWV, SIWV and ACWV and the voltages calculated by the test conversion factors of V_{LI}/V_{SI} and V_{AC}/V_{SI} under quasi-uniform field. Here, V_{AC}/V_{SI} instead of V_{ACrms}/V_{SI} is used again to calculate the voltages by the AC crest value. The values of LIWV, SIWV and ACWV are referred to IEC 62271-203, and the rated voltages are 550kV, 300kV, 245kV and 72.5kV, respectively. Regarding the voltages (open and closed square) calculated by the test conversion factors by [6.24] in Figures 6.28 (a) and (b), SI breakdown voltages V_{SI} are assumed to be equal to AC breakdown voltages V_{AC} in crest value, referring to the data in [6.30] and [6.32].

The figures show that SIWV stress is the most critical in the Range II of 300kV or higher of IEC 62271-203 under quasi-uniform field condition even if considering the mean value of the test conversion factors scattering between 1.30 and 1.66 in Table 6.7. As to the Range I, LIWV is basically the most critical stress.

Although LIWV is basically the most critical stress for a current equipment applying SF_6, it is noted that SIWV would be the most critical for the insulation design of the equipment applying N_2/SF_6 gas mixtures for IEC 62271-203.

The most critical stress under non-uniform field condition has not been well discussed, since there are not sufficient data available especially at low SF_6 content of 20% or lower and high pressure over 0.6MPa, which are practically important. However, as explained in the section 6.2.2, it should be noted that a metallic particle lowers the dielectric performance of the gas mixtures as reducing SF_6 content and increasing the gas pressure at positive LI and AC. Therefore, under non-uniform field, more detailed research would be needed to clarify the most critical stress and the effective voltage tests to find out the defects in the equipment.

6.4 Conclusion

Test conversion factors in SF_6 and N_2/SF_6 gas mixtures are reviewed and summarized based on the insulation properties including the recent data. The following remarks are derived, studying the most critical stress for the equipment when applying IEC 62271-203.

(1) Without the defects such as particle contamination and local field concentration at triple junction, LIWV is basically the most critical to the equipment applying SF_6. On the other hand, with the defects in SF_6, LI- and AC-voltage tests are essential to find out the defects in the equipment, while SI-voltage test could be eliminated due to corona stabilization effects.

(2) Without the defects in N_2/SF_6 gas mixtures, SIWV is the most critical in the Range II of the IEC. As to the Range I, LIWV is basically the most critical. Under metallic particle contamination, the dielectric performance of the gas mixtures is lowered as reducing SF_6 content and increasing the gas pressure at positive LI and AC.

(3) It is noted that SIWV would be the most critical stress for the insulation design of the equipment applying N_2/SF_6 gas mixtures for IEC 62271-203, whereas LIWV is basically the most critical stress for a current equipment applying SF_6.

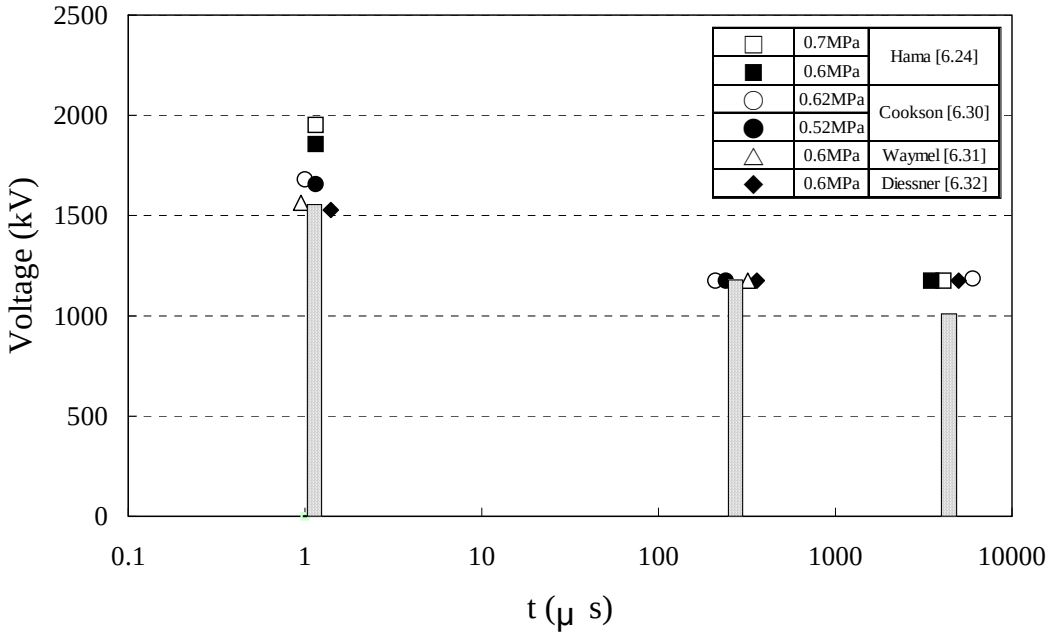

(a) Rated voltage 550kV (Range II)

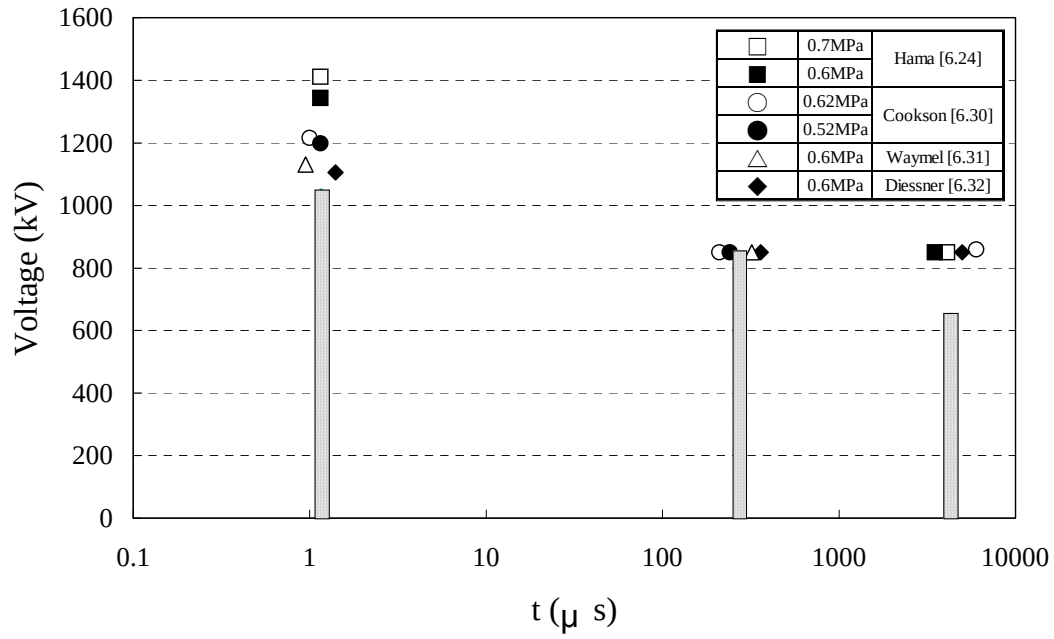

(b) Rated voltage 300kV (Range II)

Fig.6.28: Comparison between LIWV, SIWV and ACWV for GIS and the voltages calculated by the conversion factors of V_{LI}/V_{SI} and V_{AC}/V_{SI} under quasi-uniform field in N_2/SF_6 gas mixtures. The values of LIWV, SIWV and ACWV are referred to range I and II of IEC 62271-203.

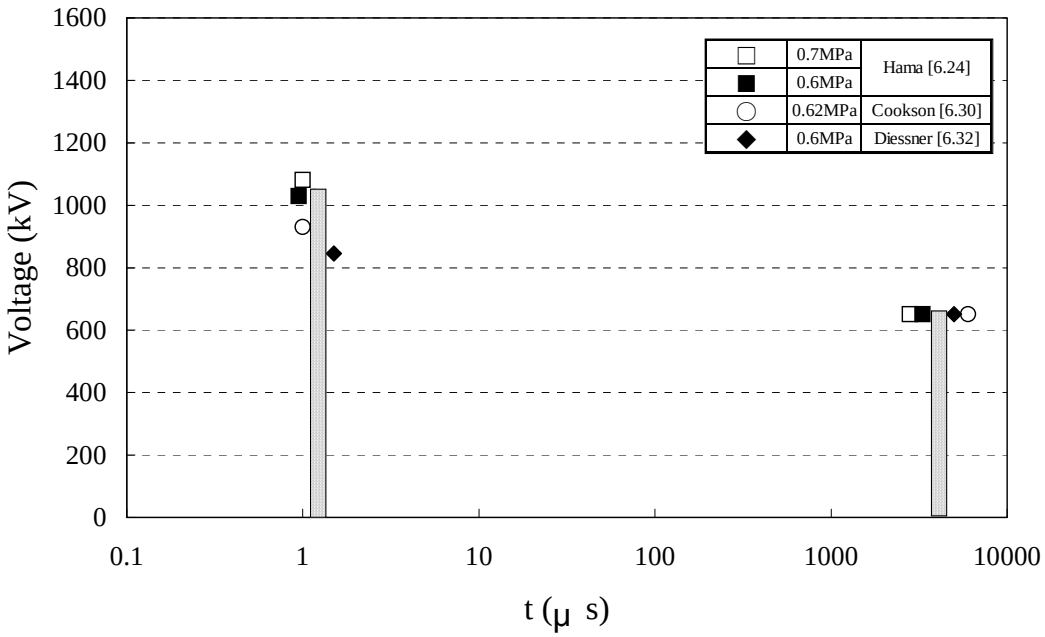

(c) Rated voltage 245kV (Range I)

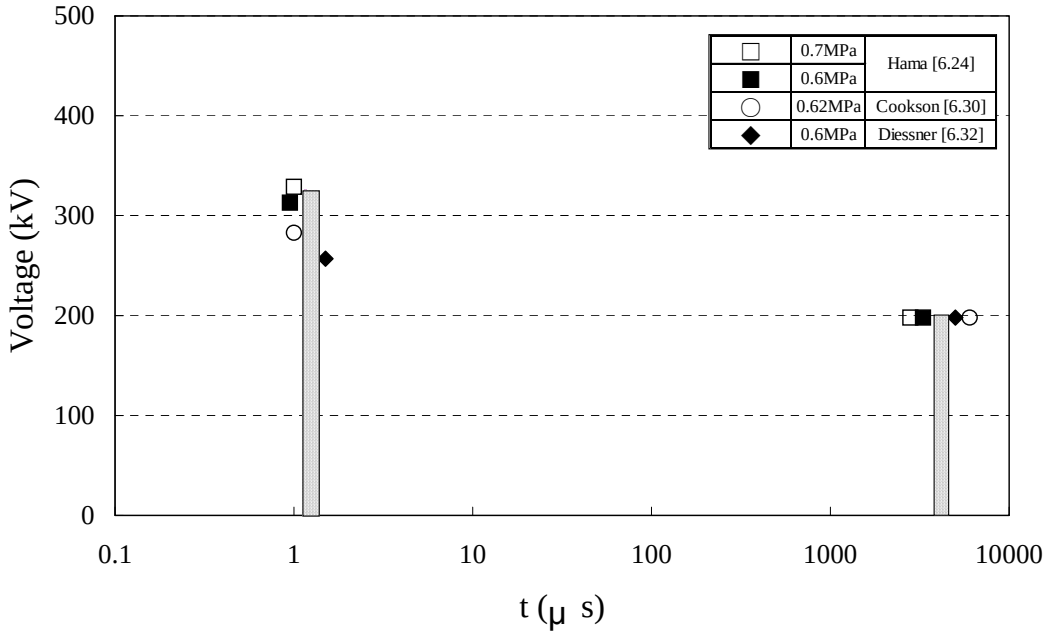

(d) Rated voltage 72.5kV (Range I)

Fig.6.28: Comparison between LIWV, SIWV and ACWV for GIS and the voltages calculated by the conversion factors of V_{LI}/V_{SI} and V_{AC}/V_{SI} under quasi-uniform field in N_2/SF_6 gas mixtures. The values of LIWV, SIWV and ACWV are referred to range I and II of IEC 62271-203.

REFERENCES of Chapter 6

[6.1] Investigation R&D Committee Chaired by Prof. T. Kawamura, "Properties on Electrical Insulation Related to Testing Voltages and Power Equipment", *Technical Reports by IEE Japan*, No.518 (1994)(in Japanese).

[6.2] Y.Kawaguchi and S.Menju, "Technical Problems of SF_6-Gas Insulation", *Toshiba Review*, Vol.25, No.2, pp.199-204 (1970)(in Japanese).

[6.3] S.Menju, K.Kimura, H.Aoyagi, K.Takahashi and H.Oono, "Dielectric Breakdown of High Pressure SF_6 between Spheres and Coaxial Cylinders", *T. IEE Japan*, Vol.93-B, No.11 (1973) (in Japanese).

[6.4] W.Mosch and W.Hauschild, "Möglichkeiten zur Berechnung der Durchschlagspannung schwach inhomogener Anordnungen im SF_6", *Elektrie* 28 H. 3, pp.152-156 (1974).

[6.5] L.G.Christophorou and R.J.Van Brunt, "SF_6/N_2 Mixtures", *IEEE Trans. Diel. and Elec. Ins.*, Vol.2 No. 5, pp.952-1003 (1995).

[6.6] A.Diessner, G.F.Luxa, W.Mosca and A.Pigini, "High Voltage Testing of SF_6 Insulated Substations on Site", *CIGRE Session 1986*, Report 33-06.

[6.7] K.Nakanishi, Y.Yoshida, Y.Shibuya and T.Nitta, "Experimental Study of the Breakdown Characteristics of a Gas-Insulated Bus", *IEEE Trans. Electrical Insulation*, Vol.EI-15, No.2, pp.111-117 (1980).

[6.8] N.Izeki, "Voltage - time Characteristics of SF_6 Gas", *Electra* N0. 101, pp. 41-59.

[6.9] H.Hama, H.Yamamoto, S.Sakuma, K.Takatsuka and T.Yamauchi, "Surface Flashover Characteristic of Disc–type Spacer System Initiated by Wedge Shaped Gas Gap and Its Improvement", *IEEE Trans. Power Delivery*, Vol.8, No.3, pp.1070-1080 (1993).

[6.10] H.Hama, K.Inami, M.Yoshimura and K.Nakanishi, "Estimation of Breakdown Voltages of Surface Flashovers Initiated from Triple Junction in SF_6 Gas", *Electrical Engineering in Japan*, Vol.116, No.5, pp.1-17 (1996).

[6.11] S.Matsumoto, H.Aoyagi, H.Murase and S.Yanabu, "Non-Uniform Field Flashover Characteristics in SF_6 Gas under Very Fast Transient Overvoltages", *T. IEE Japan* Vol.110-B, No.9 (1990) (in Japanese).

[6.12] H.Hama, K.Inami, M.Miyashita and M.Yoshimura, "Dielectric Performances of GIB Applying N_2/SF_6 Mixtures under Metallic Particle Contamination", *the XIII International Conference on Gas Discharges and their Applications*, Glasgow, pp.996-999 (2000).

[6.13] H.Hama, K.Inami, M.Yoshimura and M.Miyashita, "Dielectric Properties of Gas Insulated Bus Applying Low SF_6 Content and Highly Compressed N_2/SF_6 Gas Mixtures", *Gaseous Dielectrics IX*, pp.487-496 (2001).

[6.14] M.S.Indira and T.S.Ramu, "Motion of conducting Particles Causing Inadvertent Outages in GIS", *IEEE Trans. Diel. and Elekc. Ins.*, Vol. 7, No. 2, pp. 247-253 (2000).

[6.15] S. Zhang et al., "On the Particle-Contaminated GIS/GITL Systems with Dielectric coated Electrodes", *IEEE Power Eng. Rev.*, pp52-54, August (2001).

[6.16] S. Zhang et al., "The Impact of Electrode Dielectric Coating on the Insulation Integrity of GIS/GITL with Metallic Particle Contaminants", *IEEE Trans. Power Delivery*, Vol. 17, No. 2, pp. 318-325 (2002).

[6.17] T.Yamagiwa, T.Ishikawa and F.Endo, "Particle-initiated Breakdown Characteristics on a Ribbed Spacer Surface for SF_6 Gas Insulated Switchgear", *IEEE Trans. Power Delivery*, Vol.3, No.3, pp.954-960 (1988).

[6.18] IEC60071-2, “Insulation co-ordination Part 2: Application guide” (1996-12).
[6.19] CIGRE WG 33/23-15, “Insulation Coordination of GIS: return of experience, on site tests and diagnostic Techniques”, *ELECTRA*, N0. 176, February (1998).
[6.20] B.Hartlieb, H.Winkelnkemper, “Die Berechnung der Durchschlagspannung von SF_6-Gas-Gemischen”, etz Archiv Bd. 2 (1980) H.12 pp. 351-356.
[6.21] G.Schröder, “Entladungsentwicklung in SF_6-N_2 Gasgemischen bei schnell schwingenden Steilstoßspannungen und Blitzstoßspannung”, Diss. RWTH Aachen, Shaker Verlag Aachen (2001).
[6.22] CIGRE WG 23/21/33-15 TF 2, “Gas Insulated Transmission Lines (GIL), Appendix B: GIL Insulation Coordination, On-site Test, Long Duration Test, Monitoring and Grounding”, *Technical Brochure*, No.218 (2002).
[6.23] CIGRE Task Force D1.03.10, “N_2/SF_6 Mixtures for Gas Insulated Systems”, *Technical Brochure*, No. 260 (2004).
[6.24] H.Hama, K.Inami, M.Miyashita and M.Yoshimura, “Area Effect of Breakdown in N_2/SF_6 Gas Mixtures And Its Reflection to Insulation Design of Gas Insulated Bus”, *the XIV International Conference on Gas Discharges and their Applications*, Liverpool, pp.280-283 (2002).
[6.25] H.I.Marsden, M.D.Hopkins and C.R.Eck III, “Lightning Impulse Withstand Performance of a Practical GIC with 5 and 10 percent SF_6/N_2 Mixtures”, *ISEI-IEEE* (1998).
[6.26] H.I.Marsden, M.D.Hopkins and C.R.Eck III, “Power Frequency and SIL Withstand Performance of a GIC with 5 and 10 Percent SF_6/N_2 mixtures”, *Gaseous Dielectrics VIII*, pp.541-546 (1998).
[6.27] A.Sabot, “Insulation Co-ordination Procedure for 420kV Gas Insulated Lines (GIL)”, *ISH99*, 3.1.S18.
[6.28] Y.Hoshina, M.Sato, H.Murase, M.Toda and A.Kobayashi, “Dielectric Proprieties of SF_6/N_2 Gas Mixtures on a Full Scale Model of the Gas-insulated Busbar”, *IEEE WM* (2000).
[6.29] JEC-2350-2005, “Standard of the Japanese electrotechnical committee: Gas Insulated Switchgear” (in Japanese).
[6.30] A.H.Cookson and B.O.Pedersen, "Analysis of the High Voltage Breakdown Results for Mixture of SF_6 with CO_2, N_2 and Air", *3rd ISH*, Milan, Paper No.31.10 (1979).
[6.31] X.Waymel, “Low SF_6 Concentration SF_6/N_2 Mixtures for GIL”, *Gaseous Dielectrics VIII*, pp.345-351 (1998).
[6.32] A.Diessner, M.Finkel, A.Grund and E.Kynast, “Dielectric Properties of N_2/SF_6 Mixtures for Use in GIS or GIL”, *11th ISH*, London, Paper No.3.67.S18 (1999).
[6.33] CIGRE Guide for SF_6 Gas Mixtures, *ELECTRA*, N0. 19, August (2000).

7. SITE TESTING

In this chapter, tests after installation on site are compared between three kinds of standards in terms of the differences of purpose, test procedure and testing philosophy.

Table 7.1 shows the comparison of on-site tests after installation between IEC 62271-203 [7.1], IEEE Std C37.122-1993 [7.2] [7.3] and JEC-2350-2005 [7.4]. Tables 7.2 and 7.3 referred in the Table 7.1 show on site test voltages and test voltage for measuring PD intensity in IEC 62271-203, respectively.

Regarding the purpose of the site testing, there is not an essential difference between them. The purpose is focused on checking dielectric integrity after the completed installation and on free of defects that could cause problems under operation.

However, the test procedure and test voltage are different between IEC 62271-203/IEEE Std C37.122-1993 and JEC-2350-2005. Both the IEC and the IEEE standards specify the power-frequency voltage test (IEC: 0.45x0.8xLIWV, IEEE: 0.8-1.0 of ACWV) and the lightning impulse voltage test (IEC: 0.8xLIWV, IEEE: 0.7-1.0 of LIWV). On the other hand, only power-frequency test at reduced voltage, which is described in Annex C of IEC 62271-203, is specified in the JEC standard.

The above difference could be explained by the testing philosophy as follows. As for the IEC and the IEEE standards, it is important to detect any defects in the assembled equipment that may have been introduced during shipping or site assembly, selecting the appropriate test procedures. Voltage waveforms such as power-frequency, lightning impulse and switching impulse are specified depending on the defect types and on the rated voltage of GIS.

On the other hand, concerning the JEC standard, it is essential to check the dielectric integrity of GIS of completed installation by AC test at reduced voltage or PD and/or particle detection at the operating voltage by which testing breakdown should be avoided. Improving a quality control during transportation and on-site assembly is a basic concept instead of adopting AC tests at high voltage or lightning impulse tests.

REFERENCES of Chapter 7

[7.1] IEC 62271-203, “High- voltage switchgear and controlgear – Part 203: Gas-insulated metal-enclosed switchgear for rated voltages above 52kV”.

[7.2] IEEE Std C37.122-1993, “IEEE standard for gas-insulated substations”.

[7.3] IEEE Std C37.122.1-1993, “IEEE guide for gas-insulated substations”.

[7.4] JEC-2350-2005, “Standard of the Japanese electrotechnical committee: Gas insulated switchgear” (in Japanese).

Table 7.1: Comparison of on-site tests after installation between IEC 62271-203, IEEE Std C37.122-1993 and JEC-2350-2005.

	IEC 62271-203	IEEE Std C37.122-1993	JEC-2350-2005
Purpose	- Checking the dielectric integrity of GIS to eliminate fortuitous causes (wrong fastening, damage during handling, transportation, storage and installation, presence of foreign bodies, etc.) which might in the future give rise to an internal fault.	- Ensuring that the GIS equipment, as manufactured, shipped and assembled is free of defects that could cause problems under conditions encountered during normal operation.	- Checking the dielectric integrity of GIS of completed installation to verify the dielectric performance checked by the routine tests in the factory.
Test procedure and test voltage	- **Power-frequency voltage test (Procedure A: recommended for 170kV and below)**: Voltage specified in Table 7.2 Column 2 for 1 min. - **Power-frequency voltage test and PD measurements (Procedure B: recommended for 245kV and above)**: Voltage specified in Table 7.2 Column 2 for 1 min and PD measurements according to Table 7.3 (with $U_{\text{pre-stress}} = D_{\text{ds}}$ of Table 7.2 Column 2). - **Power-frequency voltage test and lightning impulse tests (Procedure C: recommended for 245kV and above, alternative to procedure B)**: Voltages specified in Table 7.2 for 1 min Column 2 and with three impulses of each polarity with the value specified in Table 7.2, column 4. ***** Test frequencies are referred to 10Hz to 300Hz. ***** A DC voltage test cannot be recommended.	- **Power-frequency conditioning in conjunction of PD detection**: Maximum voltage is usually in the range of 1.1–1.3 pu. (1 pu: operating voltage) - **Power-frequency voltage test (recommended for less than 362kV)**: Voltage in the range of 80–100 % of the rated low-frequency withstand level for 1 min. - **Power-frequency voltage test with PD and/or particle detection (recommended for EHV-level GIS)**: Voltage in the range of 80–100 % of the rated power-frequency withstand level for 1 min. - **Lightning impulse or oscillating impulse test (recommended for EHV-level GIS)**: Voltage of 70-80 % of the LIWV. * Test frequencies are 50Hz or 60Hz. * The power-frequency voltage test normally follows the above power-frequency conditioning period.	- **Power-frequency test at reduced voltage**: Voltage for 10 min at $1.10 \times U_r/\sqrt{3}$ (for substation with earthed neutral systems), at $1.25 \times U_r/\sqrt{3}$ (for switchgear station with earthed neutral systems) or at $1.9 \times U_r/\sqrt{3}$ (for isolated neutral systems). Here U_r is the rated voltage. Test frequencies are 50Hz or 60Hz. * The above procedure is introduced in IEC 62271-203 Annex C. * PD and/or particle detection are sometimes applied at the operating voltage to detect defects (harmful particles) under the agreement between manufacture and user. * Lightning impulse and oscillating impulse tests are not specified in the JEC-2350. The tests are subject to agreement between manufacture and user. ***** A DC voltage test cannot be recommended.
Gas pressure	- Rated gas pressure	- Rated gas pressure	- Rated gas pressure
Special test procedure	- **Power-frequency test at reduced voltage**: Voltage for 10 min at $1.10 \times U_r/\sqrt{3}$ (for earthed neutral systems), or at $1.9 \times U_r/\sqrt{3}$ (for isolated neutral systems). Here U_r is the rated voltage. If the tested units are transported without dismantling or if dismantling is limited to very simple connections and subject to agreement between manufacture and user, the site test may be reduced to the above (Annex C).	- Not specifically	- **Elimination of on-site voltage test**: Elimination of the voltage test is possible under the agreement between manufacture and user, if a special care is taken in the equipment design and in the quality control during transportation and on-site assembly in order to keep the same dielectric integrity checked by the routine test in the factory.

Testing philosophy	- Detecting any defects in the assembled equipment that may have been introduced during shipping or site assembly, selecting the appropriate test procedures. - Voltage waveforms such as power-frequency, lightning impulse and switching impulse are specified depending on the defect types and on the rated voltage of GIS.	- Detecting any defects in the assembled equipment that may have been introduced during shipping or site assembly, selecting the appropriate test procedures. - Low-frequency conditioning in conjunction of PD detection at 1.1–1.3 pu is specified by which testing breakdown should be avoided. - Voltage waveforms such as power-frequency and lightning impulse are specified depending on the defect types and on the rated voltage of GIS.	- Checking the dielectric integrity of GIS of completed installation by AC test at reduced voltage or PD and/or particle detection at the operating voltage by which testing breakdown should be avoided. - Improving a quality control during transportation and on-site assembly is a basic concept instead of adopting AC tests at high voltage or lightning impulse tests.

Table 7.2: On site test voltages in IEC 62271-203. Here, U_p and U_s are the rated lightning impulse withstand voltage and the rated switching impulse withstand voltage, respectively.

Rated voltage for equipment U_r kV (r.m.s. value)	On-site short-duration power-frequency withstand voltage U_{ds} kV (r.m.s. value)	On-site switching impulse withstand voltage U_{ss} kV (peak value)	On-site lightning impulse withstand voltage U_{ps} kV (peak value)
(1)	(2) (see Note 1)	(3)	(4)
72,5	120	-	260
100	165	-	360
123	200	-	440
145	235	-	520
170	270	-	600
245	380	680	840
300	380	680	840
362	425	760	940
420	515	840	1 140
550	560	940	1 240
800	760	1140	1 680

NOTE 1 Values of column (2) are only applicable for SF_6 insulation or when SF_6 is a major part of the gas mixture. For other insulation refer to Tables 1 and 2 of IEC 60694, applying a factor 0,8 on column (2).

NOTE 2 The on-site test voltages have been calculated as follows:

U_{ds} (on-site test value) = $U_p \times 0{,}45 \times 0{,}8$ (column 2)

U_{ss} (on-site test value) = $U_s \times 0{,}8$ (column 3)

U_{ps} (on-site test value) = $U_p \times 0{,}8$ (column 4)

All values have been rounded up to the next higher modus 5 kV.

NOTE 3 If other insulation levels than the preferred values of Tables 102 and 103 (e.g. the lower insulation levels of Tables 1 and 2 in IEC 60694) are specified, then the on-site test voltage should be calculated according to Note 2.

Table 7.3: Test voltage for measuring PD intensity in IEC 62271-203.

	System with solidly earthed neutral		System without solidly earthed neutral	
	Pre-stress voltage $U_{pre\text{-}stress}$ (1 min)	Test voltage for PD measurement $U_{pd\text{-}test}$ (>1 min)	Pre-stress voltage $U_{pre\text{-}stress}$ (1 min)	Test voltage for PD measurement $U_{pd\text{-}test}$ (>1 min)
Single-phase enclosures design (phase-to-earth voltage)	$U_{pre\text{-}stress} = U_d$	$U_{pd\text{-}test} = 1{,}2\ U_r / \sqrt{3}$	$U_{pre\text{-}stress} = U_d$	$U_{pd\text{-}test} = 1{,}2\ U_r$
Three-phase enclosures design	$U_{pre\text{-}stress} = U_d$	$U_{pd\text{-}test,\ ph\text{-}ea} = 1{,}2\ U_r / \sqrt{3}$ $U_{pd\text{-}test,\ ph\text{-}ph} = 1{,}2\ U_r$	$U_{pre\text{-}stress} = U_d$	$U_{pd\text{-}test,\ ph\text{-}ea} = 1{,}2\ U_r$

U_r: rated voltage for equipment.

U_d: power-frequency withstand test voltage as per Table 102 and 103.

$U_{pre\text{-}stress}$: pre-stress voltage.

$U_{pd\text{-}test}$: test voltage for PD measurement.

$U_{pd\text{-}test,\ ph\text{-}ea}$: test voltage for PD measurement, phase-to-earth.

$U_{pd\text{-}test,\ ph\text{-}ph}$: test voltage for PD measurement, phase-to-phase.

8. CONCLUSIONS

Insulation co-ordination related to internal insulation of gas insulated system in SF_6 and also some aspects of N_2/SF_6 gas mixtures under AC condition has been reviewed and discussed. As the equipment of the gas insulated system, GIS is dealt with in this brochure. The following items are concerned according to the flow chart for the determination of rated or standard insulation level of IEC 60071-1.

(a) Conversion in shape of field overvoltage to standard impulse waveform to determine representative voltages and overvoltages U_{rp}
(b) Safety factor K_s regarding in-service ageing and influence of prestress voltage
(c) Test conversion factor K_t

The difference of a GIS site testing between three standards is also described in terms of purpose, test procedure and testing philosophy. The concluding remarks are summarized as follows.

Field real surges of non-standard lightning impulse waveform are analyzed and the SF_6 insulation characteristics for these actual surges in SF_6 are clarified to convert the surge waveform into the standard lightning impulse waveform.

(1) It is found that the insulation requirements could not be as severe as those of the standard lightning impulse waveform, since the decay of the field overvoltage is generally large. Consequently, it could be possible in some cases to use lower withstand test voltages for GIS using SF_6.

The long-term performance of a GIS has been reviewed in terms of V-t and V-N characteristics of SF_6 insulation system. The long-term field experience of a GIS and the key components is introduced and the insulation performance after the 50 years service life is evaluated.

(2) A GIS insulation system of a proper design has a service life of 50 years and in the recent reports no significant ageing is recognized in the actual GIS after long-term operations. However, some other aspects such as metallic particles generation from the contacts, mechanical/thermal performance and gas seal performance should also be considered in a practical GIS.

The influence of AC and DC prestress on insulation performance of GIS applying IEC 62271-203 is discussed using the experimental results on insulation characteristics under LI and VFT voltages superimposed to AC or DC voltages.

(3) There is no need to consider the influence of AC prestress on a GIS insulation performance. The influence of DC prestress could also be neglected with an appropriate insulation design margin and with an effective measure against metallic particles, for example, applying a thin dielectric coating on the inner surface of GIS enclosure.

Test conversion factors in SF_6 and N_2/SF_6 gas mixtures are reviewed and summarized based on the insulation properties including the recent data. The following remarks are derived, studying the most critical stress for the equipment based on IEC 62271-203.

(4) Without the defects such as particle contamination and local field concentration at triple junction, LIWV is basically the most critical to the equipment applying SF_6. However, for the equipment applying N_2/SF_6 gas mixtures and without the defects, SIWV is the most

critical stress in the Range II (300kV or higher) of the IEC, while LIWV is basically the most critical in the Range I (245kV or lower).

Tests after installation on site are compared between IEC 62271-203, IEEE Std C37.122-1993 and JEC-2350-2005 in terms of the differences of purpose, test procedure and testing philosophy.

(5) Regarding the purpose of the site testing, there is not an essential difference between them. However, the test procedure and test voltage are different between IEC 62271-203/IEEE Std C37.122-1993 and JEC-2350-2005.

The above studies on a GIS regarding insulation co-ordination related to internal insulation are useful to make up the lack of information concerning “dielectric withstand characteristics of electrical insulation”. The results would contribute to the further compactness of a GIS with high reliability and to the reduction of SF_6 emission into the atmosphere.

As the next step, this work will be extended to internal insulation of oil-paper insulated systems.